NOTE TO USERS

The CD-ROM disc is not included in this original manuscript. It is available for consultation at the author's graduate school library.

This reproduction is the best copy available.

UMI

THE UNIVERSITY OF CALGARY

Critical Evaluation of Multiphase Flow in Pipes

by

Carlos A. Duque

A THESIS

SUBMITTED TO THE FACULTY OF GRADUATE STUDIES

IN PARTIAL FULFILLMENT OF THE REQUIREMENTS FOR THE

DEGREE OF MASTER OF SCIENCE IN CHEMICAL ENGINEERING

DEPARTMENT OF CHEMICAL AND PETROLEUM ENGINEERING

CALGARY, ALBERTA

JULY, 1998

Abstract

Mechanistic models have been reviewed. Their prediction of liquid holdup and pressure gradient have been tested against the experimental data from the Stanford database. The most important flow regimes, stratified, annular, slug, bubble and bubbly were tested. The data available for comparison was gathered mainly on laboratory test loops for air-water fluid systems.

In general, from the results of the model predictions when compared to the measured data it can be concluded that the pressure gradient is a very weak function of the liquid holdup for all the flow regimes tested. All the liquid holdup models were found to be sufficiently adequate for design purposes, that is within ± 30% average error.

The pressure gradient models showed poor performance in general. Only the models for stratified flow and slug flow, both horizontal and vertical were accurate enough to be used for design. Hence, the pressure gradient models for annular flow, both horizontal and vertical are not recommended for design.

The quality of the data was found questionable for some flow regimes; a large portion of the data appeared to be wrongly classified.

Acknowledgements

"Commit to the Lord whatever you do, and your plans will succeed." *Proverbs 16:3*

My sincerest gratitude to my supervisor, Dr. W. Y. Svrcek, for his encouragement, support and patience throughout this work.

I would also like to thank my friend, Dr. W.D. Monnery, for his vision in conceiving this work and his technical advise.

To my brother, Roberto, thanks for his assistance in the preparation of the illustrations for this work.

To my wife and children, Trudy, Camille and Lucas, thanks for their sacrifice and patience.

Finally, I am very grateful to my parents for their persisting faith, support and encouragement.

CAD.

Dedication

To my beloved wife, Trudy
and my children, Camille and Lucas

Table of Contents

List of Tables

List of Figures

Nomenclature

(Context Dependent)

A	cross-sectional area of the pipe, m^2
A_g	cross-sectional area of pipe for gas, m^2
A_l	cross-sectional area of pipe for liquid, m^2
C_o	film distribution parameter
C_L	lift coefficient
Dc	bubble critical diameter,m
D	pipe diameter, m
D_f	hydraulic diameter for film, m
D_g	hydraulic diameter for gas phase, m
D_l	hydraulic diameter for liquid phase, m
f_f	film friction factor based on Re_f
f_g	gas phase friction factor based on Re_g, equation
f_i	interfacial friction factor
f_l	liquid friction factor based on Re_l
f_m	friction factor based on Re_m
f_s	friction factor for liquid in the slug based on Re_s
f_{sg}	gas phase friction factor based on superficial velocity
f_{sl}	liquid phase friction factor based on superficial velocity
FE	liquid entrainment fraction

Fr	modified Froude number
F_B	buoyant forces in Dispersed Bubble flow, N
F_T	turbulent forces in Dispersed Bubble flow, N
g	acceleration due to gravity, m/s^2
h_g	gas depth in pipe, m
h_l	liquid depth in pipe, m
l_e	churn flow, developing length, m
l_f	film length, m
l_s	slug length, m
P	average pressure, $N/m^2/m$
dP/dx	average pressure gradient, $N/m^2/m$
Re_f	liquid film Reynolds number
Re_g	gas phase Reynolds number
Re_l	liquid phase Reynolds number
Re_m	mixture Reynolds number
Re_s	Slug Reynolds number
S_g	gas wetted perimeter with pipe wall
S_i	interface wetted perimeter between gas and liquid, m
S_l	liquid wetted perimeter with pipe wall, m
T	ratio of turbulent to bouyancy forces
u*	friction velocity, m/s
U_o	bubble rise velocity, m/s
V_g	insitu gas velocity, m/s

V_l insitu liquid velocity, m/s

V_b bubble rise velocity, m/s

V_c gas core velocity, m/s

V_d drift velocity, m/s

V_f film velocity, m/s

V_m mixture velocity, m/s

V_s average particle velocity of the slug, m/s

V_{sg} superficial gas velocity, m/s

V_{sl} superficial liquid velocity, m/s

V_t average translational velocity of the slug and bubble, m/s

X Lockhart Martinelli parameter

Y dimensionless inclination parameter

Greek Letters

α_g average insitu gas fraction in pipe

α_{gs} average insitu gas fraction in the slug

α_l average insitu liquid fraction in the pipe

α_{lf} insitu liquid fraction in the film

α_{ls} average insitu liquid fraction in the slug

β angle of inclination, $^\circ$

ε pipe roughness, m

λ no slip volume fraction

μ_g gas viscosity, Pa.s

μ_l liquid viscosity, Pa.s

μ_m mixture viscosity, Pa.s

μ_{ms} slug mixture viscosity, Pa.s

ρ_g gas density, kg/m^3

ρ_l liquid density, kg/m^3

ρ_m mixture density, kg/m^3

ρ_{ms} slug mixture density, kg/m^3

ρ_m mixture density, kg/m^3

σ surface tension, dyne/cm

τ_{wg} gas shear with pipe wall, N/m^2

τ_i interfacial shear stress between gas and liquid, N/m^2

τ_{wl} liquid shear stress with pipe wall, N/m^2

Chapter 1
INTRODUCTION

The hydraulic mechanisms of single-phase fluid flowing in a pipe are well understood and accurately predicted by the petroleum, chemical and nuclear industries. Single-phase fluid motion is characterized according to its flow regime as either laminar or turbulent. The in situ velocity can be accurately predicted by the superficial average velocity. Single-phase frictional losses are easily calculated from physical properties and the shear stress between the pipe wall and the fluid. The constitutive equation for this shear stress uses the friction factor to estimate the frictional pressure losses between the fluid and the wall. This friction factor has been correlated with the Reynolds's number and the pipe roughness given satisfactory results for single-phase flow frictional losses.

Conversely, the flow of two or more inmiscible phases in a pipe is not as well understood due to its additional complexity. There are a number of factors not present in single-phase flow, which cause this complexity. In multiphase flow, both phases occupy the pipe simultaneously competing for the available flow area. It then becomes necessary to know how the flow cross-section is being occupied by each phase. The phases move at different average velocities causing what is known as *slip* as portrayed by Govier and Aziz (1972). The distribution of the phases produces flow regimes by expanding and collapsing their gas-liquid interface. This interface between the phases complicates matters by introducing another layer of friction. The frictional gradient becomes a function of the interfacial shear stress as well. The value of this shear stress depends on the phases in contact. This complicates the finding of an appropriate closure relationship to estimate the shear stress trough an interfacial friction factor, since this varies with the flow regime. Thus, multiphase flow imposes additional complexity due to the distribution, behaviour and formation of the phases in the conduit, as well as the mechanics of the frictional losses (Taitel and Dukler (1976)). Certainly, the complications of a second phase do not exist in single-phase flow.

Whenever possible multiphase flow systems are avoided by separating the phases into individual streams because they are susceptible to flow instabilities, blockages, liquid surges (known as *slugs*), and pressure-temperature fluctuations. Also, multiphase lines can cause erosion problems when flowing at high liquid velocities. However, in many cases multiphase flow cannot be avoided. In the oil and gas industry, the transportation of two-phase flow mixtures over long distances is economically more attractive than separation of the phases for their individual transportation as shown by Corteville and Lagière (1983). In the nuclear industry multiphase flow occurs with a single component in the reactor cooling equipment. The ameliorated heat transfer characteristics of two-phase flow over single phase has promoted the use of two-phase flow in the nuclear reactor field. In the chemical industry multiphase flow is encountered in reboilers, condensers, evaporators, reactors and process piping.

Historically, empirical correlations have been used to design two-phase flow systems. The first correlations were based on very limited data, obtained in small diameter air-water systems (Lockhart and Martinelly (1949)). The fluids were treated as homogeneous mixtures and frictional losses were estimated on the basis of single-phase flow equations adjusting the Reynolds number for multiphase flow. This approach assumed a high degree of turbulence between the phases, which was the case for most of the wells discovered in the early fields. Empirical correlations can yield excellent results quickly, depending on the proper selection of variables and the data selected for the correlation. The extrapolation of these correlations to field conditions beyond the boundaries of the data used for their development can produce inaccurate results (Oliemans (1987); Baker et al. (1988); and Masud (1991)). The combination of flow regime map, holdup and pressure gradient correlations to improve prediction makes the finding of clear boundaries for these correlations to be a complex task. Gregory et al. (1985) and Nguyen et al. (1988) provided a set of guidelines for sets of correlations to use in gas-condensate and crude oil-gas systems. However, these guidelines do not cover all possible operating conditions, and piping dimensions found in field conditions.

Generalised empirical correlations do not address the complex physical phenomena occurring during multiphase flow in pipes. Thus, an impasse has been reached in which, regardless of the modification made to empirical correlations and the amount of data used to develop the correlations, it is unlikely that design calculations can be improved. Fortunately, progress in this area had already been made by the nuclear industry. Separate equations to describe the continuity equation, momentum balance, and energy balance were applied to each phase (Hetsroni (1982)). In spite of the more theoretical approach, empirical correlations and simplified closure equations were still needed for parameters such as the interfacial friction factor, fraction of liquid entrained in the gas core for annular flow, and liquid holdup in slug flow (Ansari et al. (1990)).

This is evidence of the many flaws still present in multiphase flow technology. For example, pressure drop, flow patterns, and liquid holdup in hilly terrain are poorly understood (Minami and Shoham (1995)). Also, more precise mechanistic models are required to predict three-phase flow behaviour when gas, oil and water are flowing simultaneously. Flow pattern prediction for these three-phase systems is very important for determining the presence of a free-water phase at the bottom of a pipe that could cause corrosion problems.

Due to their modelling structure mechanistic models lend themselves to piecewise improvements. Hence, many correlations and models have been proposed since the semi-theoretical based modelling began. As shown by Ansari et al. (1994) and Fernandes and Dukler (1983), enhancements in apparently unimportant parameters such as slug holdup, interfacial friction factor, and bubble-rise velocity in inclined pipe can significantly improve the calculation of the frictional losses. Unfortunately, there have been few reliable evaluations of these correlations. Most of the work has aimed to improve correlations by adjusting the main empirical parameters of the models to a new set of data, and to compare the improved model with the same data that was used to generate the new model (Rajan et al (1996); Ansari et al. (1990); and Ansary et al. (1994)). Even though these evaluation studies provide some guidelines, they are obviously biased. Consequently, design engineers must choose from an overwhelming variety of methods with little or no guidelines for making the selection.

Good estimating tools for multiphase flow behaviour and guidelines about their applicability are essential for design. Hence, a new independent and unbiased review of the most recent mechanistic methods is required. Therefore, the objective of this work is not to add a new model to an already crowded list, but to systematically test existing mechanistic models to establish their boundaries of application under different operating conditions.

Chapter 2
LITERATURE REVIEW

A vast amount of technical information on two-phase flow in pipes has been published over the last five decades. This information comes from a variety of sources involving different types of fluids and concerns. The nuclear industry has made significant contributions through the study of the transient two-phase flow of water coolant. In the petroleum industry there are unique features that create complications not encountered in other industries. The fluids involved are multicomponent mixtures whose phase behaviour is very complex. The range of pressures and temperatures is extremely broad. Pressures can range from 100 Mpa to near atmospheric conditions. Temperatures can range from 200°C to below water freezing temperatures. Pipes lengths can vary from a few meters to thousands of kilometres. Piping systems usually consist of large variety of diameters, pipe roughness, and piping layout, such as hilly terrain. Simulating multiphase flow in the petroleum industry requires the ability to predict the relationships between phase behaviour, flow rates, pressure drop, and piping geometry.

2.1 Basic Definitions and Concepts

Before tracing the history of methods to simulate two-phase flow behaviour, some of the fundamental definitions and concepts will be outlined.

2.1.1 Basic Fluid Properties

Typically in two-phase flow problems the transport properties and operating conditions (mass flow rates) are available or can be easily estimated. The mechanical details of the pipe are also known, either as a guess to a solution or as part of the constraints. Then, the volumetric flow rate can be calculated from the liquid and vapour mass fluxes as:

$$Q_g = \frac{W_g}{\rho_g} \quad and \quad Q_l = \frac{W_l}{\rho_l} \tag{2.1}$$

The superficial velocities are defined as the corresponding velocity for each phase flowing alone over the whole pipe cross sectional area:

$$V_{sg} = \frac{Q_g}{A} \quad and \quad V_{sl} = \frac{Q_l}{A} \tag{2.2}$$

The mixture velocity is defined as the sum of the gas and liquid superficial velocities:

$$V_m = V_{sg} + V_{sl} \tag{2.3}$$

The input liquid and gas phase volume fractions are defined as:

$$\lambda_l = \frac{Q_l}{(Q_l + Q_g)} = \frac{V_{sl}}{(V_{sl} + V_{sg})} \tag{2.4}$$

$$\lambda_g = \frac{Q_g}{(Q_l + Q_g)} = \frac{V_{sg}}{(V_{sl} + V_{sg})} \tag{2.5}$$

The sum of the gas and liquid volume fractions is equal to unity. As mentioned in Chapter 1, the slip between the phases causes what is known as holdup. Holdup is the in situ local liquid volume fraction. When phase slip occurs, holdup is larger than the input liquid phase volume fraction because the lighter gas phase travels at a faster velocity than the liquid phase. When stable flow conditions have been reached the liquid hold-up is a function of the momentum transfer between the fluids. Figure 2.1 helps to illustrate the definition of holdup:

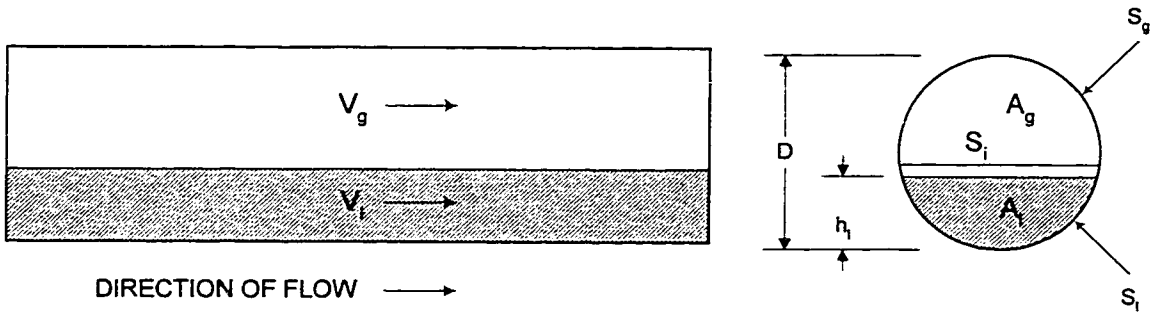

Figure 2.1 Simplified illustration of liquid holdup

The liquid occupies the area denoted as A_l of the total cross-section, whereas the gas occupies the remaining area A_G. The volume fractions measured under two-phase flow conditions are the liquid hold-up and gas volume fraction:

$$\alpha_l = \frac{A_l}{A} \tag{2.6}$$

$$\alpha_g = \frac{A_g}{A} \tag{2.7}$$

As in the case of input volume fractions the liquid holdup and the gas volume fraction also sum to unity. Due to the slip effect in horizontal and inclined pipe the liquid holdup α_l is larger than the input liquid volume fraction λ_l. The equality holds for the non-slip case or homogeneous flow conditions only, when the two phases are well mixed travelling at the same velocity ($\alpha_l = \lambda_l$). Actual or in situ phase velocities can be calculated when the liquid hold-up is known as a function of the superficial velocities as follows:

$$V_l = \frac{Q_l}{A_l} = \frac{V_{sl}}{\alpha_l} \tag{2.8}$$

$$V_g = \frac{Q_g}{A_g} = \frac{V_{sg}}{\alpha_g} \tag{2.9}$$

Note, that these velocities are larger than the corresponding superficial velocities.

2.2 Flow Regimes

During the concurrent travel of gas-liquid flow in pipes, a variety of flow regimes can exist depending on the flow rates, fluid properties and system parameters. The behaviour of the gas-liquid flow varies significantly from one flow regime to another. Consequently, an understanding of two-phase problem requires knowledge of the flow regime. The flow regime determination is also one of the most important aspects for developing two-phase flow models to predict liquid holdup and pressure drop. Classification of flow regimes is somewhat arbitrary and depends to a large extent on the interpretation of different researchers. Generally there is a gradual change of flow regimes with the flow rates rather than an abrupt change from one regime to another. Since flow regime determination is mostly done visually, there is an element of subjectivity involved in delineating the individual flow regimes.

As a result of this subjectivity, researchers have used a very large number of descriptions to characterise these flow regimes (Govier and Aziz (1972)). Hence, there is not a standard definition. Some of the regimes are alternative names for the same flow regime, while others are a subdivision of major groupings. Recently, however, there has been a realisation that the number of flow regimes used in any description should be limited.

In order to introduce the different flow regimes for vertical upward-flow and horizontal flow, a brief and simplified description of the major flow regimes is presented below.

2.2.1 Vertical Upflow

Four main regimes can be seen in vertical upflow, as illustrated in Figure 2.2. A simplified description of each flow regime will follow.

Bubbly Flow

There is a continuous upward liquid phase, with dispersed gas bubbles rising through the liquid continuum. The bubbles travel with a complex motion within the flow, without coalescing into slugs, and are generally of non-uniform size. The velocity of the bubbles exceeds that of the liquid due to buoyancy.

Slug Flow

This flow regime is often referred as slug flow in vertical systems. As the gas rate increases, bubbles coalesce into slugs, which occupy the bulk of the cross sectional area, forming characteristic bullet-shaped bubbles, called *Taylor bubbles* (Davies and Taylor 1950). The thin film of liquid that surrounds a bubble moves towards the bottoms of the slug. The liquid between Taylor bubbles often contains a dispersion of smaller bubbles. As the gas rate is increased, the length and velocity of the gas slugs increase. Slugs can occur in the downward direction, but are usually not initiated in that position.

Churn Flow

At higher gas velocities, the laminar liquid film is destroyed by gas turbulence, and the Taylor bubbles in slug flow break down into an unstable regime in which there is churning or oscillatory motion of liquid. The transition to annular flow is the point at which liquid separation between gas slugs disappears and the gas slugs coalesce into a continuous central core gas. Since Churn Flow has much more in common with slug flow, the two regimes are often lumped together and called slug flow. This flow occurs more predominantly in large diameter pipes and may not be so important in small diameter pipes where the region of churn flow is small.

Annular and Annular-Mist Flow

This configuration is characterised by liquid travelling as a film on the channel walls, and gas flowing through the centre. Part of the liquid can be carried as drops in the central gas core. This flow regime is similar to annular flow in horizontal pipe, except that the slip between phases is affected by gravity. In upflow, the annular liquid film is slowed down by gravity, which increases

the difference in velocities between gas and liquid (slip). In downflow, the reverse is true, with gravity speeding up the liquid reducing the difference in velocities between the phases. It is important to point out that the liquid film thickness is more uniform around the circumference of the pipe than in horizontal flow. At very high gas rates, the liquid is completely dispersed into the gas, eliminating the effects of orientation and direction of flow, and travelling as drops leading to the term *"mist flow"*. In the identification of vertical two-phase flow regimes, annular and mist flow are usually considered together and called *annular-mist* flow.

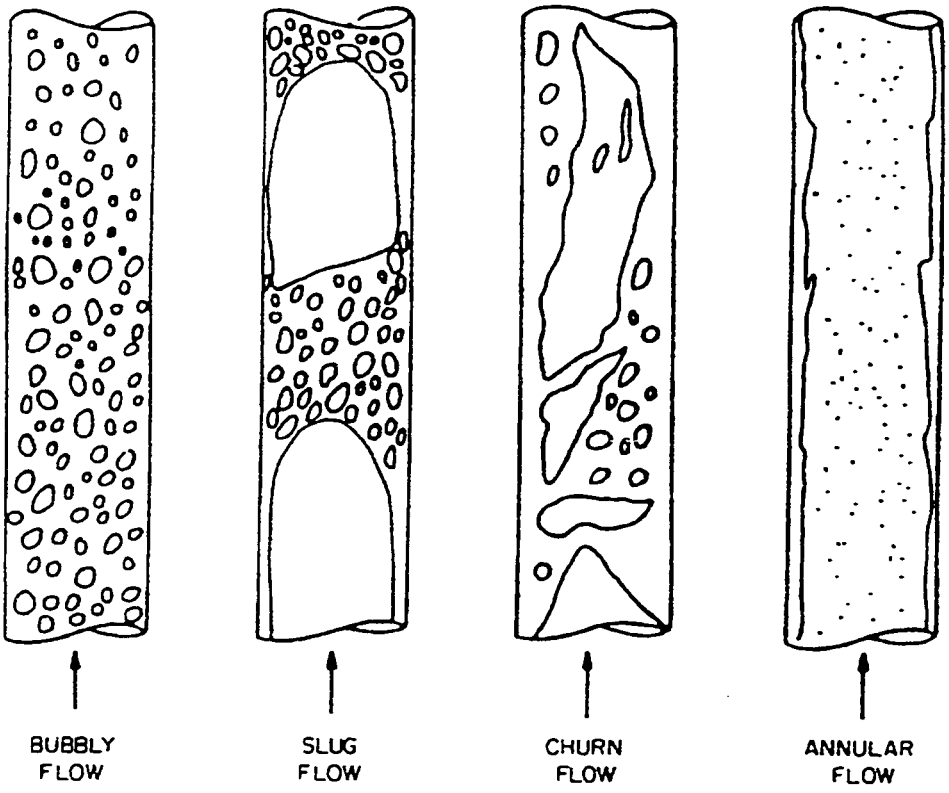

Figure 2.2 Vertical Flow Regimes

2.2.2 Horizontal Flow

When gravity acts perpendicular to the pipe axis, separation of the phases can occur. This increases the possible flow regimes that may exist in a piping system.

Dispersed Bubble Flow

Dispersed bubble flow like the equivalent pattern in vertical flow, consists of gas bubbles dispersed in a liquid continuum. However, gravity tends to make bubbles accumulate in the upper part of the pipe, except at very high velocities when the intensity of the turbulence is enough to disperse the bubbles about the cross section. Gas and liquid in situ velocities are approximately equal. In uphill flow, bubbles retain their identity over a wider range of conditions.

Stratified Flow

As the gas flow increases, the gas bubbles merge and become a continuous phase. In this flow regime, liquid flows in the lower part of the pipe with the gas above it. The interface between the phases is relatively smooth and the fraction occupied by each phase remains constant. In uphill flow, stratified flow rarely occurs and wavy flow is prevalent. In downhill flow, stratified flow is somewhat enhanced, as long as the inclination is not too steep.

Wavy Flow

As the gas rate increases even further, the gas moves appreciably faster than the liquid and the resulting shear at the interface forms liquid waves.

Slug Flow

When the gas rate reaches a certain critical value, the crests of the liquid waves touch the top of the pipe forming frothy slugs. This flow regime, like plug flow is intermittent. The gas bubbles are bigger, while the liquid slugs contain many smaller bubbles. When the slugs are highly aerated, the term, *"frothy surges"*, has been used in literature. Some researchers have used the term *"semi-slug"* to describe cases where the surges do not fill the pipe completely. However,

this might be more correctly considered as part of wavy flow.

Annular Flow

A continuous gas core with a wall film characterises this flow regime. As with the equivalent regime in vertical flow, liquid can be entrained as drops in the gas core. Gravity causes the film to be thicker on the bottom of the pipe but as the gas velocity is increased, the film becomes more uniform around the circumference.

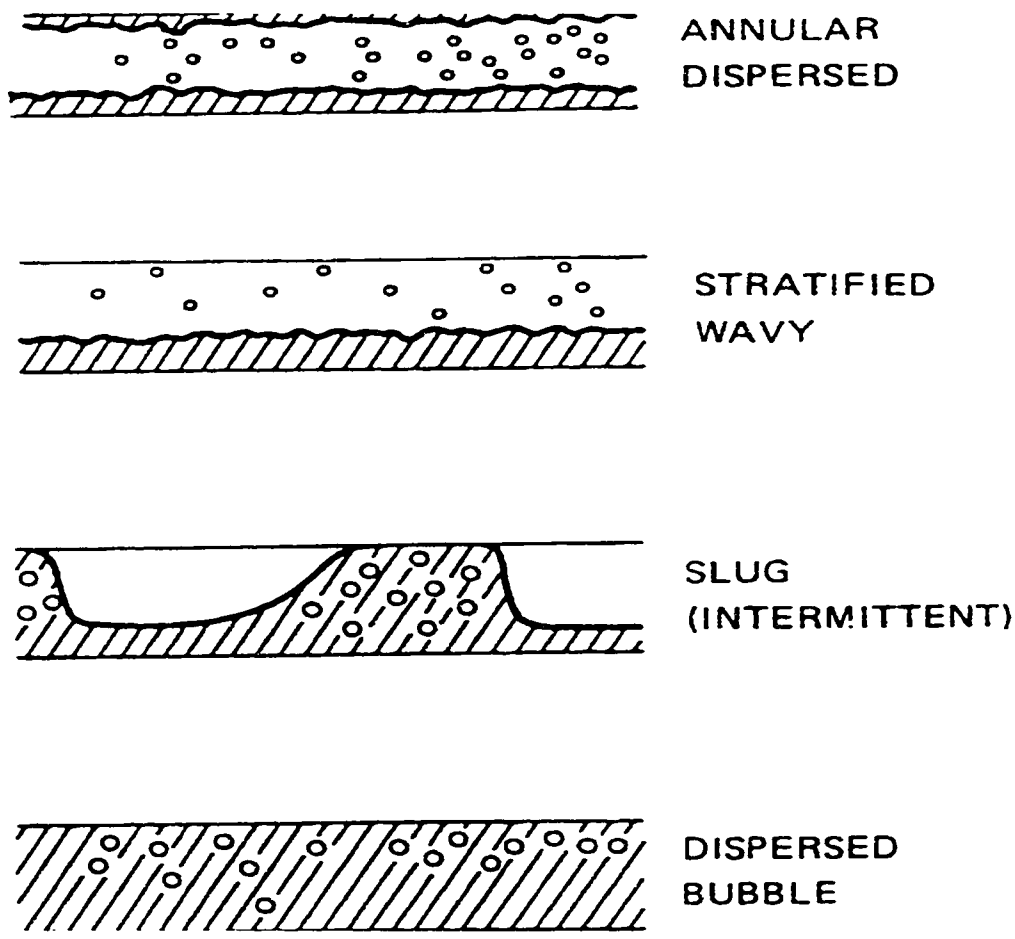

Figure 2.3 Horizontal Flow Regimes

2.3 Total Gradient Components

Consider two-phase steady state flowing through an inclined constant cross sectional area with a control volume defined by the two planes and the pipe wall as shown below:

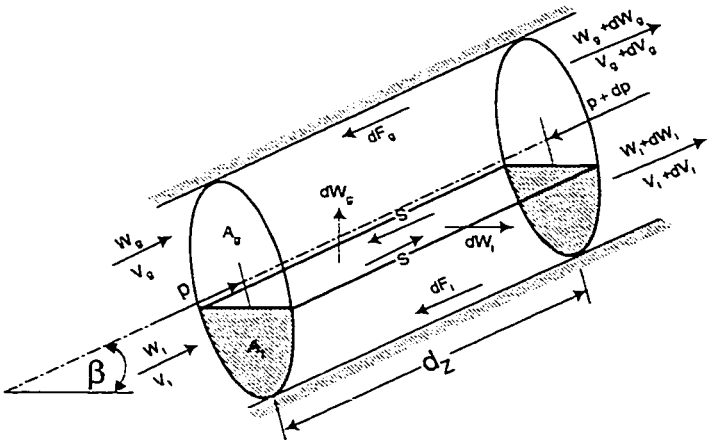

Figure 2.4 Integral Momentum Balances

The following momentum balance equations have been taken from Hetsroni (1982). A momentum balance taken around on a control volume of cross sectional A and infinitesimal thickness dx in the axial direction yields:

$$\frac{-dP}{dx} = \tau_{Wg}\frac{S_g}{A} + \tau_{Wl}\frac{S_l}{A} + \left(\alpha_g\rho_g + \alpha_l\rho_l\right)g\sin\beta + \frac{d}{dx}\left[\rho_g\frac{V_{sg}^2}{\alpha_g} + \rho_L\frac{V_{sl}^2}{\alpha_l}\right] \tag{2.10}$$

These equations express the total pressure gradient as the sum of three components due to friction, gravity and acceleration. The frictional component of the pressure drop is given by:

$$\frac{-dP}{dx} = \tau_{Wg}\frac{S_g}{A} + \tau_{Wl}\frac{S_l}{A} \tag{2.11}$$

This frictional component cannot be measured directly. It is inferred from measurements of total

pressure drop for a pipe segment and the calculated contributions of the gravity and acceleration gradients. Consequently, the resulting frictional component is subject not only to potential experimental errors, but also to the errors that are inevitably present in the estimated values of the gravitational and acceleration components.

The gravity pressure gradient or static head component is given by:

$$\frac{-dP}{dx} = \left(\alpha_g \rho_g + \alpha_l \rho_l\right) g \sin\beta \tag{2.12}$$

Note, that the holdup plays a very important role in this pressure gradient component. Thus, a good estimation of the holdup is essential for good results.

The acceleration pressure gradient component is given by:

$$\frac{-dP}{dx} = \frac{d}{dx}\left[\rho_g \frac{V_{sg}^2}{\alpha_g} + \rho_l \frac{V_{sl}^2}{\alpha_l}\right] \tag{2.13}$$

Actually, the above equation represents the changes in momentum flux in a pipe segment. To date, very few methods have been developed for predicting the changes in momentum flux in a pipe segment. As a rule, the acceleration component of the total pressure gradient is small relative to the frictional and static head components and is therefore, often neglected.

2.4 Modeling Techniques

There have been numerous correlations and methods for predicting frictional pressure drop, flow regime, and liquid holdup in gas-liquid flow systems. A few of them have attempted to consider the complex flow structure of two-phase systems from a more physically based approach. The techniques for analysing one-dimensional flows fall into several classes, which can be conveniently arranged, in ascending order of sophistication and depending on the amount of information required for their computation.

2.4.1 Homogeneous Models

Homogeneous flow theory provides the simplest technique for analysing two-phase flows. Suitable average properties are determined and the mixture is treated as a pseudo-fluid that obeys the usual equations of single-component flow. The average properties, which are required, are velocity, thermodynamic properties and transport properties. These pseudo properties are weighted averages and are not necessarily the same as the properties of either phase. The method of determining suitable properties is often to start with more complex equations and to rearrange them until they resemble equivalent equations for single-phase flow.

The assumptions upon which the homogeneous model is based on are:

- No slip, equal vapour and liquid velocities.
- No mass transfer between the phases, the attainment of thermodynamic equilibrium between the phases.
- The use of suitably defined pseudo-single phase friction factor for the two-phase flow pressure gradient.

2.4.2 Empirical Models

Correlation of experimental data in terms of chosen variables is a convenient way of obtaining design equations with a minimum of analytical work. The crudest correlations are mere mathematical exercises, readily performed with modern computers, while more advanced techniques use dimensional analysis or a grouping of several variables together on a logical basis. A virtue of correlations is that they can quickly yield excellent are easy to results. As long as they are applied to situations similar to those that were used to obtain the original data, they can be quite satisfactory, within statistical limits, which are usually known. Furthermore, since little insight into the basic phenomena is achieved by data correlation, no indication is given of ways in which performance can be improved or accuracy of prediction increased.

2.4.3 Drift-flux Model

As described by Wallis 1969, "the drift-flux model is essentially a separated-flow model in which attention is focused on the relative motion rather than on the motion of the individual phases". Although the theory can be developed in a general way, it is particularly useful if the relative motion is determined by a few key parameters and is independent of the flow rate of each phase. For example, in bubbly flow at low velocities in large vertical pipes, the relative motion between the bubbles and the liquid is governed by a balance between buoyancy and drag forces; that is, it is a function of the volume fraction but not of the flow rate. Drift-flux theory has prevalent application for the modelling of bubbly, dispersed bubble, and slug regimes in gas-liquid two-phase flow.

2.4.4 Separated-flow Model

In the separated-flow model the phases are assumed to flow side by side. Separate equations are written for each phase and the interaction between the phases is also considered. The separated flow model takes account of the fact that the two phases can have different properties and

different velocities. It may be developed with various degrees of complexity. In the most sophisticated version, separate equations of continuity, momentum, and energy are written for each phase and these equations are solved simultaneously, together with rate equations which describe how the phases interact with each other and with the walls of the pipe. In the simplest version, only one parameter, such as velocity, is allowed to differ for the two phases while conservation equations are only written for the combined flow. When the number of variables to be determined exceeds the available number of equations, correlations or simplifying assumptions are introduced. The assumptions upon which the separated flow model is based are:

- Slip between the phases.
- No mass transfer between the phases, the attainment of thermodynamic equilibrium between the phases.
- The use of simplified correlations or concepts to closure the holdup and pressure gradient equations to the independent variables of the flow.

2.5 Empirical Correlations

Since the earliest visual observation of two-phase flow, the relevancy of flow regimes in the modelling of liquid hold-up and pressure gradient has been recognised. Baker (1954) was one of the first to propose a flow regime map for horizontal flow. Baker (1961) also proposed that better predictions could be attained by developing pressure gradient correlations based on flow regime. After Baker's breakthrough, the development of overall correlations for the prediction of pressure drop and liquid hold-up, without regard to flow regime, decreased. Only correlations accompanied by a generalising principle were proposed, such as Dukler's (1964 and 1969) who used the concept of dynamic similarity to develop his overall correlation.

A large number of correlations have been published, since Baker's first correlation, for the prediction of pressure drop and liquid hold-up in two-phase flow. Most of this effort has been directed towards horizontal and vertical pipes. All of these correlations are subject to errors (sometimes very large) when applied to a particular case and considerable judgement is required

to interpret the results. It should be kept in mind that the practical application of most correlations generally requires large extrapolation from the experimental conditions. Usually air-water and or air-oil have been used as fluids in laboratory facilities. This has made scaling to high pressure gas-oil in large size pipes risky. An improvement in accuracy has been sometimes achieved by adapting the correlation on the basis of field data. This approach has exhibited a limitation of generality in application.

In spite of their shortcomings, empirical correlations have played a significant role in the development of two-phase flow theory, and there are still several empirical correlations in use by industry for the calculations of pressure loss and liquid hold-up. Govier and Aziz (1972), Gregory et al. (1980), and Brill and Beggs (1991) presented thorough reviews of the most prominent empirical correlations for flow regime map, holdup, and pressure gradient in both horizontal and vertical flow.

2.6 Flow Regime Transitions

Flow regime maps are usually generated by plotting visual observations obtained in laboratory apparatus. Because these maps depended wholly on the experiments, it has always been, the question of their applicability to field operating conditions. A more reliable approach can be obtained by developing an understanding of the physical mechanisms, which cause the flow regime transitions to take place. Then equations controlling these transitions can be developed and use to predict these transitions. Thus, physically realistic models can be obtained which incorporate the effects of flow rates, physical properties, pipe size, and pipe inclination angle. This approach is known as *mechanistic modelling.* As a consequence, it lacks the simplicity and "quick answer" features of the flow regime maps. However, with the present ready access to computing facilities, model complexity is of little importance compared to the insight into how various parameters affect the flow regime, the predicted pressure drop and gas/liquid holdup.

2.6.1 Horizontal Flow Regime Transitions

The model proposed by Taitel and Dukler (1976) is undoubtedly the most significant contribution in many years to the solution of the complex problem of flow regime prediction. They considered the conditions necessary for horizontal and slightly inclined flow regimes to exist and postulated mechanisms by which the transitions between the various flow regimes might occur. They then modelled these transitions based almost entirely on theoretical considerations that attempted to account for the effects of such parameters as pipe diameter, gas and liquid phase properties, and pipeline inclination in a systematic and semi-theoretical way.

Stratified to non Stratified Transition

Based on the model of Taitel and Dukler (1976) the mechanisms of flow regime transitions can be explained as follows. At low gas rates and low to moderate liquid rates, stratified flow can be observed. As the gas rate is increased, the formation of large waves takes place. At still higher gas rates these waves grow rapidly. Eventually, these waves grow large enough to create a bridge that blocks the pipe completely. The blocked gas flow pushes the plug forward. This causes the liquid plug to sweep up the liquid in front of it. Thus, a slug or plug is formed, and the transition to intermittent flow takes place.

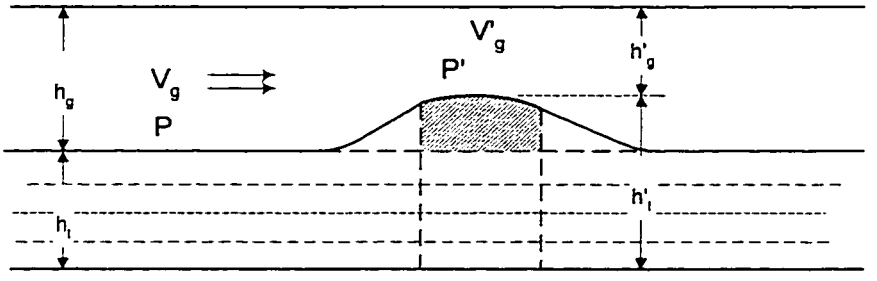

Figure 2.5 Instability for a solitary wave

Consider a wave moving on the stratified flow conditions as shown in Figure 2.5. As the faster gas moves across the top of the wave, its velocity increases from V_g to V'_g and the pressure decreases from P to P' due to the Bernoulli effect. Consider now the small piece of wave shown as crosshatched. The decreased pressure above the wave creates a force to make the wave grow. However, the force of gravity tends to pull the fluid back into the stratified liquid. A balance of forces is created that causes the wave to grow, when the pressure force exceeds the gravity force. When this happens, there will either be a transition to slug flow if the liquid level is high enough, or the liquid will wrap around the wall of the pipe because the gas flow over the waves causes the liquid to move sideways. Then annular flow will be observed. Based on the Kelvin-Helmholtz stability theory, Taitel and Dukler (1976) proposed a criterion for transition from stratified to intermittent flow regime given by:

$$Fr \geq \left[\frac{\left(1-\bar{h}_l\right)^2 \cdot \bar{A}_g}{\bar{V}_g^{\,2} \cdot \sqrt{1-\left(2\bar{h}_l-1\right)^2}} \right]^{1/2} \tag{2.14}$$

where Fr is the Froude number given by:

$$Fr = \left[\frac{\rho_g}{\rho_l - \rho_g} \right]^{1/2} \frac{V_{sg}}{\sqrt{Dg\cos(\beta)}} \tag{2.15}$$

The variables in Equation (2.14) are the dimensionless gas superficial velocity, V_{sg} and the dimensionless liquid level, $\bar{h}_l$. The basis for this criterion is that a critical gas velocity is required to create waves big enough to bridge the pipe. The condition for equilibrium stratified flow, as shown in Figure 2.6, is based on the two fluid theory. By performing a momentum balance on each phase Taitel and Dukler (1976) obtained:

$$-A_l \frac{dP}{dx} - \tau_l S_l + \tau_i S_i - \rho_l A_l g \sin(\beta) = 0 \tag{2.16}$$

$$-A_g \frac{dP}{dx} - \tau_g S_g - \tau_i S_i - \rho_g A_g g \sin(\beta) = 0 \tag{2.17}$$

where τ_l, τ_g, and τ_i are the liquid , gas and interfacial stresses respectively. S_l and S_g are the tube perimeters in contact with the liquid and the gas phases, respectively while S_i is the interfacial perimeter. Eliminating the pressure gradient dP/dx from Equations (2.16) and (2.17) results in Equation (2.18):

$$\tau_g \frac{S_g}{A_g} - \tau_l \frac{S_l}{A_l} + \tau_i S_i \left[\frac{1}{A_l} + \frac{1}{A_g}\right] - (\rho_l - \rho_g) g \sin(\beta) = 0 \tag{2.18}$$

Taitel and Dukler (1976) are evaluated the shear stresses as follow:

$$\tau_l = \frac{f_l \rho_l V_l}{2} \tag{2.19}$$

$$\tau_g = \frac{f_g \rho_g V_g}{2} \tag{2.20}$$

$$\tau_i = \frac{f_i \rho_i V_i}{2} \tag{2.21}$$

where V_l and V_g are the in situ velocities and f_l and f_g, the friction factors, are functions of liquid and gas Reynolds numbers.

$$\mathrm{Re}_l = \frac{D_l V_l \rho_l}{\mu_l} \tag{2.22}$$

$$\mathrm{Re}_g = \frac{D_g V_g \rho_g}{\mu_g} \tag{2.23}$$

The equivalent diameters D_l and D_g for the liquid and gas phases are defined as:

$$D_l = \frac{4 \cdot A_l}{S_l} \tag{2.24}$$

$$D_g = \frac{4 \cdot A_g}{S_g + S_i} \tag{2.25}$$

The friction factors need to be calculated by a correlation that accounts for the effects of pipe roughness and should cover the full range of Reynolds number, laminar through turbulent. The correlation developed by Churchill (1977) fulfils these requirements. This correlation provides the Moody's version of the friction factor as follows:

$$f = 8\left[\left(\frac{8}{\mathrm{Re}}\right)^{12} + \frac{1}{(A+B)^{1.5}}\right]^{1/12} \tag{2.26}$$

where A and B are defined as:

$$A = -2.457 \ln\left[\left(\frac{7}{\mathrm{Re}}\right)^{0.9} + 0.27\left(\frac{\varepsilon}{D}\right)\right]^{16} \tag{2.27}$$

$$B = \left(\frac{37350}{\mathrm{Re}}\right)^{16} \tag{2.28}$$

where Re is the Reynolds number and ε is the absolute pipe roughness.

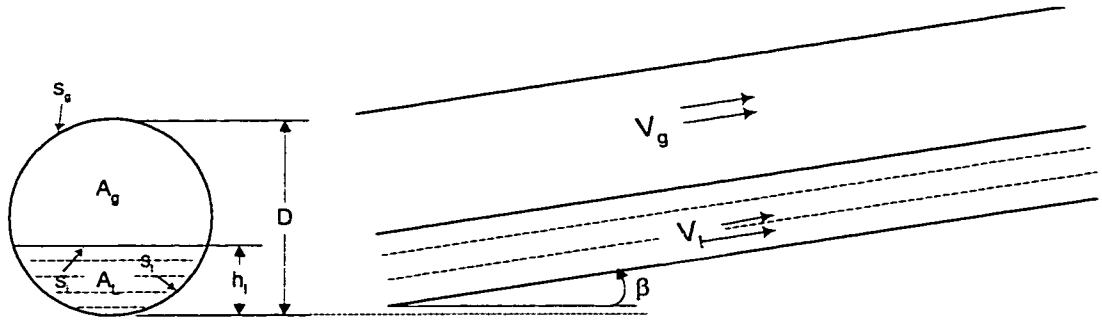

Figure 2.6 Equilibrium Stratified Flow

Taitel and Dukler (1976) introduced the concept of dimensionless variables by using the reference quantities: D for length, D^2 for area, V_{sl} and V_{sg} for the liquid and gas velocities. Denoting the dimensionless variables by ($\tilde{}$), Equation (2.18) becomes:

$$X^2 \frac{f_l \tilde{V}_l^2 \tilde{S}_l}{f_{sl} \tilde{A}_l} - \frac{f_g \tilde{V}_g^2 \tilde{S}_g}{f_{sg} \tilde{A}_g} + \frac{f_i}{f_{sg}} \tilde{V}_{sg}^2 \left[\frac{\tilde{S}_i}{\tilde{A}_l} + \frac{\tilde{S}_i}{\tilde{A}_g} \right] - 4Y = 0 \tag{2.29}$$

where X is the Lockhart-Martinelli parameter:

$$X^2 = \frac{\frac{4 f_{sl} V_{sl}^2}{2D}}{\frac{4 f_{sg} V_{sg}^2}{2D}} = \frac{\left(\frac{dP}{dx}\right)_{sl}}{\left(\frac{dP}{dx}\right)_{sg}} \tag{2.30}$$

and Y is the dimensionless inclination parameter:

$$Y = \frac{(\rho_l - \rho_g) g \sin(\beta)}{\left(\frac{dP}{dx}\right)_{sg}} \tag{2.31}$$

The parameter X can be easily calculated from the liquid and gas flow rates, fluid properties and pipe diameter. The parameter Y represents the relative forces acting on the liquid due to gravity

and pressure drop. In the above equations f_{sl} and f_{sg} are the single phase liquid and gas friction factors based on the superficial velocities. Taitel and Dukler (1976) approach the frictional friction factors by calculating them by using the correlation for smooth pipe of the Blasius form ($f = a\ (Re)^{b}$). For the interfacial friction factor Taitel and Dukler (1976) used $f_i = f_g$. For flow regime transition calculations Oliemans (1987) and Xiao et al (1990) used a constant value of 0.0142 for f_i. The different approaches adopted by different authors to evaluate the interfacial friction factor will be discussed later in Section 2.71.

All dimensionless quantities are function of $\bar{h}_l = h_l/D$ as follows:

$$\bar{A}_l = 0.25\left[\pi - \cos^{-1}\left(2\bar{h}_l - 1\right) + \left(2\bar{h}_l - 1\right)\sqrt{1-\left(2\bar{h}_l - 1\right)^2}\right] \tag{2.32}$$

$$\bar{A}_g = 0.25\left[\cos^{-1}\left(2\bar{h}_l - 1\right) - \left(2\bar{h}_l - 1\right)\sqrt{1-\left(2\bar{h}_l - 1\right)^2}\right] \tag{2.33}$$

$$\bar{S}_l = \pi - \cos^{-1}\left(2\bar{h}_l - 1\right) \tag{2.34}$$

$$\bar{S}_g = \cos^{-1}\left(2\bar{h}_l - 1\right) \tag{2.35}$$

$$\bar{S}_i = \sqrt{1-\left(2\bar{h}_l - 1\right)^2} \tag{2.36}$$

$$\bar{V}_l = \frac{\bar{A}}{\bar{A}_l} \tag{2.37}$$

$$\bar{V}_g = \frac{\bar{A}}{\bar{A}_g} \tag{2.38}$$

The occurrence of non-stratified flow can now be established. First determining the liquid level $\bar{h}_l$ from X and Y, then comparing the critical gas Froude number from Equation (2.14) with the actual gas Froude number from Equation (2.15).

All the above stability analyses are performed on the equilibrium stratified flow solution. As pointed by Barnea (1987), the solution for the steady state liquid level is not unique. Actually

multiple solutions may occur for some operating conditions in upward inclined flow. This can be observed on Figure 2.7. In this case the existence of multiple holdup values for stable stratified flow becomes a reasonable situation. Barnea and Taitel (1992) studied the existence of two possible physical solutions in the region of stratified flow. By using "structural stability analysis" they found that multiple solutions occur for upwards inclined stratified flow, at low liquid flow rates and narrow ranges of gas flow rates. When these multiple solutions occur, there are three solutions for the liquid level. The thinnest solution is always stable, the middle solution is always linearly structurally unstable and the thickest solution is almost always structurally and Kelvin-Helmholtz unstable, making it a physically impossible. Therefore, in the case of multiple solutions they concluded that the thinnest solution is physically possible, while the others are mathematical artifacts.

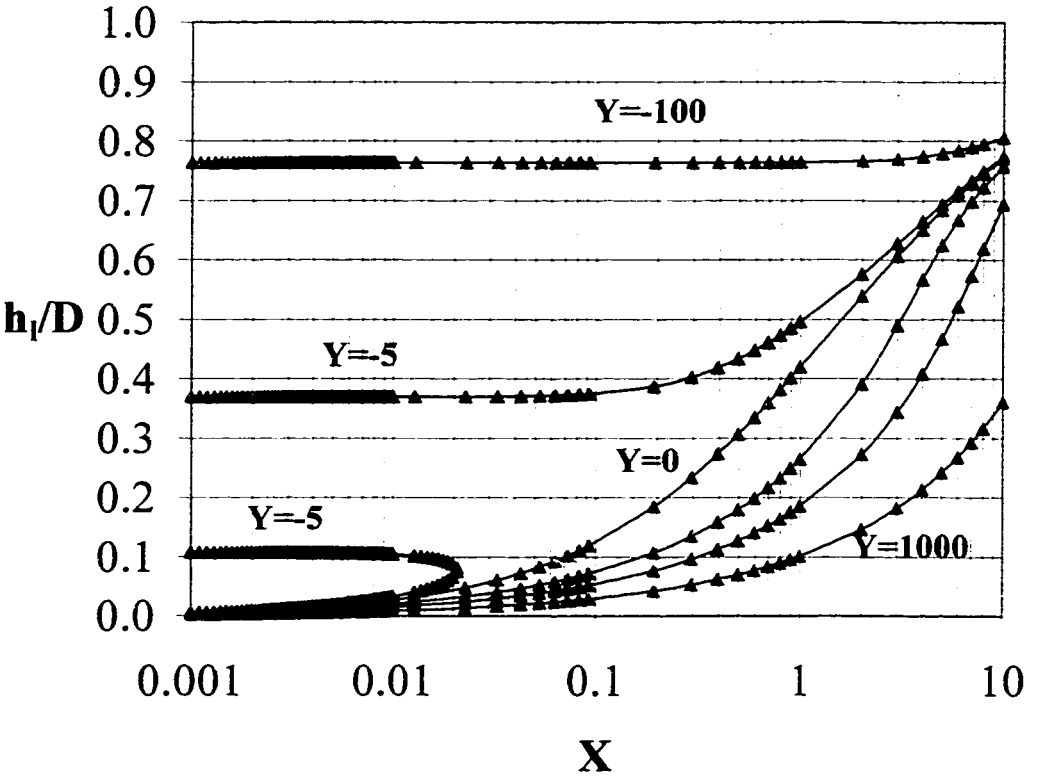

Figure 2.7 Equilibrium liquid level in Stratified Flow

For steeply downward inclined pipes, the liquid level in stratified flow is small and the liquid velocity is high. Under these conditions droplets are torn from the wavy liquid surface and deposited on the upper wall, causing a transition to non-stratified flow. Barnea et al. (1982) and Dukler-Taitel (1986) modelled this transition by considering the trajectory of droplets after they leave the interface at an initial velocity which is assumed to be the turbulent fluctuating velocity. If the height of the trajectory exceeds the distance to the upper wall, a transition to non-stratified flow occurs. This transition rule is:

$$N_L \geq \sqrt{\frac{(1-\bar{h}_l)}{\frac{f_l}{f_{sl}}}}\alpha_l \tag{2.39}$$

where N_L is the dimensionless liquid velocity defined as:

$$N_L^2 = \frac{f_{sl}F_L}{\cos(\beta)} \tag{2.40}$$

Annular to Intermittent Transition

Transition to annular flow may occur when the stratified to non-stratified test, Equation (2.14), indicates that the flow regime is non-stratified and as a result of pipe bridging by the liquid in the film when this holds enough holdup to block the passage to the gas core, Taitel and Dukler (1976) suggested that for liquid holdup values < 0.5, annular flow will develop. They inferred this transition limit based on the physical mechanism for slug flow formation. If the interface is considered a sinusoid, when the holdup > 0.5 the crest of a wave reaches the top of the pipe before the trough reaches the bottom, the wave then, blocks the gas passage and slugging results. Thus for holdup values below 0.5 annular flow exist. The above concept was developed for horizontal and near-horizontal pipes. Barnea et al. (1982) modified this criterion to account for gas holdup in the liquid slug adjacent to the transition. The revised transition criteria as proposed

by Barnea (1982) is given by:

$$\overline{h_l} \leq 0.35 \tag{2.41}$$

Intermittent to Dispersed Bubble Transition

At moderate gas and liquid rates, slug or plug flow is observed. As the liquid rate is increased, a transition to dispersed bubble flow is observed. Before this takes place, the level of the liquid film which separates each pair of slugs increases. This transition to dispersed bubble flow takes place when the turbulent fluctuations are strong enough to overcome the buoyancy forces tending to keep the gas at the top of the pipe, assuming that neither stratified nor annular flow can exist. The increased liquid rate generates forces which tend to break up the gas space above the liquid film. For horizontal and slightly inclined pipe at an angle smaller than 10 °, Taitel and Dukler (1976) suggested that the transition from intermittent to dispersed bubbles flow regime takes place when the turbulence in the liquid phase overcome the buoyancy forces leading to the following transition rule:

$$T^2 \geq \frac{2\pi \alpha_l^2 \alpha_g D}{\left(\frac{f_l}{f_{sl}}\right) S_l} \tag{2.42}$$

where T is the ratio of the turbulent to buoyancy forces, defined as :

$$T^2 = \frac{\left(\frac{dP}{dx}\right)_{sl}}{(\rho_l - \rho_g) g \cos(\beta)} \tag{2.43}$$

The liquid holdup and the liquid friction factor in Equation (2.42) are evaluated from the solution of stratified flow model.

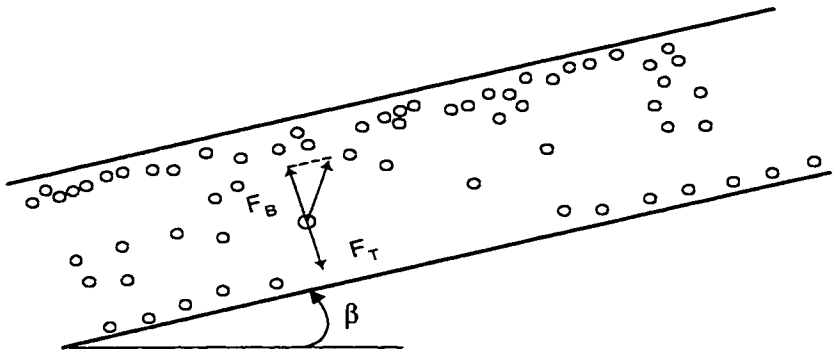

Figure 2.8 Equilibrium of forces in Bubble Flow

Barnea (1986) introduced a different approach, which is based on fully dispersed bubble flow as shown in Figure 2.8. Two dominant forces act on the bubble: a buoyant force which tends to lift the bubble to the upper part of the pipe and a turbulent force which tends to disperse it in the liquid. It is assumed that these two forces are approximately equal for the transition from intermittent to dispersed bubble. Barnea estimated the turbulent forces acting on the bubble from Levich (1962):

$$F_T = \frac{1}{2}\rho_l \bar{v}^2 \frac{\pi d_b^2}{4} \tag{2.44}$$

where $\bar{v}$ is the radial velocity fluctuations which can be estimated using the friction velocity u^*:

$$\bar{v}^{1/2} = u^* = vl\sqrt{\frac{f_l}{2}} \tag{2.45}$$

where f_l is the liquid phase friction factor. The buoyant forces acting on the bubble are:

$$F_B = (\rho_l - \rho_g) g \cos(\beta) \frac{\pi d_b^3}{6} \tag{2.46}$$

At the transition:

$$F_T \geq F_B \tag{2.47}$$

by substituting equations (2.44), (2.45) and (2.46) into (2.77) yields:

$$v_l \geq \left[\frac{8(\rho_l - \rho_g)g\cos(\beta)d_b}{3\rho_l f_l}\right]^{1/2} \tag{2.48}$$

Davison and Schuler (1960) developed a simple equation for the stable bubble diameter, d_b, as:

$$\frac{\pi d_b^3}{6} = 1.378\left(\frac{\pi D^2 V_{sg}}{4}\right)^{1.2} g^{-3/5} \tag{2.49}$$

This correlation was developed for low viscosity liquids and bubble formation in a stagnant pool of liquid. By substituting Equations (2.49), with $v_l = V_{sl}/\alpha_l$ and g = 9.81 m/s^2 into Equation (2.48) the transition criteria becomes:

$$V_{Sl} \geq 4.56\,\alpha_l\left[\frac{(\rho_l - \rho_g)\cos(\beta)D^{0.8}V_{sg}^{0.4}}{\rho_l f_l}\right]^{1/2} \tag{2.50}$$

Stratified Smooth to Stratified Wavy Transition

When a liquid film flows with a smooth surface, there exists a certain rate at which energy is dissipated due to viscosity of the liquid. Additional energy is needed to generate and sustain a steady wavy motion, even if waves do not grow. This energy can be provided by pressure and shear forces from the gas phase. These waves will be maintained if the energy transferred from the gas to the liquid exceeds the additional energy dissipated by the waves themselves. When in

stratified flow the gas velocity is sufficiently high, but not too high to cause a transition to non-stratified flow, interface waves will form. Waves will be initiated when pressure and shear work on a wave overcome viscous dissipation in the waves. Although the phenomenon of wave generation is not completely understood, Taitel and Dukler (1976) proposed the following criterion for the transition from smooth to wavy flow:

$$V_g \geq \left[\frac{4\mu_l (\rho_l - \rho_g)\cos(\beta)}{s\,\rho_l \rho_g V_l} \right]^{1/2} \tag{2.51}$$

which in dimensionless form can be expressed as:

$$K \geq \frac{2}{\bar{V}_g \sqrt{\bar{V}_l\, s}} \tag{2.52}$$

where s is the sheltering coefficient, with a value of 0.01 as suggested by the authors. K is the product of the modified Froude number and the square root of the Reynolds number of the liquid phase:

$$K^2 = \left[\frac{\rho_g V_{sg}^2}{(\rho_l - \rho_g) D\, g \cos(\beta)} \right] \left[\frac{\rho_l D V_{sl}}{\mu_l} \right] \tag{2.53}$$

Since the right hand side of Equation (2.51) depends only on the liquid level of stratified flow, $\bar{h}_l$, the critical value for K can be calculated from the stratified flow solution.

2.6.2 Vertical Flow Regime Transitions

Taitel et al. (1980) presented the fundamentals for mechanistic modelling of flow regime transitions for upward two-phase flow. They identified four distinct flow regimes and formulated the transition boundaries for them. The four flow regimes are bubble, slug, churn and annular flow regimes. Later, modifications to the transition mechanisms have been made to extend these mechanisms to inclined angles as well. Barnea (1986) combined the transition mechanism for different inclination angles into one unified model with the aim of constructing a general method independent of the angle of inclination. As a result of all this work, the flow regime can be determined through the transition mechanisms for bubble, slug, churn and annular flow.

Bubbly-Slug Transition

At low flow rates of liquid and gas, a dynamic equilibrium between coalescence and breakup of bubbles determines whether the flow pattern will be bubbly or slug flow. Once agglomeration and coalescence of small bubbles take place to a significant degree, large Taylor bubbles are formed and a transition from bubbly flow into slug flow occurs. As has been shown this largely depends on the volume fraction of the gas. The volume fraction of the gas, (gas holdup) is the fraction of the cross-sectional area of the pipe occupied by gas. When this volume fraction is larger than 0.25, the bubbles are very closely packed and a transition from bubbly to slug flow takes place. The equation relating the liquid and gas superficial velocities, V_{sl} and V_{sg} at which the transition from Bubbly to Slug flow regime takes place is:

$$V_{sl} = 3 \cdot V_{sg} - 1.15 \cdot \left[\frac{g(\rho_l - \rho_g)\sigma}{\rho_l^{\,2}} \right]^{1/4} \tag{2.54}$$

The quantity in square brackets depends only on physical properties. Once these are fixed, the transition boundary can be defined. Barnea et al. (1986) introduced inclination dependency to

the above transition in the following way:

$$V_{sl} = 3 \cdot V_{sg} - 1.15 \cdot \left[\frac{g(\rho_l - \rho_g)\sigma}{\rho_l^2} \right]^{1/4} \sin(\beta) \tag{2.55}$$

In small pipe sizes, this transition does not exist, because for these small pipes the rise velocity of the small deformable bubbles is much larger than that for Taylor bubbles. As a result, the small bubbles tend to overtake or catch up with the occasional Taylor bubble and combine with it. These small deformable bubbles are formed when the surface tension forces overcome the turbulent forces as observed by Hinze (1955). This tends to create the condition of slug flow by a different mechanism. Taitel et al. (1980) suggested that bubbly flow could not exist when pipe and, bubble diameters are smaller than the following critical diameter D_c.

$$D_c = 19.0 \cdot \left[\frac{(\rho_l - \rho_g)\sigma}{\rho_l^2 \cdot g} \right]^{1/4} \tag{2.56}$$

Barnea et al. (1985) also proposed another condition for bubbly flow to exist. There is a minimum angle of inclination for which bubbly flow cannot exist. This is due to bubble migration to the top wall of the pipe, which occurs when the radial component of the buoyancy forces surpasses the lift forces. This critical angle is given by:

$$\frac{\cos(\beta)}{\sin^2(\beta)} = 0.75 \cos(45^\circ) \frac{U_o^2}{g} \cdot \left[\frac{C_L \gamma^2}{d} \right] \tag{2.57}$$

where U_o is the bubble rise velocity, for which Harmathy (1960) proposed the following:

$$U_o = 1.53 \left[\frac{g(\rho_l - \rho_g)\sigma}{\rho_l^2} \right]^{1/4} \tag{2.58}$$

In Equation (2.57) C_L is the lift coefficient that can range from 0.4 to 1.2, γ is the distortion coefficient of the bubble, ranging from 1.1.to 1.5, and d is the bubble size, normally between 4 to 10 mm. Tests and theory have shown that β fluctuates between 55° to 70° (Barnea .et al. 1985).

Finely-Dispersed Bubble Transition

At high liquid flow rates, turbulent forces act to break and disperse the gas phase into small bubbles. These forces are greater than the surface tension forces tending to prevent breakup. Defining these forces and equating them result in this equation that specifies the values of V_{sl} and V_{sg} at along this transition. This transition was originally given by Taitel et al. (1980) and modified by Barnea et al. (1982) to account for coalescence resulting in:

$$\left[\frac{0.4\sigma}{g(\rho_l-\rho_g)}\right]^{0.5}\left[\frac{\rho_l}{\sigma}\right]^{0.6}\left[\frac{0.092\cdot\nu_L^{0.2}}{D^{1.2}}\right]^{0.4}\left(V_{sl}-V_{sg}\right)^{1.12}=1.49-8.52\left[\frac{V_{sg}}{V_{sl}+V_{sg}}\right]^{0.5} \qquad (2.59)$$

Equation (2.59) is valid for a gas volume fraction less than 0.52. For larger pipes, where $D > D_c$, bubbly flow exists at low liquid rates. When V_{sl} exceeds the transition V_{sl} as given by Equation (2.59), the nature of the bubbles changes. They are smaller, and they move essentially rectilinearly upward. This is a subtle and not easily observed transition, although it can have a large effect on heat and mass transfer Barnea et al. (1982).

In small pipes, slug flow exists at low gas rates rather than bubbly flow, as discussed above. Then, as the liquid rate is increased so that V_{sl} exceeds the transition V_{sl} as given by Equation (2.59), a transition is observed from slug to bubbly flow, finely dispersed bubbles are formed in the region where V_{sl} exceeds the transition V_{sl} as given by Equation (2.59). Now as the gas rate is increased, the volume fraction of gas increases and the bubbles become more closely packed. But it is impossible to pack spherical bubbles more closely than $\alpha = 0.52$ (maximum void for a rectangular packing array). At this point there must be coalescence even in the presence of very high turbulence levels. Thus, for liquid and as flow rates where $\alpha > 0.52$, dispersed bubbly flow

can no longer exist. This condition is given by:

$$V_{sl} = 0.92 \cdot V_{sg} - 0.5 \cdot \left[\frac{g(\rho_l - \rho_g)\sigma}{\rho_l^2} \right]^{1/4} \tag{2.60}$$

The second term of Equation (2.59), which accounts for slippage between the phases, is usually less than three percent of V_{sl} and therefore can be neglected. By doing so, the assumption of homogeneous flow with no slippage can be assumed.

Slug-Churn Transition

Barnea (1982) considered Churn flow as an entrance phenomenon leading to slug flow downstream. In the region of the entrance, short slug and Taylor bubbles are created and these tend to move at different velocities. Successive Taylor bubbles overtake one another, and with each merger, the bubble doubles in length and the liquid dumps to the slug below. This gives rise to the chaotic appearance characteristic of churn flow.

As the bubbles and slugs get larger, further down the pipe, their velocity becomes more uniform and fewer overtakings take place. Eventually, sufficiently far downstream, the merging stops, and a stable slug length and slug frequency are observed. According to Barnea (1982) the length necessary for stable slugs to be established can be estimated by calculating the time for successive bubbles to overtake until a stable bubble length is reached. This time multiplied by the velocity of the Taylor bubble gives the developing or entry length, l_e. Barnea (1982) defined this transition as:

$$\frac{l_e}{D} = 42.6 \left[\frac{V_{sl} + V_{sg}}{\sqrt{gD}} + 0.28 \right] \tag{2.61}$$

Once the tube length and diameter is specified, l_e/D can be set. Then the relationship between V_{sl}

and V_{sl} can be calculated from Equation (2.59). Thus, there are a series of curves defining the transition for different values of l_e/D. The transition between slug and churn flow can be found at any position along the tube by using the distance from the entry to the point of observation.

Transition to Annular Flow

For high gas flow rates, the flow regime becomes annular. The liquid flows upward in the form of a wavy film along the wall with droplets entrained in the gas core. It is suggested that annular flow cannot exist unless the gas velocity in the gas core is sufficient to lift the largest entrained liquid droplets. When the gas rate is insufficient, the droplets fall back, accumulate, form a bridge, and churn or slug flow will take place. Based on this mechanism, the condition for annular flow is given by:

$$V_{sg} = 3.1\left[\frac{g\sigma(\rho_l - \rho_g)\sin(\beta)}{\rho_g^2}\right]^{1/4} \tag{2.62}$$

When V_{sg} exceeds V_{sg} given by Equation (2.61) annular flow exists.

Barnea (1986) proposed two mechanisms for gas core blockage during annular flow leading to intermittent flow:

1. blockage due to partial downflow of liquid near the wall (liquid film instability),
2. blockage due to large supply of liquid in the film (liquid film bridging).

Barnea (1986) obtained the condition for the instability of the liquid film (mechanism 1) from the simultaneous solution of the following equations expressed in dimensionless form:

$$Y = \frac{1+75\alpha_l}{(1-\alpha_l)^{2.5}\alpha_l} - \frac{1}{\alpha_l^3}X^2 \tag{2.63}$$

and

$$Y = \frac{2 - 1.5\alpha_l}{(1 - 1.5\alpha_l)^{2.5}\alpha_l^3} X^2 \tag{2.64}$$

where X and Y are defined as in Equations (2.30) and (2.31), respectively. Equation (2.63) gives the solution for the liquid holdup in annular flow and Equation (2.64) gives the liquid holdup at the boundary of film instability. The transition boundaries can be plotted as a function of the dimensionless parameters X and Y, Figure 2.9. The locus for transition (1) is depicted by line (a) and obtained by simultaneous solution of Equations (2.63) and (2.64) as mentioned earlier. According to Barnea (1986) liquid film bridging occurs when the conditions for slugging are satisfied. Barnea suggested that the slugging transition is as follows:

$$\frac{A_L}{A\,R_{sm}} = \frac{\alpha_L}{R_{sm}} \geq 0.5 \tag{2.65}$$

where A is the pipe cross sectional area and R_{sm} is the minimum liquid holdup in the resulting liquid bridge that will ensure blockage of the gas passage. This minimum value is related to the maximum packing of bubbles in the liquid slug (R_s = 0.48). At lower values of R_s slugging cannot occur due to the high gas volume fraction. By replacing the value of α_l with $0.5R_{sm}$ (α_l=0.24) in Equation (2.63) yields the transition for liquid film bridging. As shown in Figure 2.9 the locus for this transition is depicted by line (b).

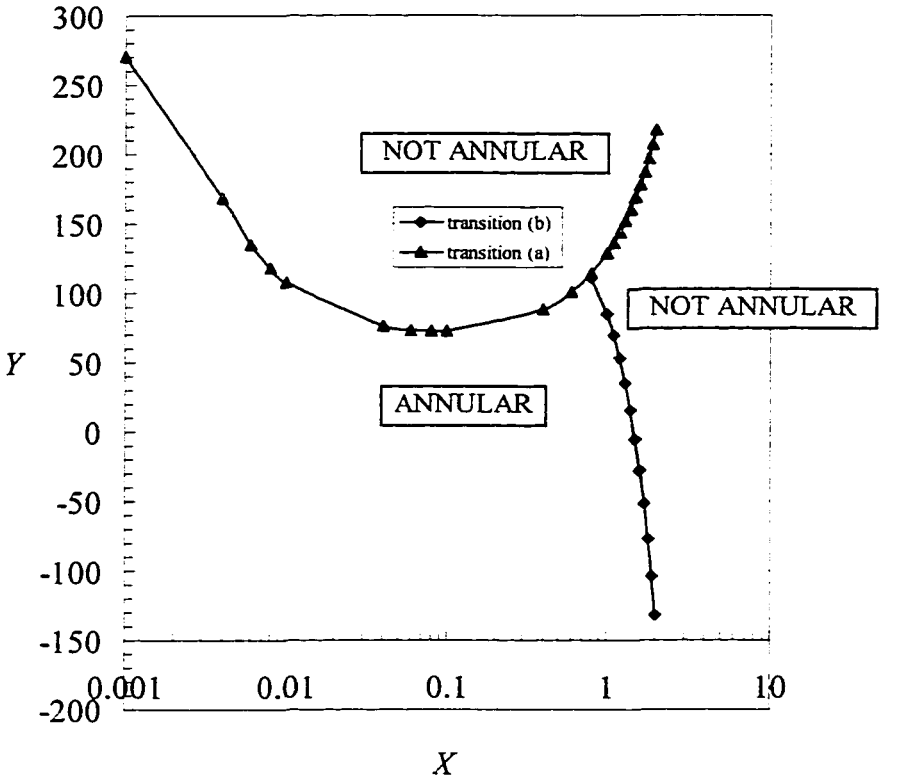

Figure 2.9 Generalized map for Annular-Intermittent Transition

Mandhane et al. (1974) developed a flow regime map for horizontal flow using the gas and liquid superficial velocities as coordinates. This is the best empirical map for air-water systems in laboratory scale, but does account for pipe sizes or inclination angle variations. Taitel and Dukler (1976) found excellent agreement between the Mandhane map and their flow regime transition mechanism expressed in the same coordinates system. The Design Institute for Multiphase Flow, (DIMP), found as a result of a study sponsored by the American Institute of Chemical Engineers, (AIChE), that the best flow regime maps where those based on physical modelling of the transition mechanisms (Dukler and Taitel (1982) and (1984)).

2.7 Mechanistic Liquid-holdup and Pressure Gradient Models

2.7.1 Horizontal Stratified Flow

The mechanistic description of holdup and pressure loss predictions for stratified flow can be obtained from the two-fluid approach developed by Taitel-Dukler (1976) and modified by Oliemans (1987). By using a simplified one dimensional approach and assuming steady state, isothermal flow without mass transfer between the fluids, Taitel-Dukler (1976) obtained individual momentum equations for the liquid and gas phases. These two momentum equations result in two equations with two unknowns, the liquid holdup and the pressure gradient. To solve these equations a number of constitutive empirical correlations have to be introduced.

The momentum balance on each phase yields equations for the two fluids as shown in Equation (2.16) and (2.17) earlier:

$$-A_l \frac{dP}{dx} - \tau_l S_l + \tau_i S_i - \rho_l A_l g \sin(\beta) = 0 \tag{2.66}$$

$$-A_g \frac{dP}{dx} - \tau_g S_g - \tau_i S_i - \rho_g A_g g \sin(\beta) = 0 \tag{2.67}$$

The variables in Equation (2.66) and (2.67) were defined and described earlier in Section 2.61. It was shown also, that by eliminating the pressure gradient from (2.66) and (2.67) gives what was shown before as Equation (2.18):

$$\tau_g \frac{S_g}{A_g} - \tau_l \frac{S_l}{A_l} + \tau_i S_i \left[\frac{1}{A_l} + \frac{1}{A_g} \right] - (\rho_l - \rho_g) g \sin(\beta) = 0 \tag{2.68}$$

where τ_l, τ_g, and τ_i are the liquid, gas and interfacial stresses, respectively. In these equations S_l, S_g and S_i are the perimeters for gas against the pipe wall, liquid against the pipe wall and for the interface. The shear stresses, τ_l, τ_g, and τ_i are the liquid, and gas and interfacial stresses, respectively, shown earlier as Equations (2.19), (2.20) and (2.21). In these Equations f_l and f_g, are the Fanning friction factor which are evaluated using the actual average velocities and hydraulic diameters. For the interfacial shear stress an additional complication is the determination of the interfacial velocity V_i and the interfacial roughness ε_i.

Note that all the variables mentioned depend on the height of the liquid layer h_l, hence on the liquid holdup α_l as depicted in Figure 2.10.

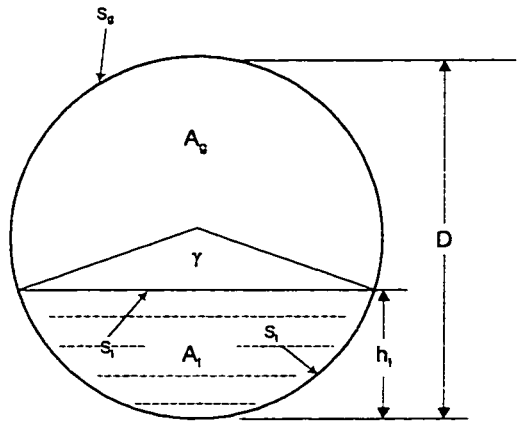

Figure 2.10 Inclined Stratified Flow

For stratified flow, the liquid holdup α_l and the perimeters are related to the top angle γ, shown in Figure 2.10 and defined as:

$$\alpha_l = \frac{\gamma - \sin(\gamma)}{2\pi} \tag{2.69}$$

The depth h_l is a function of the angle γ as described by the following relationship:

$$\gamma = 2\cos^{-1}\left(1 - \frac{2h_l}{D}\right) \tag{2.70}$$

It is convenient to rewrite the equation for the liquid holdup given by Equation (2.68) in the dimensionless form defined by Taitel and Dukler (1976) and presented earlier as Equation (2.29) as follows:

$$X^2 \frac{f_l \overline{V}_l^2 \overline{S}_l}{f_{sl} \overline{A}_l} - \frac{f_g \overline{V}_g^2 \overline{S}_g}{f_{sg} \overline{A}_g} + \frac{f_i}{f_{sg}} \overline{V}_r^2 \left[\frac{\overline{S}_i}{\overline{A}_l} + \frac{\overline{S}_i}{\overline{A}_g}\right] - 4Y = 0 \tag{2.71}$$

Here $V_r=V_g - V_l$ is the relative velocity that measures the difference between the gas velocity, V_g and the interfacial velocity V_i. The dimensionless parameters were described earlier by Equation (2.32) to (2.38) with the exception of $\bar{V}_r$ which is defined as $\bar{V}_r = V_r/V_{sg}$. In Equation (2.71) the dimensionless liquid height $\bar{h_l} = h_l/D$ can be determined as a function of the Lockhart and Martinelli parameters X and the gravity parameter Y. The liquid hold-up then follows from:

$$\alpha_l = \frac{1}{\pi}\left[\cos^{-1}\left(1-2\bar{h}_l\right) - \left(1-2\bar{h}_l\right)\bar{S}_l\right] \tag{2.72}$$

where:

$$\bar{S}_l = \sqrt{1-\left(1-2\bar{h}_l\right)^2} \tag{2.73}$$

In order to solve the stratified flow equations for liquid holdup a method for the calculation of the liquid interface velocity, V_i, the interfacial friction factor, f_i, and to compute the interfacial shear, τ_i, are require. For the interfacial friction factor, f_i ,a number of correlations have been published. Taitel and Dukler use $f_i = f_g$ in their stratified flow model, while Shoham and Taitel (1984) in their study on stratified turbulent-turbulent gas-liquid flow in horizontal and inclined pipes proposed a constant value $f_i = 0.0142$, corresponding to a fully developed rough interface due to the presence of small waves as reported by Cohen and Hanratty (1968).

In the Oliemans (1987) model the interfacial friction factor f_i is calculated in the same manner as the friction factor for gas and liquid and a relative roughness ε_i/D_g. Consequently, determination of the friction factor requires knowledge of the effective roughness of the gas-liquid interface ε_i. Oliemans (1987) used the Cohen and Hanratty (1968) relationship for the equivalent sand grain roughness of the gas-liquid interface (ε_i) with the root-mean-square wave height (Δh) described by:

$$\varepsilon_i = 3\sqrt{2}\,\Delta h \tag{2.74}$$

Laboratory measurements on air/water channel flow provide the wave data to determine the interfacial roughness. For values of Δh larger than the height of the liquid layer h_l, ε_i is calculated by using h_l instead of Δh as follows:

$$\varepsilon_i = \begin{cases} 3\sqrt{2}\,\Delta h \;\; for\;\; \Delta h < h_l \\ 3\sqrt{2}\,h_l \;\; for\;\; \Delta h \geq h_l \end{cases} \tag{2.75}$$

Oliemans (1986) used the value of highly turbulent liquid flow for the liquid interface velocity $V_i = V_l$. For all methods, the pressure gradient is computed by eliminating the interfacial shear from Equations (2.66) and (2.67) resulting in:

$$\frac{-dP}{dx} = \frac{\tau_l S_l + \tau_g S_g}{A} + \left[\frac{A_l \rho_l}{A} + \frac{A_g \rho_g}{A}\right] g\,\sin(\beta) \tag{2.76}$$

Note, that this equation includes the frictional and gravitational pressure gradients, the acceleration and term has been omitted assuming that is negligeable.

2.7.2 Horizontal Annular Flow

One of the most significant developments in annular flow modelling for horizontal flow has been the work of Xiao et al. (1990). They extended the two-fluid approach to a fully developed steady state annular flow model. They assumed a uniform film thickness around the pipe, and the gas core was assumed to behave as a homogeneous fluid, no slip between the phases within the core. In a similar procedure to that for stratified flow, by using a simplified model they determined liquid holdup from the parameters X and Y as shown in Figure 2.11, Oliemans et al. (1986). Here, the two fluids are the liquid film and the gas core, which includes the gas and the entrained liquid droplets. Figure 2.12 shows the geometry of annular flow in a horizontal and inclined pipe. A momentum balances on the liquid film and the gas core yields:

$$-A_f \frac{dP}{dx} - \tau_f S_f + \tau_i S_i - \rho_l A_f \, g\sin(\beta) = 0 \tag{2.77}$$

$$-A_c \frac{dP}{dx} - \tau_i S_i - \rho_c A_c \, g\sin(\beta) = 0 \tag{2.78}$$

Where τ_f and τ_i are the liquid film, gas core and interfacial stresses, respectively defined as:

$$\tau_f = \frac{f_f \rho_l V_f^2}{2} \tag{2.79}$$

$$\tau_i = \frac{f_i \rho_c \left(V_c - V_f\right)^2}{2} \tag{2.80}$$

A_f and A_c are the cross sectional areas occupied by the liquid and gas, respectively, S_f, and S_i are the perimeters for liquid against the pipe wall and for the interface ρ_f and ρ_c are the liquid film and gas core densities.

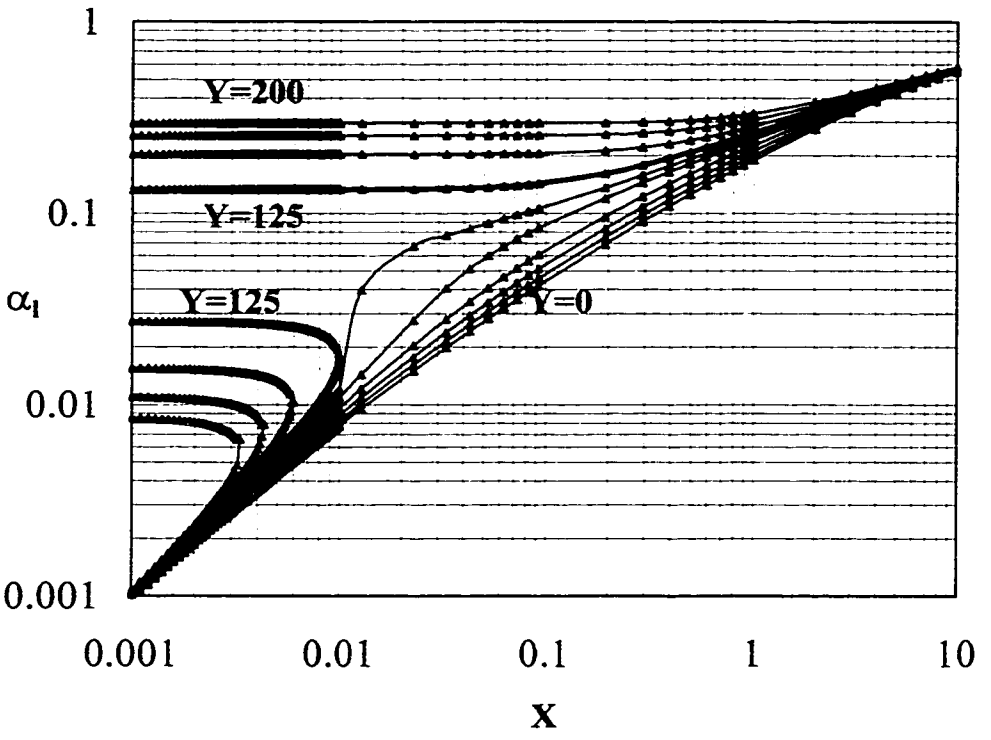

Figure 2.11 Liquid holdup for Inclined Annular Flow

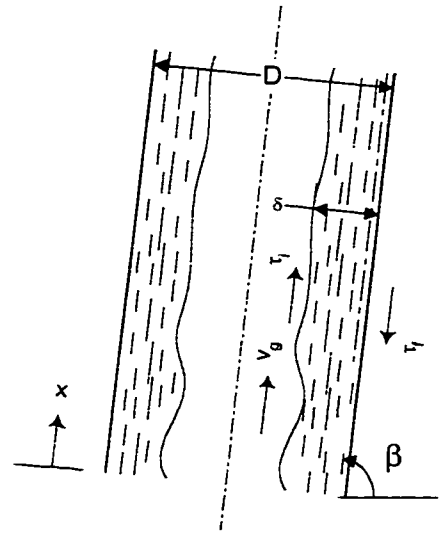

Figure 2.12 Geometry for Inclined Annular Flow Model

As in the stratified flow model eliminating the pressure gradient from each momentum balance equations yields the combined momentum, balance equation:

$$\tau_i S_i \left[\frac{1}{A_f} + \frac{1}{A_c}\right] - (\rho_l - \rho_c) g \sin(\beta) - \tau_f \frac{S_f}{A_f} = 0 \tag{2.81}$$

Similarly to the stratified flow case, all the geometric parameters in Equation (2.81) can be expressed as a function of the dimensionless average film thickness δ/D, Barnea (1986):

$$\left.\begin{aligned} S_f = \pi D, \quad S_i = \pi(D - 2\delta) \\ A_f = \pi(D\delta - \delta^2) \quad \text{and} \quad A_c = \pi\left(\frac{D}{2} - \delta\right)^2 \end{aligned}\right\} \tag{2.82}$$

Although Xiao et al. (1990) did not present these relationships, they did show an expression for the liquid holdup as a function of the dimensionless average film thickness δ/D:

$$\alpha_l = 1 - \left(1 - 2\frac{\delta}{D}\right)\left[\frac{V_{sg}}{V_{sg} + V_{sl}FE}\right] \tag{2.83}$$

where FE is the fraction of liquid entrainment.

To complete the annular flow model, closure relationships for the interfacial friction factor and the liquid entrainment fraction are needed. Xiao et al. used the liquid entrainment correlation proposed by Oliemans et al. (1986) for vertical flow, since only few correlations have been developed from experimental data for horizontal annular flow. This correlations is as follows:

$$\frac{FE}{1-FE} = 10^{\beta 0}\rho_l^{\beta 1}\rho_g^{\beta 2}\mu_l^{\beta 3}\mu_g^{\beta 4}\sigma^{\beta 5}D^{\beta 6}V_{sl}^{\beta 7}V_{sg}^{\beta 8}g^{\beta 9} \tag{2.84}$$

where the β exponents are regression coefficients, which were regressed by Oliemans et al (1986) such as to make the left hand side of Equation (2.116) dimensionless. The above correlation was not based on any physical model, yet it was the empirical correlation that best fitted the Harwell databank for annular dispersed flow experiments. Table 2.1 in Section 2.7.5 shows the regressed values for the β exponents.

Similarly to stratified flow, Xiao et al. calculated the core friction factor f_c and the interface friction factor f_f from the Colebrook (1939) correlation for Reynolds number and relative pipe roughness. The hydraulic diameters are a function of the film thickness as follows:

$$\left.\begin{aligned} D_l &= \frac{4\delta(D-\delta)}{D} \\ D_c &= D - 2\delta \end{aligned}\right\} \tag{2.85}$$

The core density ρ_c and the core viscosity μ_c are function of the core liquid holdup as follows:

$$\rho_c = \alpha_c \rho_l + (1-\alpha_c)\rho_g \tag{2.86}$$

$$\mu_c = \alpha_c \mu_l + (1-\alpha_c)\mu_g \tag{2.87}$$

where the core liquid holdup is given by:

$$\alpha_c = \frac{V_{sl} \cdot FE}{V_{sg} + V_{sl} \cdot FE} \tag{2.88}$$

The liquid film velocity V_f and the gas core velocity V_c were calculated by Xiao et al. by performing an overall liquid volumetric flow rate balance for the film, and the core which lead to the following relationship for their respective velocities:

$$V_f = \frac{V_{sl} \cdot (1-FE)}{4\frac{\delta}{D}\left[1-\frac{\delta}{D}\right]} \tag{2.89}$$

$$V_c = \frac{V_{sg} + V_{sl} \cdot FE}{\left[1-\frac{2\delta}{D}\right]^2} \tag{2.90}$$

The expression for the pressure gradient was obtained by combining Equations (2.77) and (2.78) yielding:

$$\frac{-dP}{dx} = \tau_f \frac{S_l}{A} + \left[\frac{A_f \rho_l}{A} + \frac{A_c \rho_c}{A}\right] g \sin(\beta) \tag{2.91}$$

The total pressure gradient is the summation of the frictional pressure gradient and the gravitational pressure gradient. As in stratified flow the acceleration pressure gradient is neglected.

Hewitt & Hall-Taylor (1970) summarized early studies for annular flow. The classical treatment for annular flow uses the triangular relationship between the film flow rate, the film thickness, and the pressure gradient. This treatment ignores the variations of the film thickness, and the deposition-entrainment rates. These phenomena are important for horizontal and inclined annular flow. Unlike the vertical flow case, the liquid film thickness in the horizontal and inclined configurations is not uniform, but is usually thicker at the bottom than at the top of the pipe. Therefore, two-dimensional models have been proposed to incorporate these mechanisms by James et al. (1987) and Laurinat et al. (1985). However, in these models, complex mathematical formulations are involved, and lengthy numerical methods are often required for this solution. Manabe et al. (1997) developed a new model that accounts for the non-uniformity of the liquid film around the pipe that is an extension of the Xiao et al. (1990) model, where the physical representation of the film liquid distribution assumes a rectangular cross-sectional area as illustrated by Figure 2.13.

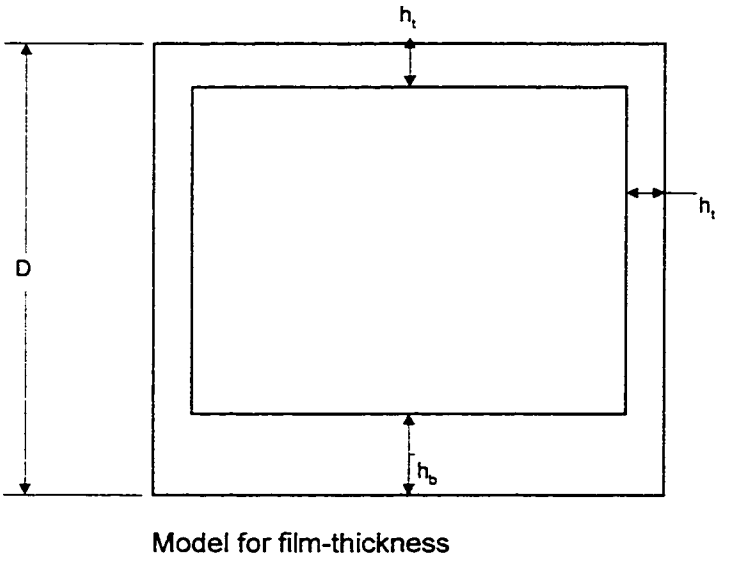

Figure 2.13 Manabe's Model for Film Thickness Distribution

They derived the following relationship between the film thickness distribution and the liquid holdup:

$$\alpha_L = \frac{3h_{ft}}{D} + \frac{h_{fb}}{D} \tag{2.92}$$

By introducing the dimensionless number N in Equation (2.92) and rearranging they obtained the following relationship between the two film thickness:

$$\left(\frac{h_{ft}}{D}\right)^3 - N\left[\frac{h_{fb}}{D} - \frac{h_{ft}}{D}\right] = 0 \tag{2.93}$$

where N is given by:

$$N = \frac{4.22\rho_c\mu_l^2 V_{sg}}{g\sigma\rho_l(\rho_l - \rho_g)D^2\cos(\beta)} \tag{2.94}$$

They determined the average liquid holdup in the same manner shown earlier for Xiao et al. They solved Equation (2.93) for h_{ft} and h_{fb} once the average liquid holdup was determined. They calculated the wall-liquid stresses using Xiao's definitions for liquid film velocity V_f, the gas core velocity V_c, interfacial friction factor f_i, and liquid entrainment fraction. The frictional factors were computed by using a Balsius type correlation. The film thickness distribution was accounted by Manabe's model in their expression for the pressure gradient:

$$-\frac{dP}{dx} = \left(\tau_{lb}\frac{S_l}{4A} + \tau_{lt}\frac{3S_l}{4A}\right) + \left(\frac{A_f\rho_L}{4A} + \frac{A_c\rho_c}{4A}\right)g\sin(\beta) = 0 \tag{2.95}$$

In Manabe's expression for the pressure gradient the gravitational term is not unit consistent. Thus Equation (2.95) has been corrected by adding the required area, A, term.

2.7.3 Horizontal Slug Flow

Dukler and Hubbard (1975) presented the first mechanistic model to predict liquid holdup and pressure drop for slug flow in horizontal pipes. A shortcoming of the model is that it requires the values of slug frequency and liquid holdup in the slug which are difficult to estimate. Nicholson et al. (1978) modified the model by suggesting the use of empirical correlations for the slug holdup and the slug length. In an attempt to close the model equations, Taitel and Dukler (1977) introduced a method for predicting the slug frequency. Based on the concept of boundary layer relaxation, Maron et al. (1982) developed a simple model for slug flow in horizontal pipes.

Recently, Taitel and Barnea (1990) presented a general approach to determine the hydrodynamics of the liquid film of a slug unit using a very detailed one-dimensional flow model. The disadvantage of this general approach is the requirement for numerical integration. They also tested a model with uniform liquid level in the film zone, which surprisingly gave good results. Xiao et al. (1990) proposed a simplified version of the Taitel and Barnea (1990) model. They assumed uniform liquid level in the film zone and a fully developed slug flow with no entrance or exit losses.

Figure 2.14 shows the slug geometry, which consists of two parts. The bubble has a separated flow configuration, with a liquid film at the bottom of the pipe for near-horizontal flow and completely surrounding it for near-vertical flow. The liquid cylinder contains gas bubbles and has a dispersed bubble flow configuration. Model-wise it is a hybrid system of the two model types already treated; two fluid modelling of the separated flow part and drift flux modelling of the dispersed flow part. The slug propagates at the translational velocity V_t, which can be obtained from the Bediksen (1984) correlation:

$$V_t = C_o V_m + 0.35\sqrt{gD}\sin(\beta) + 0.54\sqrt{gD}\cos(\beta) \tag{2.96}$$

Where the value of C_o depends on the liquid velocity profile in the slug body, ranging from C_o = 1.2 for turbulent flow and C_o = 2 is for laminar flow. The velocity of dispersed bubbles in the slug body is given by:

$$V_b = 1.2V_m + 1.53\left[\frac{g(\rho_l - \rho_g)\sigma}{\rho_l^2}\right]^{1/4} \alpha_L^{0.1} \sin(\beta) \tag{2.97}$$

According to Ansari (1988) $\alpha_l^{0.1}$ is included to account for the effect of "*bubble swarm*" in the slug body. Xiao et al (1990) used the correlation developed by Gregory et al. (1978) for liquid holdup in the slug body:

$$\alpha_s = \frac{1}{1 + \left(\frac{V_s}{8.66}\right)^{1.39}} \tag{2.98}$$

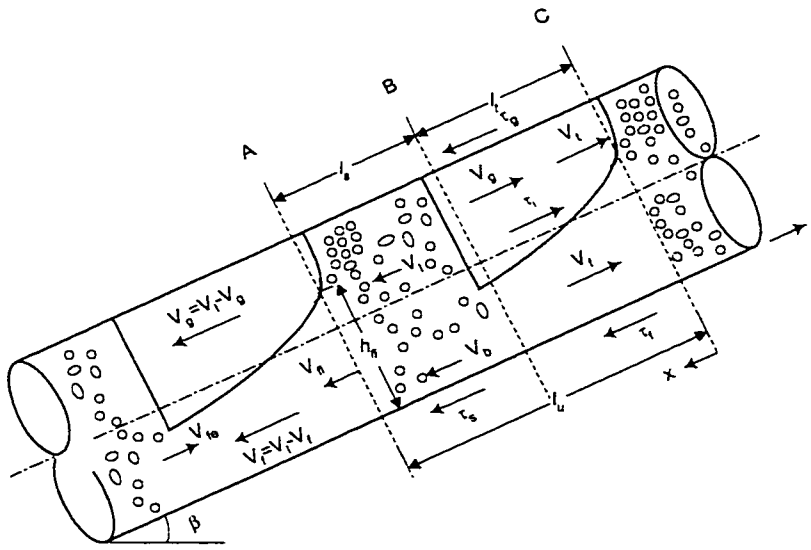

Figure 2.14 Geometry for Inclined Slug Flow Model

For slug length they used the correlation developed by Scott (1987), which is valid for D < 0.0381m:

$$\ln(l_s) = -26.6 + 28.5(\ln(D) + 3.67)^{0.1} \tag{2.99}$$

If $D > 0.0381$ m, l_s is assumed to be $30D$.

Because a uniform liquid level was assumed along the film zone, a combined momentum balance similar to stratified flow can be obtained for the film zone:

$$\tau_f \frac{S_f}{A_f} - \tau_g \left[\frac{S_g}{A_g} + \frac{\tau_i}{\tau_g} \left(\frac{S_i}{A_f} + \frac{S_i}{A_g} \right) \right] + (\rho_l - \rho_g) g \sin(\beta) = 0 \tag{2.100}$$

The average pressure gradient for slug flow was calculated by using a force balance over a slug unit:

$$\frac{-dP}{dx} = \frac{1}{l_u} \left[\frac{\tau_s S_l l_s}{A} + \left(\frac{\tau_f S_l + \tau_f S_g}{A} \right) l_f \right] + \rho_u g \sin(\beta) \tag{2.101}$$

Where ρ_u is the average fluid density of a slug unit:

$$\rho_u = \alpha_l \rho_l + (1 - \alpha_l) \rho_g \tag{2.102}$$

The shear stresses for the film and the gas are analogous to those of stratified flow. The frictional factors are functions of the film and gas velocities, which are calculated from material balances performed over the film and slug units. Xiao et al. (1990) used a constant value of 0.0142 for the interfacial friction factor. The slug shear stress is a function of the mixture velocity and the mixture properties calculated from the slug liquid holdup α_s.

The average liquid holdup for the slug unit was defined as:

$$\alpha_l = \frac{\alpha_s \cdot V_t + V_b(1-\alpha_s) - V_{sg}}{V_t} \tag{2.103}$$

2.7.4 Horizontal Dispersed Bubble and Bubble Flow

The homogeneous flow approach is commonly used for modelling dispersed bubble flow. For bubble flow, the drift-flux model, which account for the slip between the phases, is used. Wallis (1969) covered in detail drift flux mechanism in his book. Xiao et al. (1990) used a homogeneous pseudo single-phase model with average properties to describe bubble flow. Their non-slip homogeneous liquid holdup uses the liquid input phase volume fraction as given earlier in Equation (2.4):

$$\alpha_l = \frac{V_{sl}}{V_{sg} + V_{sl}} \tag{2.104}$$

Their equation for the pressure gradient as pseudo single-phase fluid is:

$$-\frac{dP}{dx} = \frac{f_m \rho_m V_m^2}{2 \cdot D} + \rho_m \cdot g \sin(\beta) = 0 \tag{2.105}$$

where:

$$V_m = V_{sg} + V_{sl} \tag{2.106}$$

$$\rho_m = \alpha_L \rho_l + (1-\alpha_L)\rho_g \tag{2.107}$$

$$\mu_m = \alpha_L \mu_l + (1-\alpha_L)\mu_g \tag{2.108}$$

The friction factor f_m is calculated using the mixture Reynolds number and the relative roughness. In the drift-flux version for dispersed bubble flow the actual gas velocity is supposed to represent the centre-line velocity in the pipe which, in the case of turbulent flow, is assumed to be 25%

greater than the mixture velocity V_m. Moreover, the gas bubbles experience a bubble rise velocity V_b due to their buoyancy, which is calculated by the Harmathy (1960) correlation shown earlier as U_o in Equation (2.58):

$$V_b = 1.53\left[\frac{g(\rho_l - \rho_g)\sigma}{\rho_l^2}\right]^{1/4} \tag{2.109}$$

Once the actual gas velocity is known, the gas hold-up can be obtained from its definition as:

$$\alpha_l = \frac{V_{sg}}{V_g} \tag{2.110}$$

Once the liquid holdup has been determined, it is possible to compute the contribution to the pressure gradient from gravity and acceleration in the same manner as for the homogeneous model, by using the mixture properties. However, these properties are estimated using the in situ liquid holdup from Equation (2.110).

2.7.5 Vertical Annular Flow

Oliemans et al. (1986) carried out a comprehensive study on the reliability of the prediction of liquid holdup, liquid entrainment and pressure gradient by annular flow models based on the two-fluid approach. They proposed a new two-fluid model and introduced correlations for the liquid holdup, interfacial friction factor and entrainment liquid fraction. They tested these correlations with the Harwell databank.

Their two fluid model was based on the geometry for annular flow similar to the one shown for incline annular flow in Figure 2.12. They based their model on typical assumptions valid for two-

fluid modelling. Such as one-dimensional, steady-state, concurrent upward flow, no mass transfer between the phases, and uniform circumferential liquid film distribution. They also assumed no-slip between the liquid entrained in the gas core and the gas.

Their version of momentum balances around the pipe core and the whole-pipe results in:

$$-A\frac{dP}{dx}-\tau_f S_f-\left(\alpha_f\rho_l-\alpha_c\rho_c\right)A\,g\sin(\beta)=0 \tag{2.111}$$

$$-A_c\frac{dP}{dx}-\tau_i S_i-\rho_c A_c\,g\sin(\beta)=0 \tag{2.112}$$

By eliminating *dP/dx*, the following relationship is obtained:

$$\tau_f\frac{S_f}{A}-\tau_i\frac{S_i}{A_c}+\alpha_f\left(\rho_l-\rho_c\right)g\sin(\beta)=0 \tag{2.113}$$

Where τ_f, and τ_i are the liquid film and interfacial stresses, respectively. Note, that this equation is a function of the liquid holdup α_f. The parameters A and A_c are the whole pipe and gas core cross sectional areas. S_f and S_i are the perimeters for liquid against the pipe wall and for the interface, and ρ_f and ρ_c are the liquid film and gas core densities. The definition of these parameters is equivalent to those presented for the horizontal annular model in Section 2.7.2.

The shear stresses occurring in these equations are defined as follows:

$$\tau_f=\frac{f_f\rho_l V_f^2}{2} \tag{2.114}$$

$$\tau_i=\frac{f_i\rho_c\left(V_c-V_i\right)^2}{2} \tag{2.115}$$

The above equations can be solved as long as closure relationships are available. A similar

procedure to the one carried for stratified flow arrives at an expression for the liquid holdup as a function of the Lockhart-Martinelli parameter X, and the dimensionless gravity parameter Y as follows:

$$Y = \frac{1+75\alpha_l}{(1-\alpha_l)^{2.5}\alpha_l} - \frac{1}{\alpha_l^{3}} X^2 \tag{2.116}$$

This equation assumes no liquid entrainment and a smooth pipe wall. The definition of the parameters X, and Y used by Oliemans et al. differs slightly from previous definitions for the dimensionless gravity parameter Y:

$$X^2 = \frac{\frac{4 f_{sl} V_{sl}^2}{2D}}{\frac{4 f_{sg} V_{sg}^2}{2D}} = \frac{\left(\frac{dP}{dx}\right)_{sl}}{\left(\frac{dP}{dx}\right)_{sg}} \tag{2.117}$$

$$Y = \frac{(\rho_l - \rho_g) g D \sin(\beta)}{2 f_{sg} V_{sg}^2} \tag{2.118}$$

The interfacial friction factor used by Oliemans et al. was based on the Wallis (1969) expression for rough or wavy annular flow:

$$f_i = f_{sg}(1+80\alpha_l) \tag{2.119}$$

The interface velocity required for the evaluation of the interfacial shear stress comes from an analysis of velocity profiles for laminar and turbulent single-phase flow:

$$h_f^+ \le 30 \quad \Rightarrow \quad V_i^+ = \frac{\tanh(0.074 h_f^+)}{0.074} \tag{2.120}$$

$$h_f^+ > 30 \quad \Rightarrow \quad V_i^+ = 2.44\ln\left(h_f^+\right) + 4.9 \tag{2.121}$$

where $V_i^+ = V_i / V_f^*$ and $h_f^- = \rho_l V_f^* h_f / \mu_l$. The wall friction velocity is given by $V_f^* = V_f(f/2)^{0.5}$.

They correlated the interfacial roughness factor in a similar manner to, the Cohen and Hanratty (1968) relationship for the equivalent sand grain roughness of the gas-liquid interface (ε_i) with the root-mean-square wave height (Δh) described by Equation (2.74). They used the average film thickness instead in a relationship such as:

$$\varepsilon_i = C h_f \tag{2.122}$$

They correlated the constant C against the Weber number We, and found the following relationship fitted best the Harvell data bank:

$$C = \frac{30}{We} \tag{2.123}$$

Where the Weber number is defined as:

$$We = \frac{\rho_c V_r^2 h_f}{\sigma} \tag{2.124}$$

The velocity measures the relative velocity between the gas core velocity and the interfacial velocity as $V_r = V_c - V_i$. They correlated the liquid entrainment factor to the equation shown before as (2.84). Table 2.1 shows the values for the parameters regressed by Oliemans et al (1986).

Table 2.1 Parameter estimate for entrainment correlation model Oliemans (1986)

Parameter	Value
β^0	-2.52
β^1	1.08
β^2	0.18
β^3	0.27
β^4	0.28
β^5	-1.80
β^6	1.72
β^7	0.70
β^8	1.44
β^9	0.46

Finally, by solving for *dP/dx* in either Equation (2.111) or (2.112) the pressure gradient can be calculated.

Rajan et al (1996) proposed a similar model to the Ansari et al. (1990). The geometry for this two-fluid model can be illustrated by Figure 2.12. The linear momentum balances for the liquid film and gas core are given by:

$$-A_f \frac{dP}{dx} - \tau_f S_f + \tau_i S_i - \rho_l A_f \, g\sin(\beta) = 0 \tag{2.125}$$

$$-A_c \frac{dP}{dx} - \tau_i S_i - \rho_c A_c \, g\sin(\beta) = 0 \tag{2.126}$$

Rajan et al. assuming the liquid film to be of uniform thickness, δ. All the dimensionless geometric parameters can be expressed as function of this film thickness. These parameters are equivalent to those for horizontal annular flow given by Equations (2.82) and (2.85).

Shear stress for the liquid film, the gas core and the interface are also equivalent to the horizontal annular flow as proposed by Xiao et al (1990) model. Rajan et al. neglected the contribution of the interfacial velocity in the interfacial shear stress. The liquid entrainment fraction correlation

used by Rajan et al was the one proposed by Wallis (1969).

$$FE = 1 - \exp(-0.125(v_{crit} - 1.5))$$
$$where \tag{2.127}$$
$$v_{crit} = 10000 \cdot \frac{V_{sg}\mu_g}{\sigma_l}\sqrt{\frac{\rho_g}{\rho_l}}$$

For the interfacial friction factor, Rajan et al used the Wallis correlation adapted for thin films:

$$Z = \frac{f_c}{f_{sc}} = 1 + 300\frac{\delta}{D} \quad for\ FE > 0.9 \tag{2.128}$$

which was adapted for thick films as follows:

$$Z = \frac{f_c}{f_{sc}} = 1 + 16\left(\frac{\rho_l}{\rho_g}\right)^{\frac{1}{3}}\frac{\delta}{D} \quad for\ FE < 0.9 \tag{2.129}$$

In a similar manner to the Olieman model, by eliminating *dP/dx* from Equations (2.125) and (2.126) and substituting geometrical properties the following expression is obtained after simplifying some terms:

$$Y_m = \frac{Z}{(1-\alpha_{lf})^{2.5}\alpha_{lf}} - \frac{1}{\alpha_{lf}^{3}}X_m^2 \tag{2.130}$$

where the modified Lockhart and Martinelli parameters are defined as:

$$X_m^2 = \frac{(1-FE)^2 \frac{f_f}{f_{sl}} \left(\frac{dP}{dx}\right)_{sl}}{\left(\frac{dP}{dx}\right)_{sc}} \tag{2.131}$$

$$Y_m = \frac{(\rho_l - \rho_g) g \sin(\beta)}{\left(\frac{dP}{dx}\right)_{sc}} \tag{2.132}$$

The non-entrainment liquid holdup, α_{lf}, is the fraction of the pipe area occupied by the liquid film, and was defined in terms of film thickness as:

$$\alpha_{lf} = 4\frac{\delta}{D}\left(1-\frac{\delta}{D}\right) \tag{2.133}$$

The total pressure gradients may be determined from either of the following two equations for the liquid film and the gas core, respectively:

$$\left(\frac{dP}{dx}\right)_f = \left[\frac{X_m^2}{\alpha_{lf}^3} - \frac{Z}{(1-\alpha_{lf})^{1.5}\alpha_{lf}}\right]\left(\frac{dP}{dx}\right)_{sc} + \rho_l g \sin(\beta) \tag{2.134}$$

$$\left(\frac{dP}{dx}\right)_f = \left[\frac{Z}{(1-\alpha_{lf})^{1.5}\alpha_{lf}}\right]\left(\frac{dP}{dx}\right)_{sc} + \rho_c g \sin(\beta) \tag{2.135}$$

2.7.6 Vertical Slug Flow

The first thorough physical model for slug flow was developed by Fernandes et al. (1986). By introducing the analysis of the slug unit made up of the Taylor bubble and the liquid slug behind it, Fernandes et al. (1986) formulated overall mass and momentum balance equations to explain the mechanisms of slug flow. Their model could not predict the slug length, and the liquid holdup of the slug was determined indirectly through empirical correlations. Sylvester (1987) proposed a simplified version of this model, which incorporated correlations for the liquid holdup of the slug and the slug length. These models used an important assumption of fully developed slug flow. Figure 2.15 shows the geometry for a fully developed slug unit. Ansari et al (1994) presented a modified version of Sylvester (1987) model.

An overall gas and liquid mass balance over a control volume equivalent to a slug unit cell, considering a cylindrical bubble with a flat nose in an incompressible liquid, yields:

$$V_{sg} = \beta V_{gtb}(1-\alpha_{ltb}) + (1-\beta)V_{gls}(1-\alpha_{lls}) \tag{2.136}$$

$$V_{sl} = (1-\beta)V_{lls}\alpha_{lls} - \beta V_{ltb}\alpha_{ltb} \tag{2.137}$$

where, $\beta = L_{tb}/L_{su}$. The Taylor bubble translational velocity is considered as a superposition of the velocity of a single bubble in a stagnant liquid column, V_{tb} and the mixture velocity, V_m:

$$V_{tb} = 1.2V_m + 0.35\left[\frac{gD(\rho_l - \rho_g)}{\rho_l}\right]^{1/2} \tag{2.138}$$

Similarly, the velocity of the gas bubbles in the liquid slug is given by:

$$V_{gls} = 1.2V_m + 1.53\left[\frac{g(\rho_l - \rho_g)\sigma}{\rho_l^2}\right]^{1/4} \alpha_{lls}^{0.1} \tag{2.139}$$

The velocity of the falling film, V_{ltb}, can be correlated with the film thickness δ using the Brotz expression, and under the assumption of bubble-free film with cylindrical shaped bubbles gives:

$$V_{ltb} = 9.916\left[gD\left(1-\alpha_{gtb}^{0.5}\right)\right]^{1/2} \tag{2.140}$$

The last relationship required for closure is the liquid slug volume fraction that can be obtained by the correlation developed by Sylvester (1987):

$$\alpha_{gls} = \frac{V_{sg}}{0.425 + 2.65V_m} \tag{2.141}$$

The system of equations presented by Ansari et al. (1994) can be solved iteratively to obtain all eight unknowns that define the developed slug flow model.

Finally, the expression for the elevation and frictional pressure gradient across the slug unit was given by:

$$\left(\frac{dP}{dx}\right) = \frac{f_{ls}\rho_{ls}V_m^2(1-\beta)}{2D} + \left[(1-\beta)\rho_l + \beta\rho_g\right]g\sin(\beta) \tag{2.142}$$

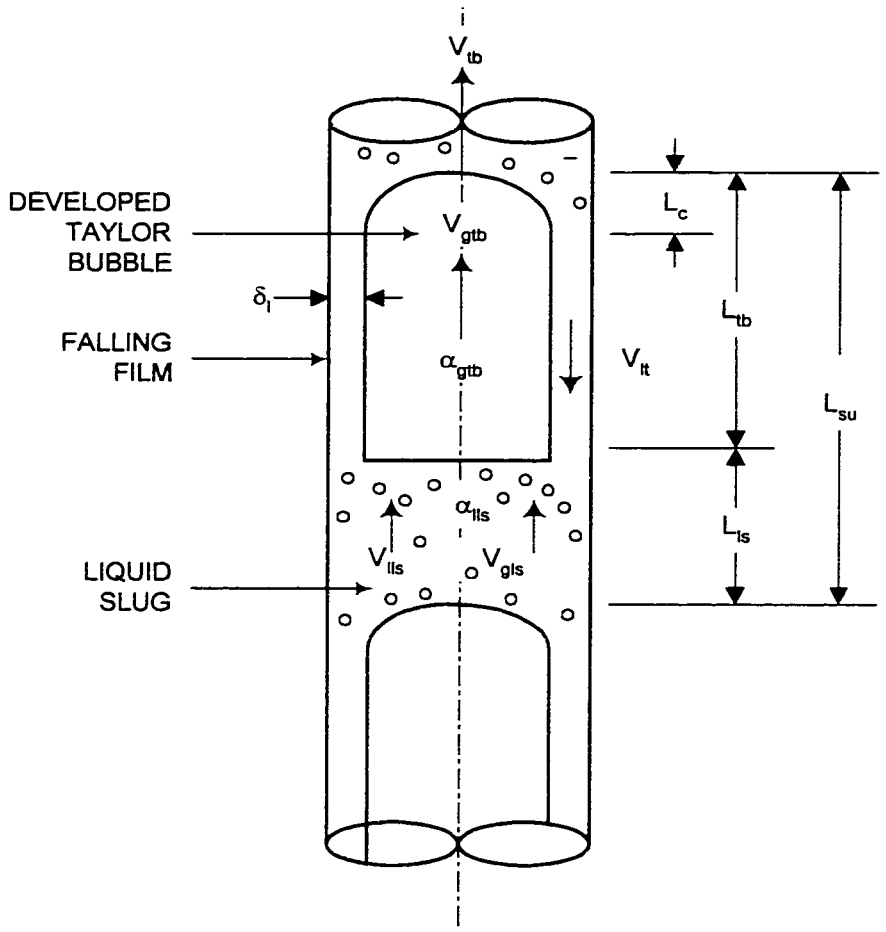

Figure 2.15 Geometry for Slug and Churn Vertical Flow Model

2.7.7 Vertical Bubbly Flow

For bubble vertical flow the non-slip homogeneous flow assumption holds. In the case of dispersed bubble flow a drift-flux model is commonly used. For vertical flow the actual gas velocity becomes:

$$V_g = C_o \cdot V_m + V_b \tag{2.143}$$

The parameter C_o, known as the distribution parameter, reflects the effect of the center line velocity and usually ranges form 1.2 to 1.25 depending on the system. Zuber and Hench (1962) modified Equation (2.109) to account for bubble swarm effects as follows:

$$V_b = 1.53\left[\frac{g(\rho_l - \rho_g)\sigma}{\rho_l^2}\right]^{1/4} \alpha_l^n \tag{2.144}$$

However, the value of n varies from one study to another, and Ansari at al. (1990) used a value of 0.1 in their work. Combining Equations (2.143) and (2.144) an implicit equation for the liquid holdup is obtained:

$$\frac{V_{sg}}{1-\alpha_l^n} - C_o V_m = 1.53\left[\frac{g(\rho_l - \rho_g)\sigma}{\rho_l^2}\right]^{1/4} \alpha_l^n \tag{2.145}$$

Again, as in the horizontal drift–flux model, once the liquid holdup has been determined, it is possible to compute the contribution to the pressure gradient from gravity and acceleration in same manner as for the homogeneous model, by using the mixture properties.

2.8 Summary

This chapter provided a detailed literature review of the mechanistic models to predict flow regime transitions, liquid holdup, and frictional pressure gradient in horizontal and vertical flow. The flow regime transition methods recommended by DIMP (Dukler and Taitel (1982) and (1984)) with enhancements from the unified approach presented by Barnea (1982) were identified as the most accurate ones. The work by Xiao et al (1990), for the prediction of liquid holdup and the frictional pressure gradient in horizontal flow, was found the most comprehensive model. For vertical flow, the work by Ansari and Sylvester (1994) was identified as a very promising method for its balance theoretical basis coupled with flexible closure correlations.

Chapter 3
METHODOLOGY

3.1 Models to be Evaluated

The approach for the evaluation of mechanistic models was based on the work of Xiao et al. (1990) for horizontal flow and the work of Ansari et al. (1994) for vertical flow. The models developed by Taitel and Dukler (1976), Oliemans (1986) and Rajan (1996) for stratified and annular flow regimes were also selected for comparisons as part of this study. Using this approach, a variety of the early and more recent models will be evaluated. Note also, that the given models selected are those that can be modelled with the fluid and operating data typical of test loop experiments. The evaluated flow regimes and their corresponding models are Table 3.8.

Table 3.1 Models Selected for Evaluation

Flow Regime	Orientation	Model
Stratified	Horizontal	Taitel & Dukler 76 Oliemans 87
Annular	Horizontal	Xiao & Shoham et al. 90 Oliemans 86
Slug	Horizontal	Xiao & Shoham et al. 90
Bubble	Horizontal	Ansari & Sylvester 94
Annular	Vertical	Rajan et al 96
Slug	Vertical	Ansari & Sylvester 94
Bubbly	Vertical	Ansari & Sylvester 94

3.2 Calculation Methodology

The calculation method was based on a single point hydrodynamic analysis using the test loop data as input. The different models were numerically evaluated with Excel Visual Basic functions written to solve for liquid holdup and pressure gradient. In order to reduce the scatter of the data, theoretical flow regime transition maps were generated for each data sub-set using superficial gas and liquid velocity as the coordinates. The data sets outside their flow regime boundaries were considered faulty and disregarded from further analysis.

3.2.1. Flow regime maps

For horizontal flow, the **Stratified-Intermittent** flow regime transition, Equations (2.14) and (2.29) were solved simultaneously for *Vsl* and $\overline{h}_l$. The **Intermittent-Dispersed Bubble** flow regime transition Equation (2.50) was solved for *Vsl,* assuming *fl* from the equilibrium stratified flow solution. The **Intermittent–Annular** flow regime transition was obtained from the solution of Equation (2.41).

For vertical flow only the **Bubbly-Slug** and **Annular** transitions were reproduced since these cover all the flow regimes under analysis, namely bubbly, annular and slug flow. The **Bubbly-Slug** transition was obtained from Equations (2.55) by direct evaluation. The **Annular-Non-Annular** transition was determined from Equation (2.62).

3.2.2. Holdup and Pressure Gradient

The overall steps for the calculation of liquid holdup and pressure gradient for stratified, annular, slug, bubble and bubbly flow in a pipe are summarised as follows. The input parameters from the loop test database are the physical properties, operating conditions, the pipe diameter, the relative pipe roughness, and the angle of inclination.

In the case of **Stratified** flow Equations (2.71) and (2.76) are iteratively solved for the dimensionless liquid level $\overline{h}_l$. A value for $\overline{h}_l$ is assumed and all the geometric parameters determined for Equations (2.32) to (2.38). Once a value for $\overline{h}_l$ is found that solves Equation (2.71) within a specified tolerance the iteration is halted. The liquid holdup is then calculated from Equation (2.72) and the pressure gradient is obtained from Equation (2.76).

In the horizontal **Annular** flow the procedure is very similar. First Equation (2.81) is iteratively solved for δ/D, the dimensionless film thickness. Once the solution for equation (2.81), is found, the core and film velocities, as well as the core and film liquid holdups can be evaluated from Equations (2.83) to (2.90). The overall liquid holdup can be calculated from Equation (2.83) and the pressure gradient is obtained from Equation (2.91).

Because **Slug** flow is a hybrid type model, the calculations are divided in two zones, the slug and the film zone. In the slug zone, the velocities and liquid holdup are obtained from the empirical correlations, Equations (2.96) to (2.98). The film zone is solved by assuming Stratified flow, with a solution procedure identical to the one described earlier for Stratified flow. The pressure gradient can be obtained from Equation (2.101) and the average liquid holdup from Equation (2.103).

For **Bubble** flow, the procedure is very simple; the liquid holdup is directly obtained from Equation (2.104) and (2.110) for the homogeneous and drift flux models, respectively. The pressure gradient is calculated from equation (2.105) for both models.

For the vertical **Annular** flow regime model proposed by Oliemans (1986), Equation (2.117) is iteratively solved for liquid holdup. Then, either Equations (2.111) or (2.112) can be used to determine the pressure gradient. The Rajan et al. (1996) model for liquid holdup is very similar to its horizontal counterpart, whereas the pressure gradient can be obtained from the core or film momentum balances, Equations (2.134) or (2.135).

For the vertical **Slug** flow model presented by Ansari et al (1996), the system of Equations (2.136) to (2.141) can be iteratively solved for the liquid holdup in the Taylor bubble. The overall liquid holdup is equivalent to the expression for horizontal slug flow, and the pressure gradient can be determined from Equation (2.142) once the liquid holdup in the Taylor bubble is known.

The equation for liquid holdup in the **Bubbly** flow regime is implicit in liquid holdup, Equation (2.145). Thus, the liquid holdup must be again solved by iteration. The pressure gradient is obtained from an Equation (2.105).

3.3 Experimental Database

In order to test the predictive capabilities of the selected mechanistic models a database of experimental data is required. This database should contain measured data for liquid holdup, pressure gradient and must also provide physical properties, in order to avoid adding another level of uncertainty to the evaluation. The database compiled by the Stanford University (Petalas and Aziz (1994)) satisfied these requirements, and was therefore used in this work. This database includes data from two main sources:

1. The University of Calgary's Multiphase Flow Databank (203 data sets and a total of 20,271 measurements).
2. The University of Tulsa's Well Flow Data Bank (1,775 data sets of actual well data).

The test loop data from the Stanford database was categorised based on pipe orientation, flow regime, and fluid type. The selection of the experimental data aimed to cover a wide range of conditions from air-water to hydrocarbon fluid systems, from small pipe at low pressures to large diameter pipe at high pressures. The conditions included all the flow regimes under evaluation. Tables 3.2 to 3.7 show the data sets extracted from the Stanford database for stratified, annular (horizontal and vertical), slug (horizontal and vertical), bubble and bubbly flow regimes. Most of the data for liquid holdup available in the database was limited to air-water systems, with the

exception of the horizontal stratified flow where some hydrocarbon fluid data was available. Also, most of the pressure gradient data available for systems other than laboratory scale air-water system did not include the liquid holdup data. For pressure gradients in vertical flow, the liquid holdup and pressure gradient data were only available for air-water systems.

Table 3.2 Horizontal Stratified Flow Data sets

Category	Data-Set #1	Data-Set #2	Data-Set #3	Data-Set #4	Data-Set #5
Flow Regime	Stratified Smooth	Stratified Wavy	Stratified Wavy	Stratified Smooth	Stratified Smooth
Orientation	Horizontal	Horizontal	Horizontal	Horizontal	Horizontal
Data Type	Laboratory	Laboratory	Laboratory	Field	Laboratory
Gas Fluid	Air	Air	Hydrocarbon Gas	Hydrocarbon Gas	Air
Liquid Fluid	Water	Water	Hydrocarbon Liquid	Hydrocarbon Liquid	Water
Flow Regime Recorded	YES	YES	YES	YES	YES
Liquid Holdup Recorded	YES	YES	NA	NA	NA
Pressure Drop Recorded	YES	YES	YES	YES	YES

Table 3.3 Horizontal Annular Flow Data sets

Category	Data-Set #6	Data-Set #7	Data-Set #8	Data-Set #9
Flow Regime	Annular-mist	Annular-mist	Annular-mist	Annular-mist
Orientation	Horizontal	Horizontal	Horizontal	Horizontal
Data Type	Laboratory	Laboratory	Field	Laboratory
Gas Fluid	Air	Hydrocarbon Gas	Hydrocarbon Gas	Air
Liquid Fluid	Water	Hydrocarbon Liquid	Hydrocarbon Liquid	Water
Flow Regime Recorded	YES	YES	YES	YES
Liquid Holdup Recorded	YES	NA	NA	NA
Pressure Drop Recorded	YES	YES	YES	YES

Table 3.4 Horizontal Slug Flow Data sets

Category	Data-Set #10	Data-Set #11
Flow Regime	Slug	Slug
Orientation	Horizontal	Horizontal
Data Type	Laboratory	Field
Gas Fluid	Air	Hydrocarbon Gas
Liquid Fluid	Water	Hydrocarbon Liquid
Flow Regime Recorded	YES	YES
Liquid Holdup Recorded	YES	NA
Pressure Drop Recorded	YES	YES

Table 3.5 Horizontal Bubble Flow Data sets

Category	Data-Set #12	Data-Set #13
Flow Regime	Bubble	Bubble
Orientation	Horizontal	Horizontal
Data Type	Laboratory	Field
Gas Fluid	Air	Hydrocarbon Gas
Liquid Fluid	Water	Hydrocarbon Liquid
Flow Regime Recorded	YES	YES
Liquid Holdup Recorded	YES	NA
Pressure Drop Recorded	YES	YES

Table 3.6 Vertical Annular Flow Data sets

Category	Data-Set #14
Flow Regime	Annular
Orientation	Vertical
Data Type	Laboratory
Gas Fluid	Air
Liquid Fluid	Water
Flow Regime Recorded	YES
Liquid Holdup Recorded	YES
Pressure Drop Recorded	YES

Table 3.7 Vertical Slug Flow Data sets

Category	Data-Set #15
Flow Regime	Slug
Orientation	Vertical
Data Type	Laboratory
Gas Fluid	Air
Liquid Fluid	Water
Flow Regime Recorded	YES
Liquid Holdup Recorded	YES
Pressure Drop Recorded	YES

Table 3.8 Vertical Bubbly Flow Data sets

Category	Data-Set #16
Flow Regime	Bubbly
Orientation	Vertical
Data Type	Laboratory
Gas Fluid	Air
Liquid Fluid	Water
Flow Regime Recorded	YES
Liquid Holdup Recorded	YES
Pressure Drop Recorded	YES

3.4 Statistical Results

The liquid holdup and pressure gradient results from the model equations were compared with the experimental data. Since both liquid holdup and pressure gradient are influenced by several factors and vary considerably over the range of database, several statistical parameters were used to test the accuracy of the model predictions.

Statistical Parameters

For a given observation i, the difference between the calculated value, y_{calc}, and the observed value, y_{exp}, is given by e_i as follows:

$$e_i = y_{calc} - y_{\exp} \tag{3.1}$$

where y denotes either the liquid holdup or the pressure gradient. Similarly, the relative error is

defined as:

$$\varepsilon_i = \frac{y_{calc} - y_{exp}}{y_{exp}} \tag{3.2}$$

The statistical parameters used in this work are the average percent error, ε_1, the absolute average percent error, ε_2, and the standard deviation σ, expressed mathematically as:

$$\varepsilon_1 = \frac{1}{n}\sum \varepsilon_i \cdot 100 \tag{3.3}$$

$$\varepsilon_2 = \frac{1}{n}\sum |\varepsilon_i \cdot 100| \tag{3.4}$$

$$\sigma = \sqrt{\frac{1}{n-1}\sum \left(|\varepsilon_i \cdot 100| - \varepsilon_1\right)^2} \tag{3.5}$$

Note that, the standard deviation was used as a measure of the spread or variation of the predicted values with respect to the experimental values.

3.5 Summary

This chapter first presents the models selected for evaluation. For horizontal flow, the Xiao et al. (1990) mechanistic models were used as well as the Oliemans (1986 and 1987) for stratified and annular flow, respectively. The vertical flow models selected were based on the work by Ansari and Sylvester (1994), as well as the Rajan et al. (1996) for slug flow. Procedures for solving the set of equations describing each model were presented in detail. Computer programs were written to implement these procedures.

The database assembled by the University of Stanford was selected for testing. This database contains extensive test loop laboratory data, mainly for air-water systems. For each data set, the

physical properties, flow rate, pipe diameter, absolute roughness, flow regime, as well as pressure gradient are given. Liquid holdup was partially available. The selection of the flow regimes used for testing were constrained by their availability in the database.

Flow regime maps in typical superficial velocity coordinates were selected as a data-screening tool. The methodology proposed for testing the models against the data collected was based on typical statistical parameter, such average percent error and standard deviation.

Chapter 4
ANALYSES OF RESULTS

The presentation of the results is classified based on the pipe orientation and the flow regimes. The experimental data as well as the results for the theoretical predictions for liquid holdup and pressure gradient are plotted for comparison purposes. The statistical parameters discussed in Section 3.4 were computed and presented in tabular form.

4.1 Horizontal Stratified Flow

4.1.1. Liquid Holdup

Data Set # 1

Theoretical flow regime transition maps were generated for each data sub-set using superficial gas and liquid velocity as the coordinates. The procedure to generate these maps was outlined in Section 3.2.1. Because of the high level of accuracy in predicting flow regime transitions for air-water systems, as demonstrated by Taitel and Dukler (1982; 1984), these maps provide an indication of the reliability of the data. For purposes of this study, data inside specific flow regime boundaries is considered to be valid data, which is consistent with the classification in the database. Data outside the boundaries is considered faulty and was discarded from further analysis. For data set 1, these flow regime maps are shown in Figures 4.1 to 4.4. The sub set SU-96 is shown in Figure 4.1. Almost all the data is within the stratified regime boundaries, except for two data points located in the vicinity of this transition.

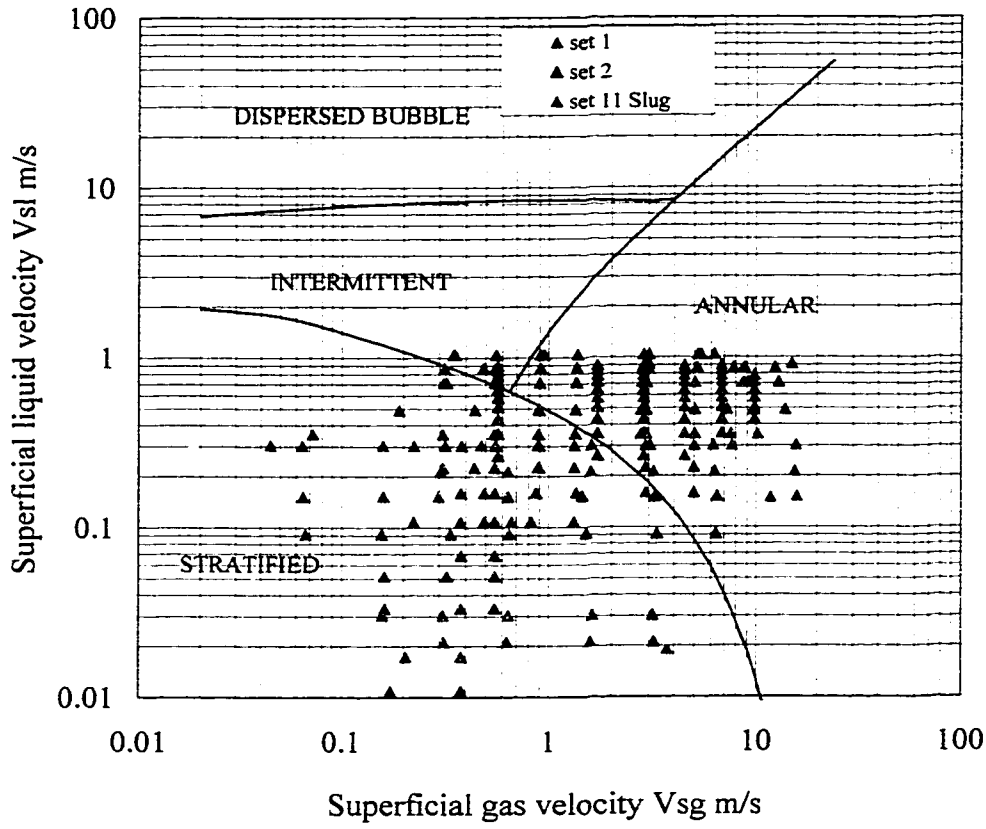

Figure 4.1 Flow Pattern Map
Flow Data Sets # 1and 2 SU-96

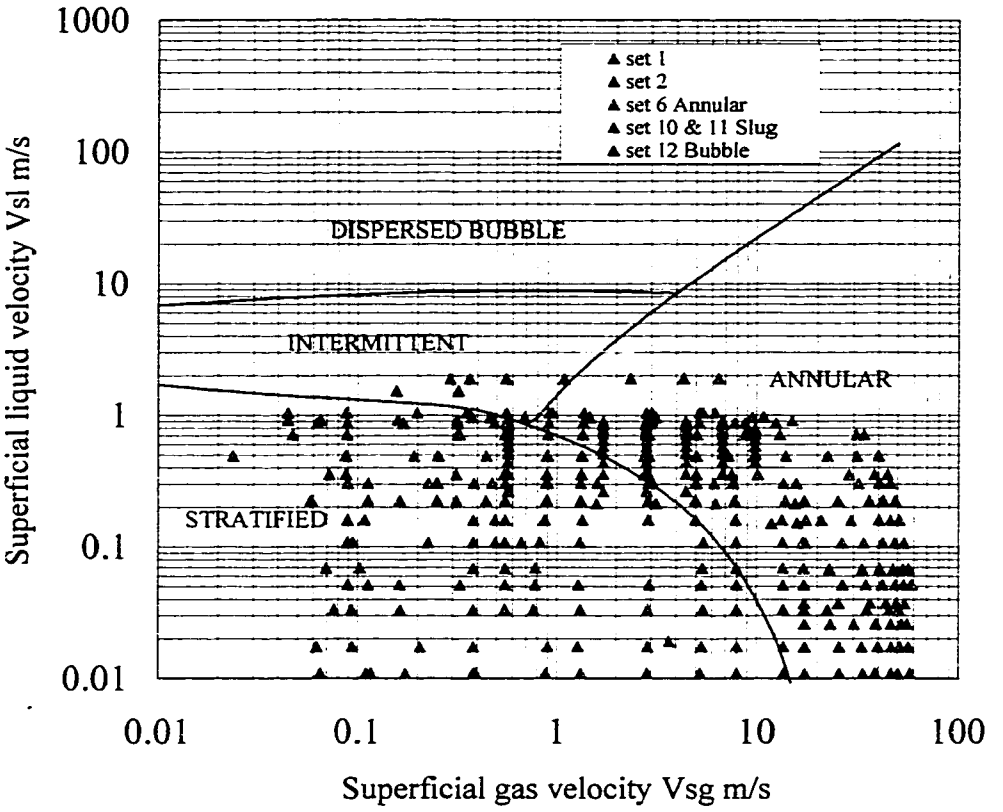

Figure 4.2 Flow Pattern Map
Flow Data Sets # 1 and 2 SU-199
Flow Data Sets # 6 SU-199
Flow Data Sets # 10 and 11 SU-199
Flow Data Sets # 12 SU-199

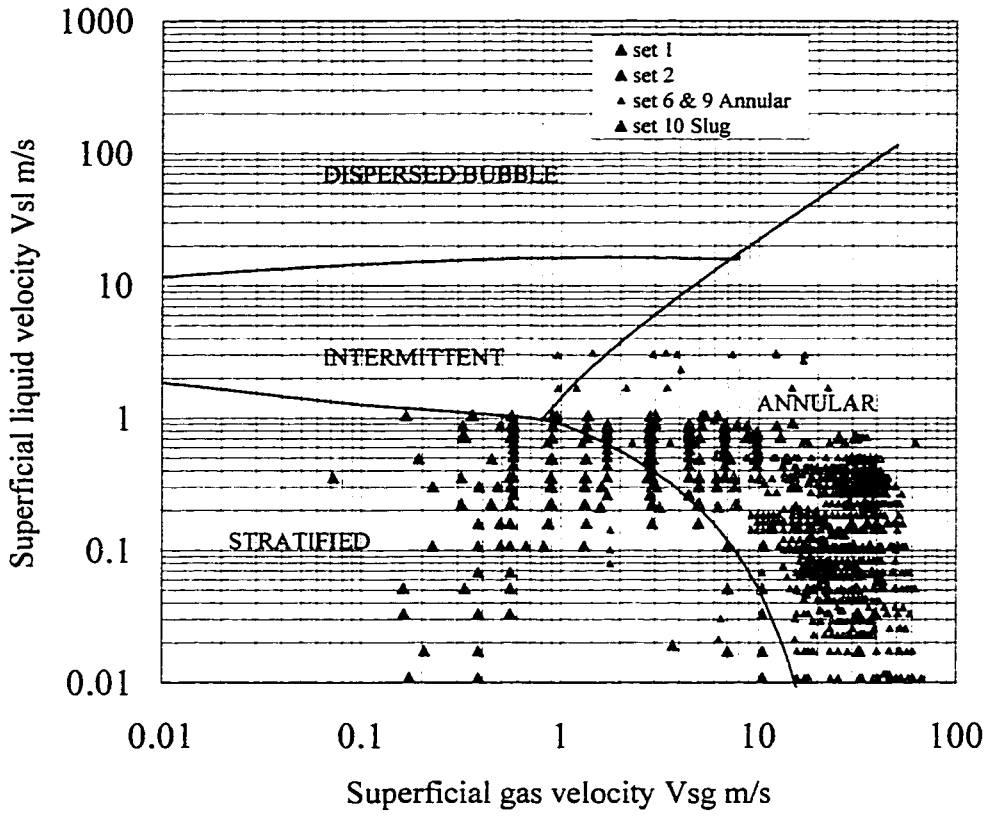

Figure 4.3 Flow Pattern Map
Flow Data Sets # 1 and 2 SU-200
Flow Data Sets # 6 & 9 SU-200
Flow Data Sets # 10 SU-200

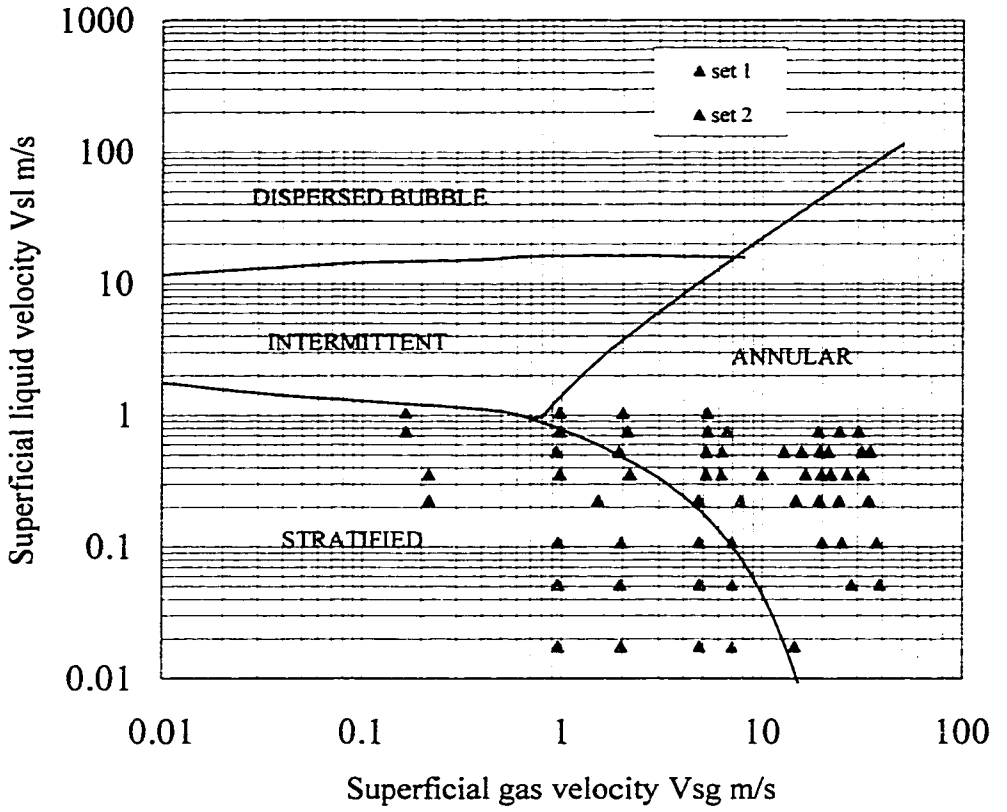

Figure 4.4 Flow Pattern Map
Flow Data Sets # 1 and 2 SU-205

The sub set SU-199 shown in Figure 4.2 exhibits a similar behaviour to sub set SU-96. In sub sets SU-200 and SU-205 the data is distributed almost evenly between stratified and annular flow regimes. The data points outside the stratified flow regime display velocities greater than 10 m/s for *Vsg* and greater than 0.2 for *Vsl*. Note, that sub set SU-200 is inclined upward flow, with and angle of 2.7 °, while sub set 205 is inclined downward with an angle of –6.2 °.

In Figure 4.5 the measured liquid holdup is compared with the calculated holdup from Taitel and Dukler and Oliemans methods. In spite of the obvious scattering of the calculated data, the agreement between the measured and calculated values is actually good. The high density of points around the low holdup zone ($\alpha_L < 0.2$) could be the cause for this good agreement. The results for liquid holdup were also plotted against the Martinelli parameter X with the different liquid holdup models as a parameter, as shown in Figure 4.6. All the curves for these models follow the same trend, which is to increase with an increasing of the X parameter reaching an asymptote value close to 1 at X values greater than 10. The holdup values calculated according to Taitel and Dukler's model overpredict the measured holdup for the entire range of X parameter values. The holdup calculated using the Olieman's model underpredicts the liquid holdup for X ranging from 0.01 to 1. At X=1 there is a crossover by the Olieman's model trending to the same values as the Taitel and Dukler model.

The degree of slippage between the phases is shown by the difference of the homogeneous and measured liquid holdup. This difference is large along the X values up to X=10, and converges to an asymptotic value for X values greater than 10. For the region with $X > 10$, the gas velocity values are large as well which is a typical condition of homogeneous flow.

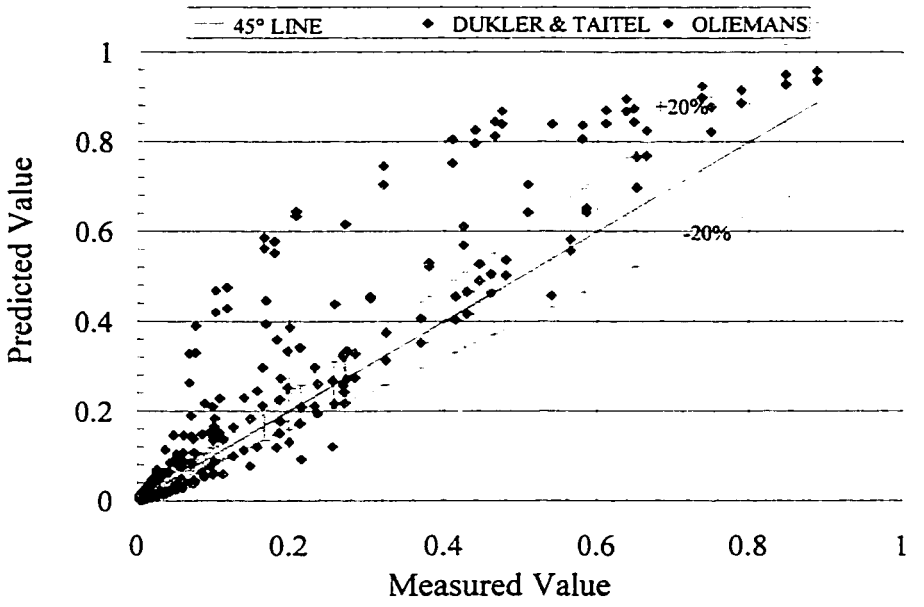

Figure 4.5 Holdup Stratified Flow
SMFD Dataset #1

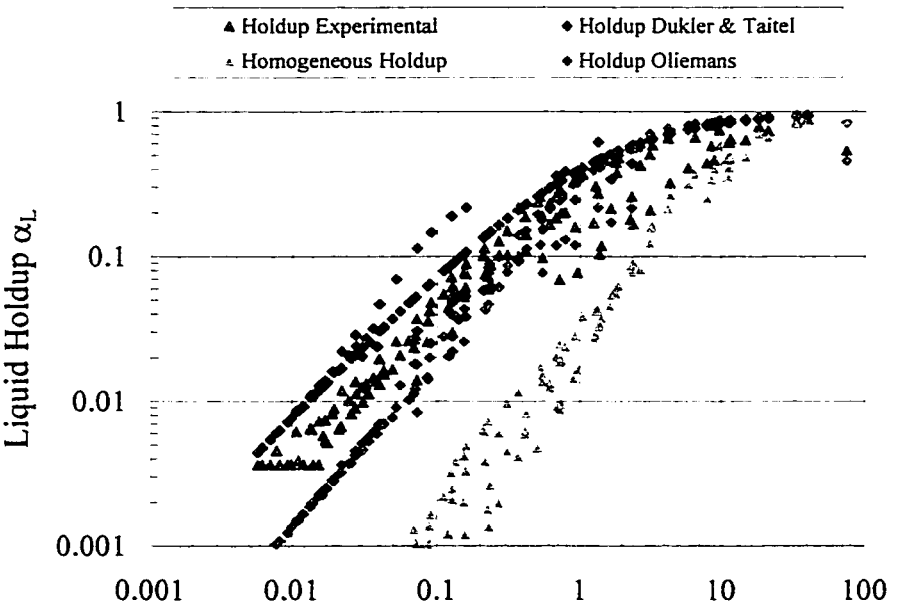

Figure 4.6 Liquid Holdup in Stratified Flow
SMFD Dataset #1

In the Oliemans model the liquid holdup is a function of the interfacial friction factor, through the interfacial roughness and the liquid velocity as described earlier in Section 2.7.1. The Taitel and Dukler model uses the superficial gas friction factor instead. The experimentally equivalent interfacial friction factor was obtained using the Oliemans model and the measured liquid holdup as parameter. Equation (2.69) was solved by iterating on the dimensionless liquid level $\bar{h}_l$ until it matched the measured liquid holdup. In order to evaluate the quality of the Olieman's interfacial friction factor, the ratio of theoretical and experimental equivalent friction factor to the superficial gas friction factor were plotted against the Martinelli parameter defined earlier in Equation (2.30). For data set 1 these two curves are shown in Figure 4.7. The theoretical friction factor trends well with the experimental based friction factor.

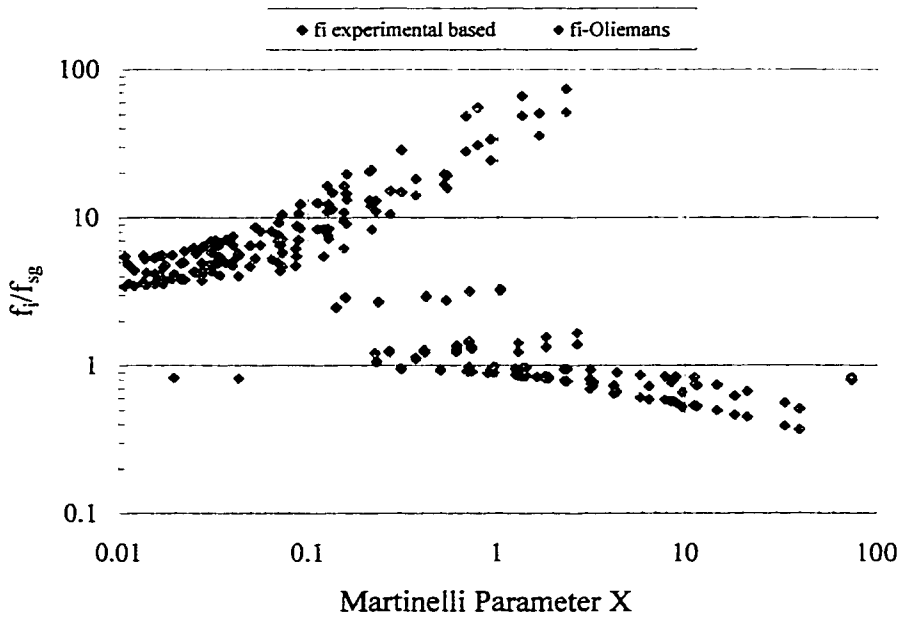

Figure 4.7 Interface / Superficial Gas Friction Factor Ratio
SMFD Dataset # 1

There are three distinct zones. The first of these zones covers the X range from 0.01 to 2 with the values for f_i/f_{sg} increasing from 4 to 80. The second zone covers the X range from 0.2 to 40 with the values for f_i/f_{sg} almost constant at 1. The first and second zones overlap each other creating a third transition zone which covers the X range from 0.2 to 2. In this zone it is not clear what value of the f_i/f_{sg} should be used. The difference between the theoretical friction factor and the experimental based one varies with the zone. In both zones the experimental equivalent friction factor is underpredicted. In the first zone the theoretical friction factor is about two times smaller than the experimental based friction factor. In the second zone the largest value for this ratio is about 1.2. This behaviour also indicates that the liquid holdup is a decreasing function of f_i/f_{sg}.

Since the data in each sub sets was generated by different authors using different experimental set ups, a similar analysis were performed for each of the data sub sets of data set 1 (SU-96 to SU-205). Figure 4.8 compares the measured liquid holdup to the theoretically predicted liquid holdup from Taitel and Dukler and Oliemans methods for sub set SU-96. The average percent errors shown in Table 4.1 fluctuates between 21 and 14.4 respectively, with the majority of the points within the ± 20 percent error band as shown by Figure 4.8. The agreement between the measured and calculated liquid holdup is excellent for values of X below 4.

Table 4.1 Statistical Comparison of Liquid Holdup Results for Stratified Flow

Data Set	SU	No of Points	Model	ε_1	ε_2	σ
1	96	30	Taitel and Dukler	21.5	21.5	18.3
1	199	74	Taitel and Dukler	109.8	109.9	80.6
1	200	23	Taitel and Dukler	107.1	107.1	46.5
1	205	2	Taitel and Dukler	64.9	57.2	23.8
1	96	30	Oliemans	14.4	21.1	27.1
1	199	74	Oliemans	0.445	69.1	96.7
1	200	23	Oliemans	-6.76	58.4	54.9
1	205	2	Oliemans	-35.03	35.0	17.0
2	ALL	80	Taitel and Dukler	79.14	79.1	58.5
2	ALL	80	Oliemans	-14.9	23.0	26.0

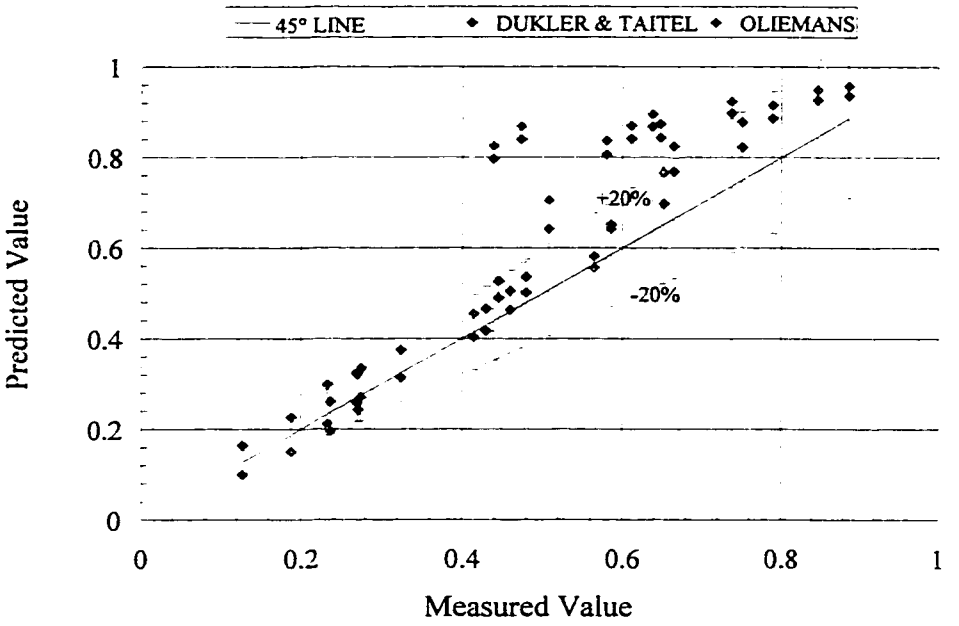

Figure 4.8 Holdup Stratified Flow
SMFD Dataset #1 SU-96

Figure 4.9 also confirms this agreement at liquid holdup values below 0.4. This corresponds to a mixture velocity from 0.3 to 30 m/s, as shown in Figure 4.10, while the superficial gas velocity ranges from 0.3 up to 30 m/s. It should be mentioned that at the low end of liquid holdup where the Martinelli parameter X is small the gas velocity is dominant. For sub set 199 the fit is not as good as sub set 96 as shown in Figure 4.11. The correlation coefficients are around 0.8, which indicates a poor fit. The degree of scatter is large too as indicated by the high value of the standard deviation, which is about 90 percent. Again, the holdup region below 0.1 is in good agreement with the measured data. This poor performance of the models could be attributed to the high scatter of the experimental points as shown in Figure 4.12. A definite good agreement is observed for values of the Martinelli parameter X below 0.4.

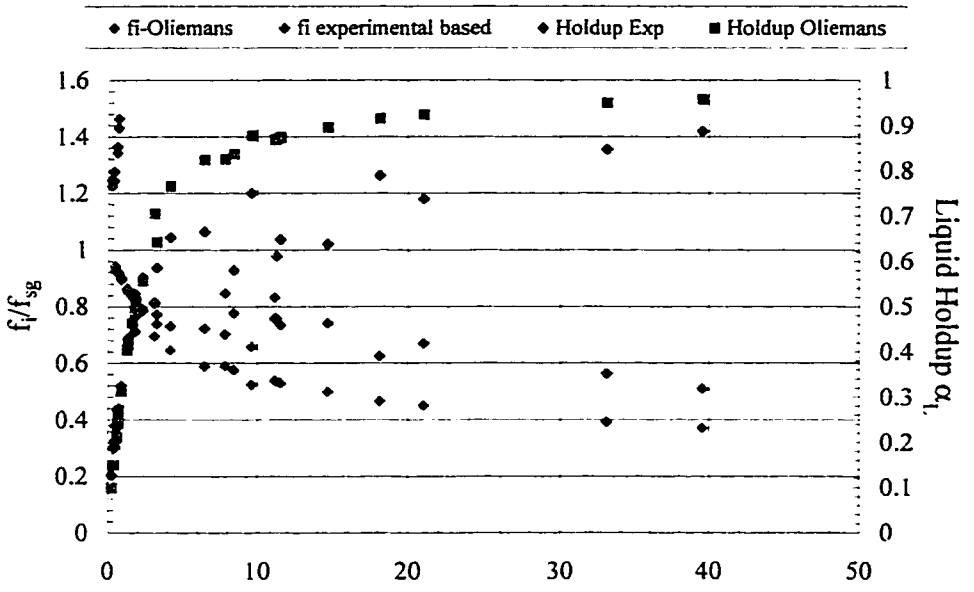

Figure 4.9 Interface / Superficial Gas Friction Factor Ratio
and Liquid Holdup in Stratified Flow
SMFD Dataset #1 SU-96

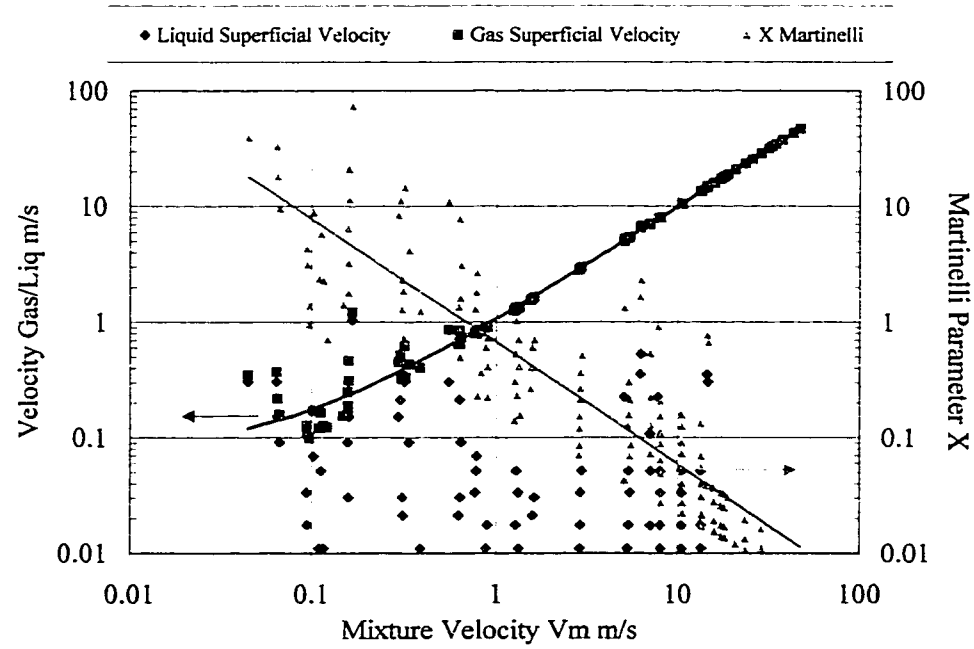

Figure 4.10 Gas-Liquid Superficial Velocities v/s Mixture Velocity
SMFD Dataset # 1

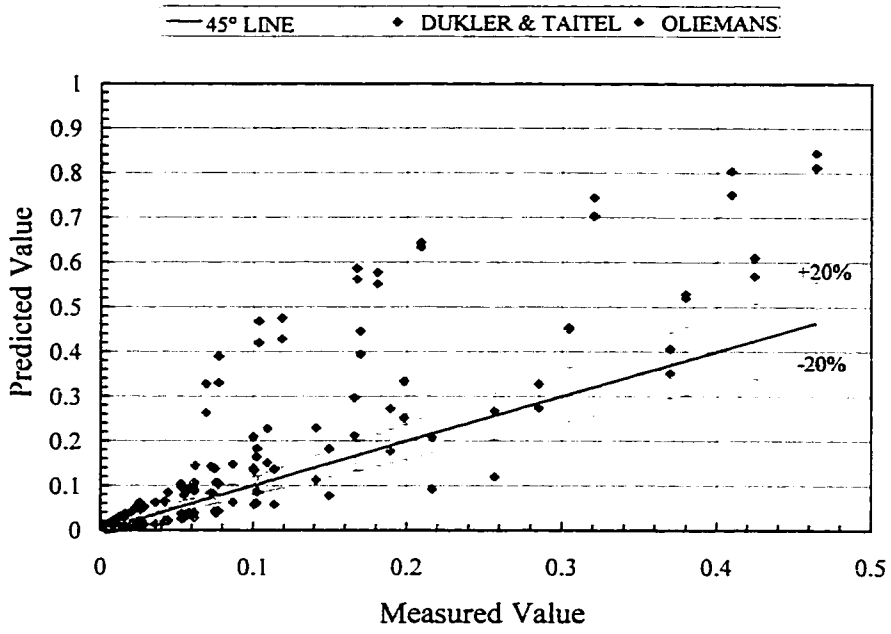

Figure 4.11 Holdup Stratified Flow
SMFD Dataset #1 SU-199

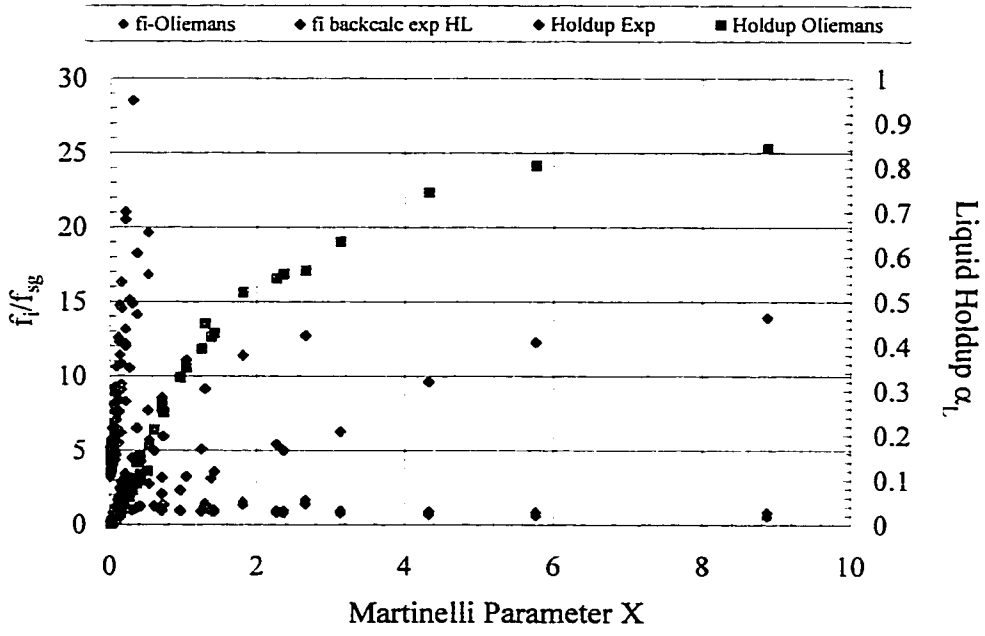

Figure 4.12 Interface / Superficial Gas Friction Factor Ratio
and Liquid Holdup in Stratified Flow
SMFD Dataset #1 SU-199

In sub set SU-200 the Oliemans model predicts the liquid holdup quite well as shown in Figure 4.13. All the valid points are within the ± 20 percent; however, the Taitel and Dukler model does not predict the liquid holdup as accurately. This could be attributed to the inclined upward flow, with an angle of 2.7 °.

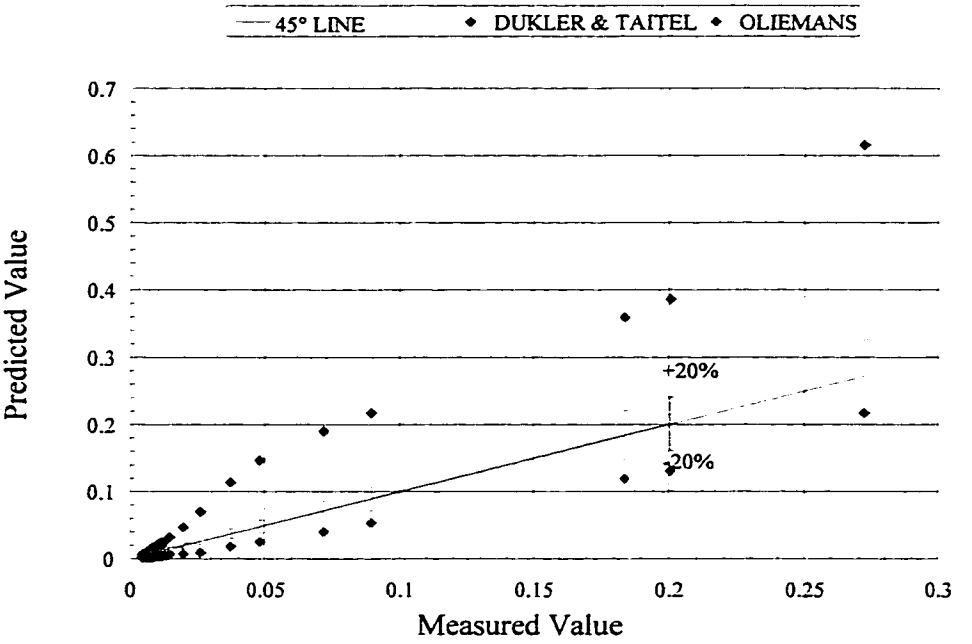

Figure 4.13 Holdup Stratified Flow
SMFD Dataset #1 SU-200

Note, that in Figure 4.14 for sub set SU-205 exhibits the same behaviour as sub set SU-200. Again sub set SU-205 is inclined downward with an angle of –6.2 °.

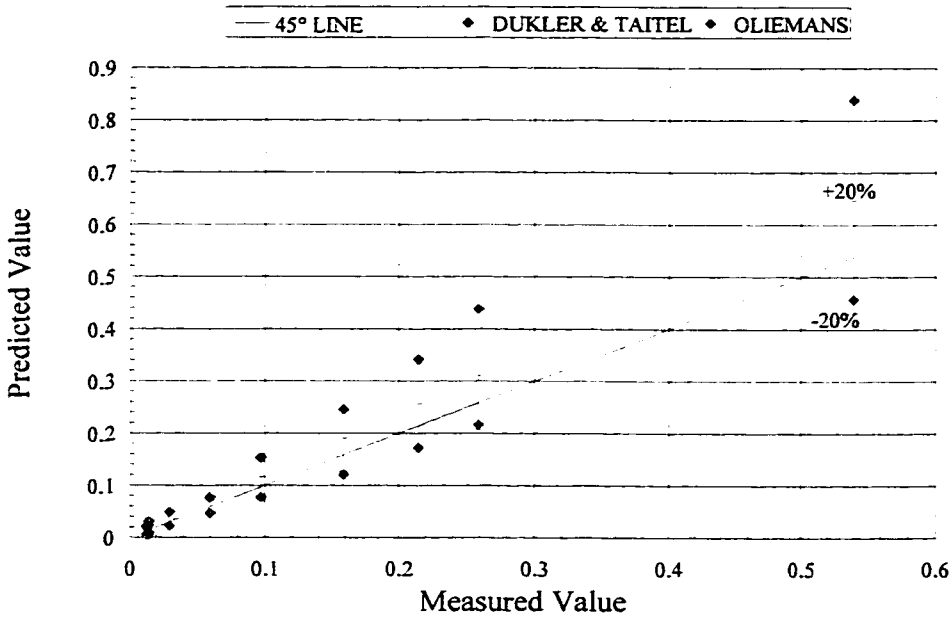

Figure 4.14 Holdup Stratified Flow
SMFD Dataset # 1 SU-205

Data Set # 2

As shown in Table 3.1 the only other data set containing liquid holdup information is data set 2. For data set 2 most of the flow regime maps were shown in Figures 4.1 to 4.4. For the sub set SU-96 almost all data points are within the stratified regime boundaries. For the sub sets SU-199 and SU-200 almost all the data points are outside the stratified flow boundaries, while for sub set SU-205 the data points are distributed between stratified and annular flow. The flow regime maps for sub sets SU-21 and SU-53 are shown in Figures 4.15 and 4.16, respectively. These figures show, for SU-21, that all the data points are outside the stratified flow regime boundaries and that all the points are outside for SU-53. Because of these results the data points for sub sets SU-199 and SU-200 were considered faulty and were discarded from further analysis.

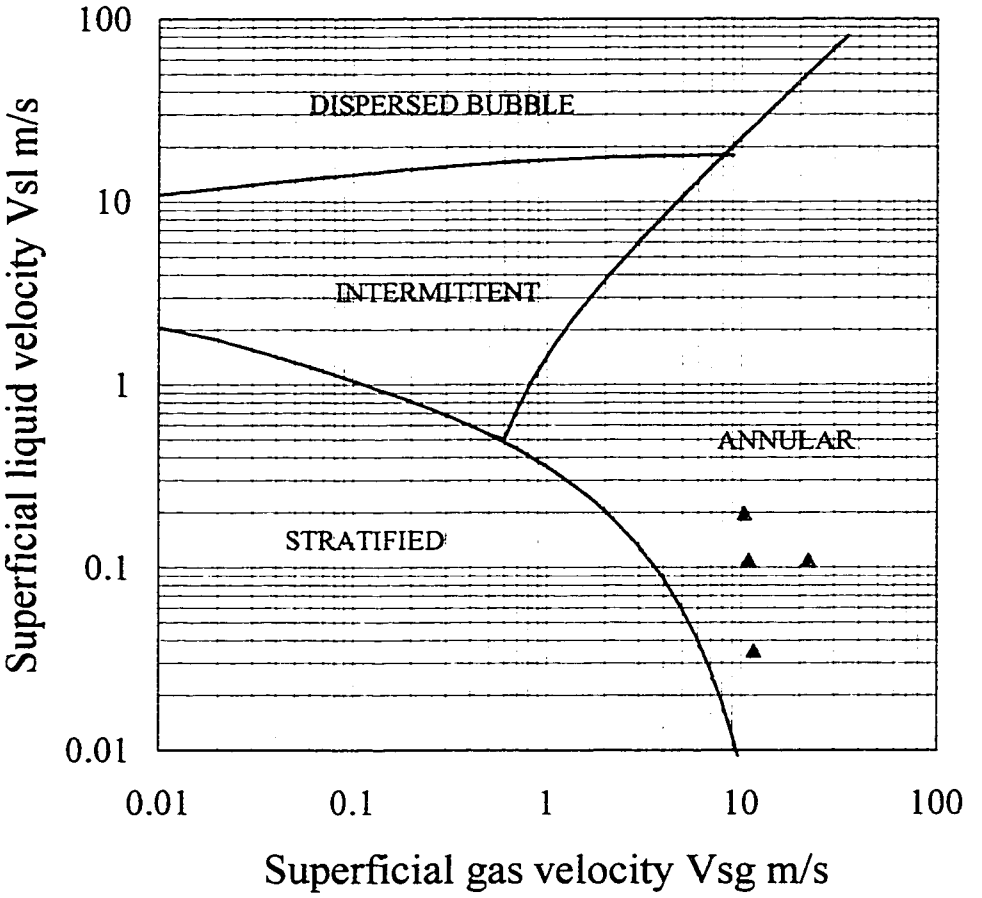

Figure 4.15 Flow Pattern Map Stratified Flow Data Sets # 2 SU-21

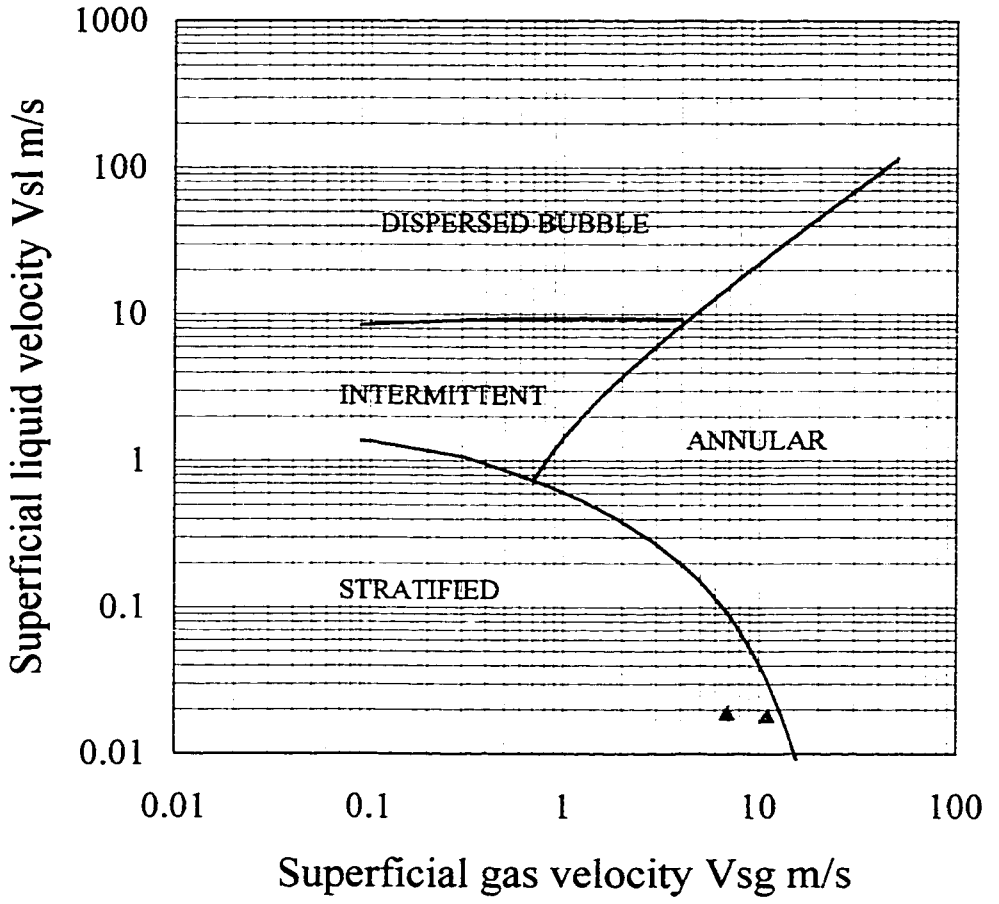

Figure 4.16 Flow Pattern Map Stratified Flow Data Sets # 1 SU-53

Figure 4.17 shows the measured liquid holdup compared with the calculated holdup from Taitel and Dukler and Oliemans methods. The Oliemans method underpredicts the liquid holdup with an average percent error of −15%, while the Taitel and Dukler method overpredicts the liquid holdup with an average percent error of 79%, which coincide with the trends observed for set 1. The agreement between the data predicted with the Oliemans model with the measured data is very good, with all the valid points within the ± 20 percent band; however, the Taitel and Dukler model does not predict the liquid holdup as accurately. The results for liquid holdup were also plotted against the Martinelli parameter X, as shown in Figure 4.18. All the curves for these models follow the same trend, which is the liquid holdup being an increasing function of X.

A plot similar to Figure 4.7 for data set 1 was prepare for data set 2, Figure 4.19. The trend for the interface to gas friction factor ratio, f_i/f_{sg}, is very similar to data set 1; however, there is only one distinct zone. This zone covers the range for X from 0.01 to 1 with the values for f_i/f_{sg} increasing from 4 to 80.

The physical properties and operating conditions for data sets 1 and 2 are quite similar. Both data sets are for air-water fluid systems at low pressures and moderate temperatures. Their pipe sizes are very similar ranging from ½ to 1½ inches in diameter. Their only difference lies in their flow regimes, data set 1 being stratified smooth, while data set 2 is stratified wavy. Basically they are the same system, which explains their similar behaviour.

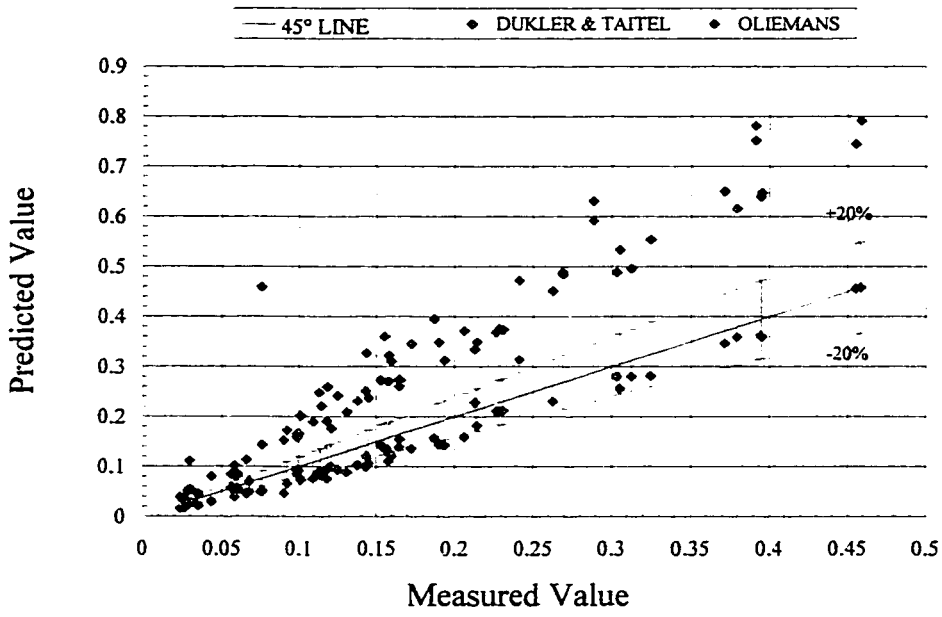

Figure 4.17 Holdup Stratified Flow
SMFD Dataset # 2

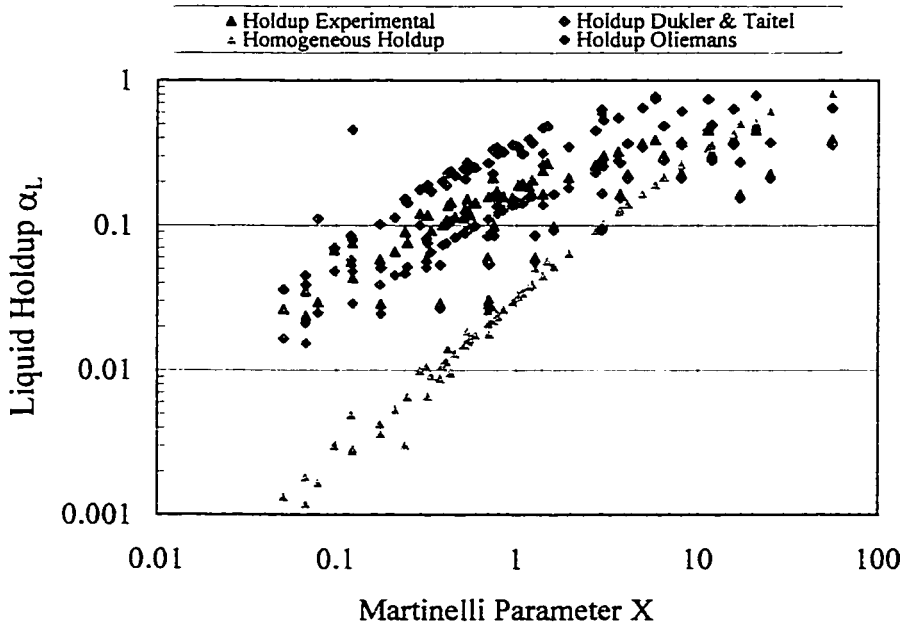

Figure 4.18 Liquid Holdup in Stratified Flow
SMFD Dataset 2

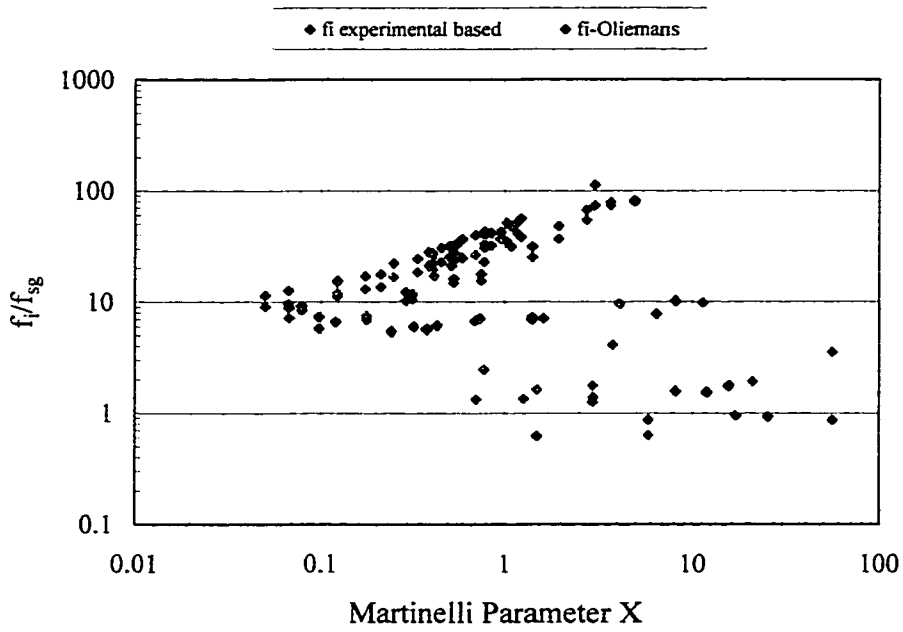

Figure 4.19 Interface / Superficial Gas Friction Factor Ratio
SMFD Dataset # 2

4.1.2. Pressure Gradient

Data Set # 1

Figure 4.20 shows an excellent agreement between the measured and calculated pressure gradients, with the majority of the points within the ± 20 percent error band. The Olieman's model overpredicts the pressure gradient and the Taitel and Dukler's model underpredicted it, as indicated by their average percent errors, ε_l, are 79% and –15%, respectively.

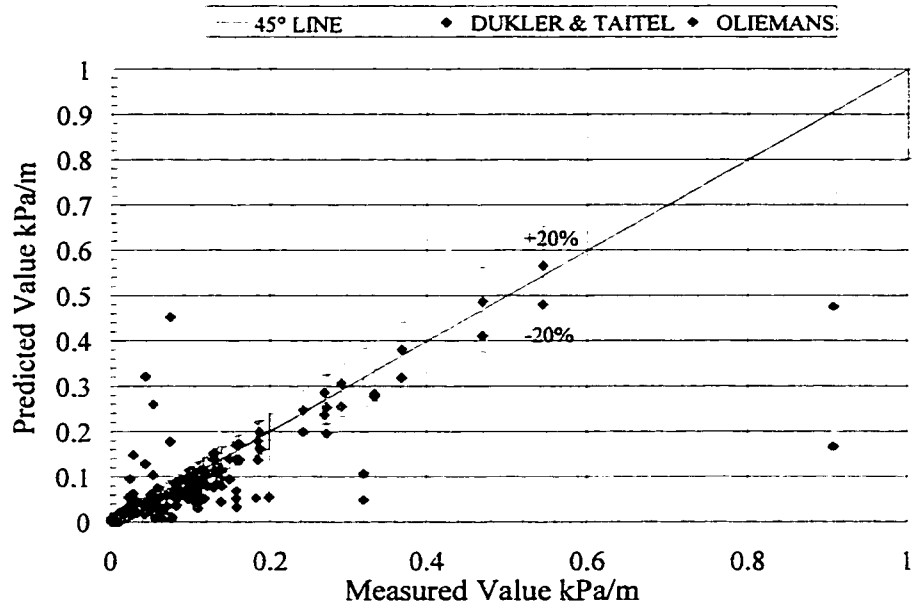

Figure 4.20 Pressure Gradient Stratified Flow
SMFD Dataset #1

An alternative plot of the results presents the pressure gradient against the mixture velocity for the predictive methods as well as the measured ones. This plot is shown for set 1 in Figure 4.21. This figure shows the good agreement of the two models at mixture velocities > 10 m/s. For mixture velocity values < 10 m/s, a high degree of scattering in the measured values is noted. The pressure gradient was calculated with the Oliemans model using the dimensionless liquid level $\bar{h}_l$ obtained from the measured liquid holdup, as shown in Figure 4.22. The pressure gradient calculated this way follows the Oliemans model quite closely; however, it does not improve the agreement with the measured values as expected. This does not necessarily mean that the model is not sensitive to the interfacial friction factor correlation, but that the data is questionable in the low mixture velocity region (below 10 m/s).

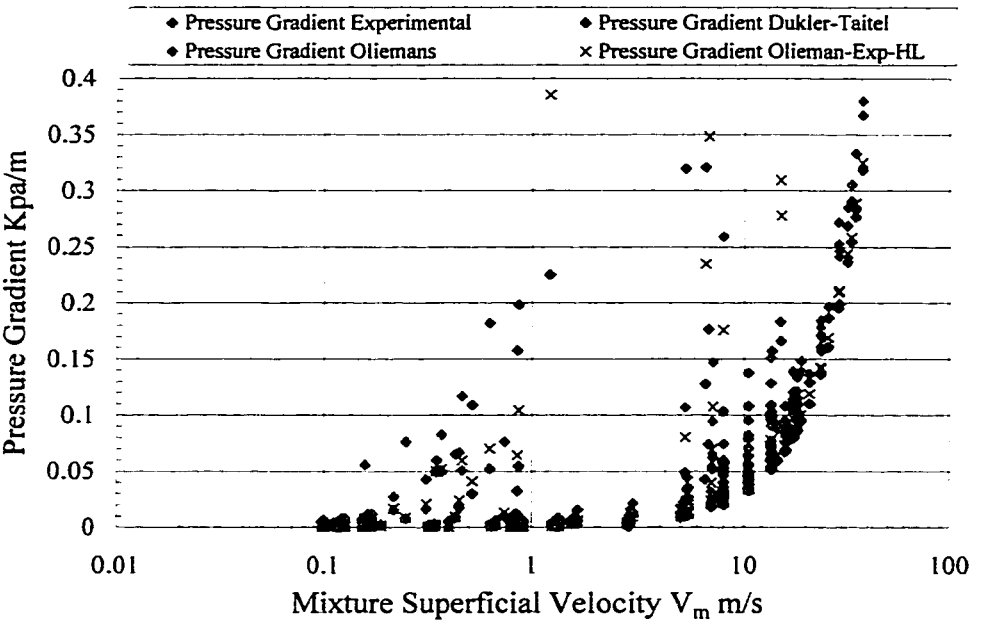

Figure 4.21 Pressure Gradient in Stratified Flow
SMFD Dataset #1

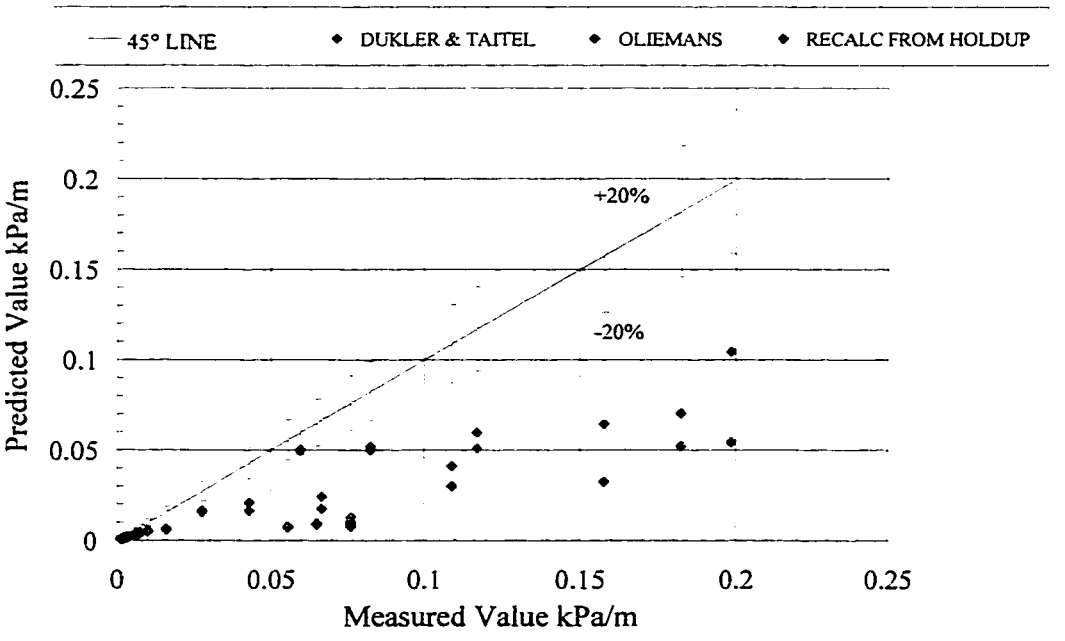

Figure 4.22 Pressure Gradient Stratified Flow
SMFD Dataset #1 SU-96

Similar to the analysis performed on liquid holdup, the sub sets were also individually studied. For sub set 96 shown in Figure 4.22, the agreement is poor. However, subset 199 and 200, display a very good match as shown in Figures 4.23 and 4.24, while sub set 205 shown in Figure 4.25 does not show good results. Those sub sets in poor agreement with the measured values have low values of mixture velocity below 10. The sub sets with good agreement have larger mixture velocity values that translate into gas superficial velocities ranging from 10 to 100 m/s as shown in Figure 4.10. The good match for the mixture velocity region above 10 m/s coincides with part of the region in which good liquid hold predictions were achieved, namely between 10 and 30 m/s.

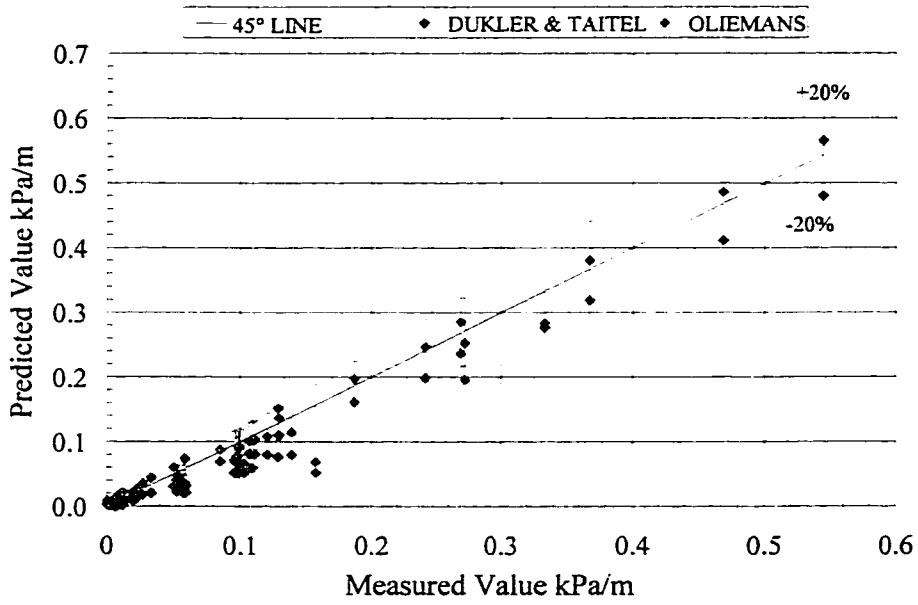

Figure 4.23 Pressure Gradient Stratified Flow
SMFD Dataset #1 SU-199

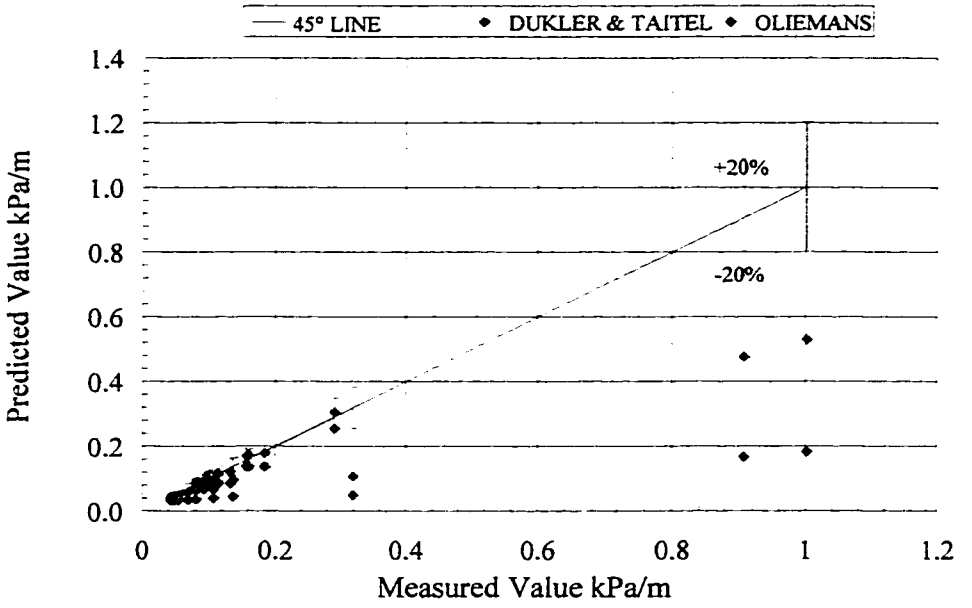

Figure 4.24 Pressure Gradient Stratified Flow
SMFD Dataset #1 SU-200

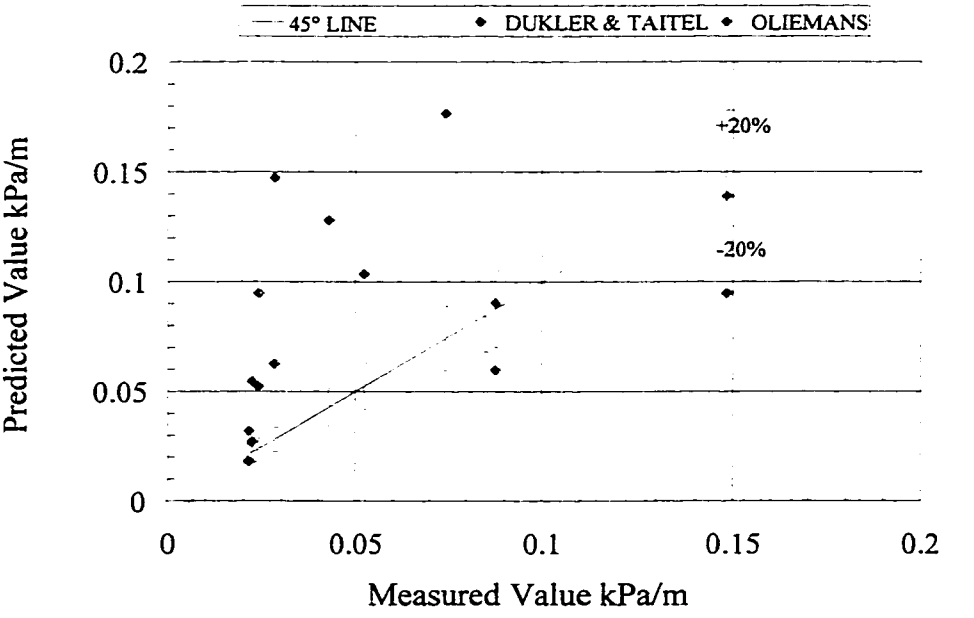

Figure 4.25 Pressure Gradient Stratified Flow
SMFD Dataset #1 SU-205

Data Set # 2

Figure 4.26 shows that the agreement between the predicted and measured values of pressure gradient is very poor. As shown in Table 4.2 the average error percent for the pressure gradient is1800 for the Taitel and Dukler model and 4400 for the Oliemans model. This is due to the large amount of data points near zero values (< 0.01), which give an artificial large percent error. These near zero points were removed and the average percent were reduced to 36% and 193% for the Taitel and Dukler and Oliemans models, respectively.

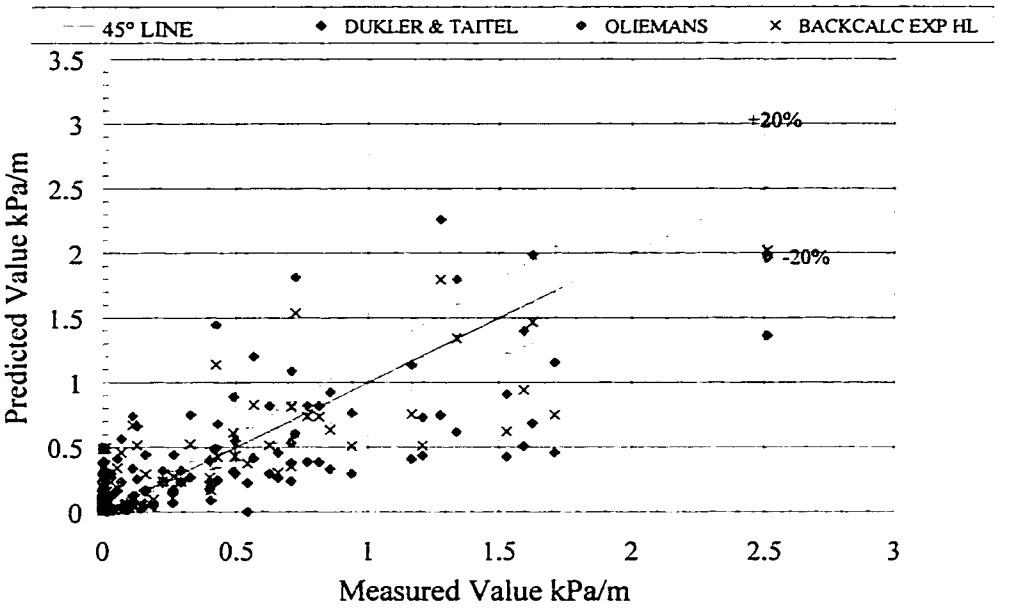

Figure 4.26 Pressure Gradient Stratified Flow
SMFD Dataset # 2

Table 4.2 Statistical Comparison of Pressure Gradient Results for Stratified Flow

Data Set	SU	No of Points	Model	ε_1	ε_2	σ
1	96	30	Taitel and Dukler	-57.3	57.3	17.3
1	199	74	Taitel and Dukler	-29.2	71.9	103.9
1	200	23	Taitel and Dukler	-25.9	43.2	53.5
1	205	2	Taitel and Dukler	33.7	61.5	80.4
1	96	30	Oliemans	-58.1	58.1	18.3
1	199	74	Oliemans	10.7	84.3	184.2
1	200	23	Oliemans	2.17	41.6	139.5
1	205	2	Oliemans	211.6	243.8	213.7
2a	ALL	80	Taitel and Dukler	1869.6	1949.0	6912.0
2a	ALL	80	Oliemans	4413.8	4475.2	16210.4
2b	ALL	80	Taitel and Dukler	36.5	111.7	296.3
2b	ALL	80	Oliemans	193.1	221.0	568.2
3	ALL	80	Taitel and Dukler	-40.7	40.7	9.1
3	ALL	80	Oliemans	41.5	41.5	20.7
4	ALL	75	Taitel and Dukler	-47.4	65.5	62.8
4	ALL	75	Oliemans	-11.2	77.9	114.5
5	ALL	80	Taitel and Dukler	367.1	132.0	205.8
5	ALL	80	Oliemans	195.4	207.4	247.8

Data Set # 3

As shown in Figure 4.27 all the data points are within the stratified regime boundaries. Therefore, this data set is considered valid for further analysis.

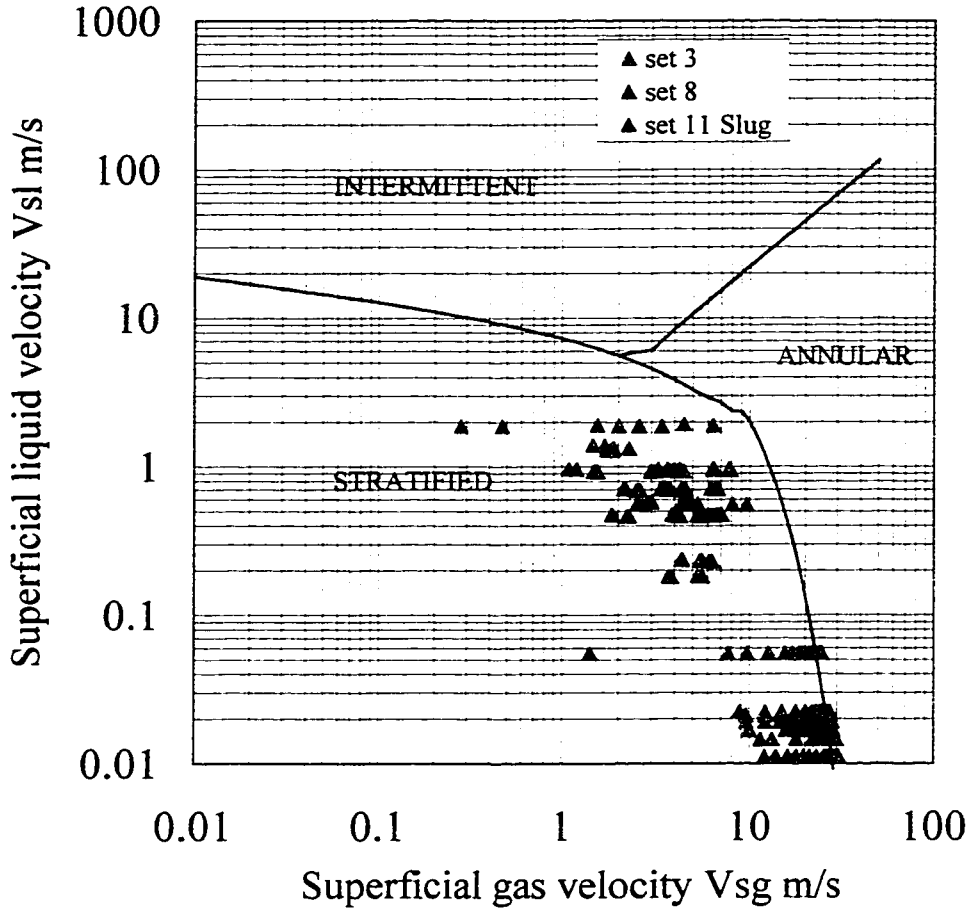

Figure 4.27 Flow Pattern Map
Sets # 3 SU-80
Sets # 8 SU-80
Sets # 11

Figure 4.28 shows that the agreement between the predictive and measure values of pressure gradient is poor, most of the points are outside the ± 20 percent error band. As shown in Table 4.2 the average percentage errors are –40% for the Taitel and Dukler model and 41% for the Oliemans model. Again, the trend is similar to previous findings, where the Taitel and Dukler model underpredicts the pressure gradient and the Olieman model overpredicts it. The fluid system tested here is hydrocarbon liquid and hydrocarbon gas with properties and operating conditions are similar to those of sets 1 and 2.

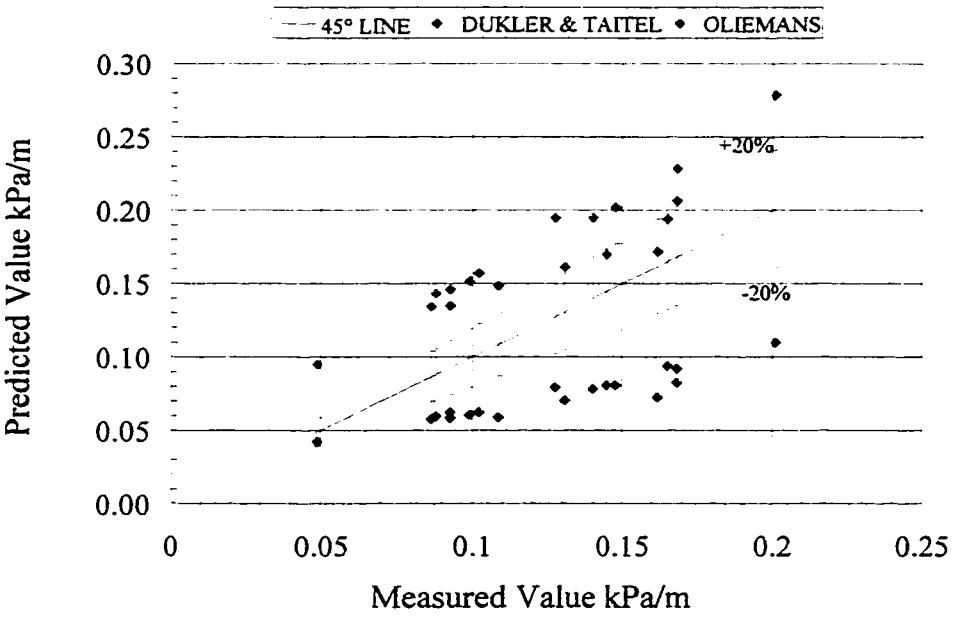

Figure 4.28 Pressure Gradient Stratified Flow
SMFD Dataset # 2 SU-80

Data Set # 4

Figures 4.29 and 4.30 show the flow regime maps for the sub set SU-109 and SU-110, respectively. In Figure 4.29 most of the data points are outside the stratified regime boundaries, while in Figure 4.30 almost all data points are within the stratified regime boundaries. Both data sub sets were considered for the pressure gradient predictions.

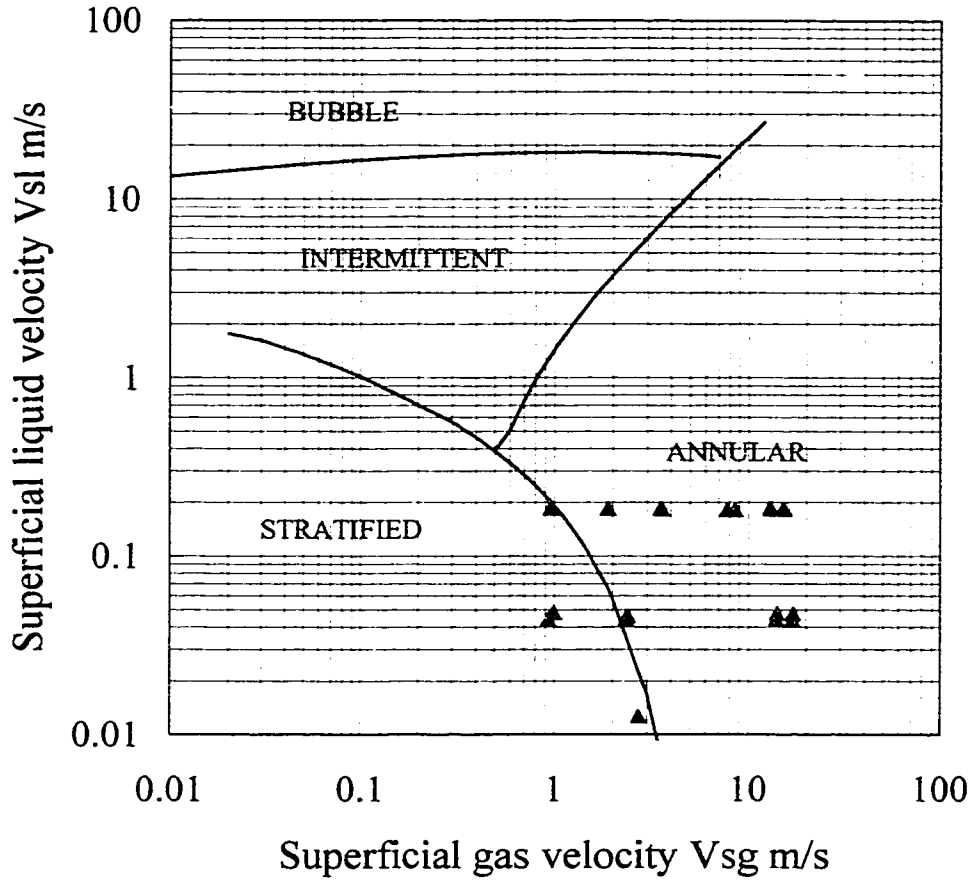

Figure 4.29 Flow Pattern Flow
Data Sets # 4 SU-109

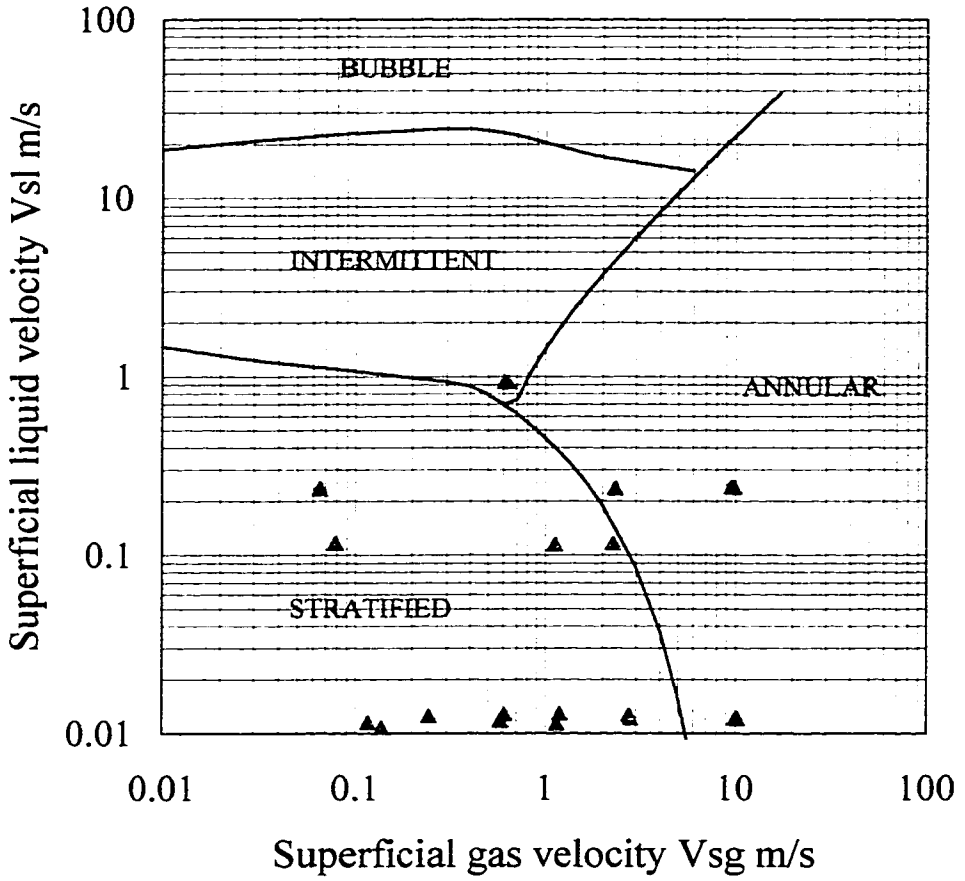

Figure 4.30 Flow Pattern Map
Data Sets # 4 SU-110

Figure 4.31 shows that the agreement between the predictive and measure values of pressure gradient is good with most of the data points inside the ± 20 percent error band. The points outside the ± 20 percent error band coincide with the point outside the stratified flow regime boundaries, which corresponds to mixture velocities > 10 m/s as shown in Figure 4.32. Table 4.2 shows the average percentage errors being –47% for the Taitel and Dukler model and –11% for the Oliemans model. Here, both models seem to underpredict the pressure gradient. The liquid and gas components for this system are both hydrocarbons, operating at pressures between 2000 to 4000 kPag and with density ratios of 29 to 58. In spite of these differences the system behaved in a similar manner to the previous data sets tested so far.

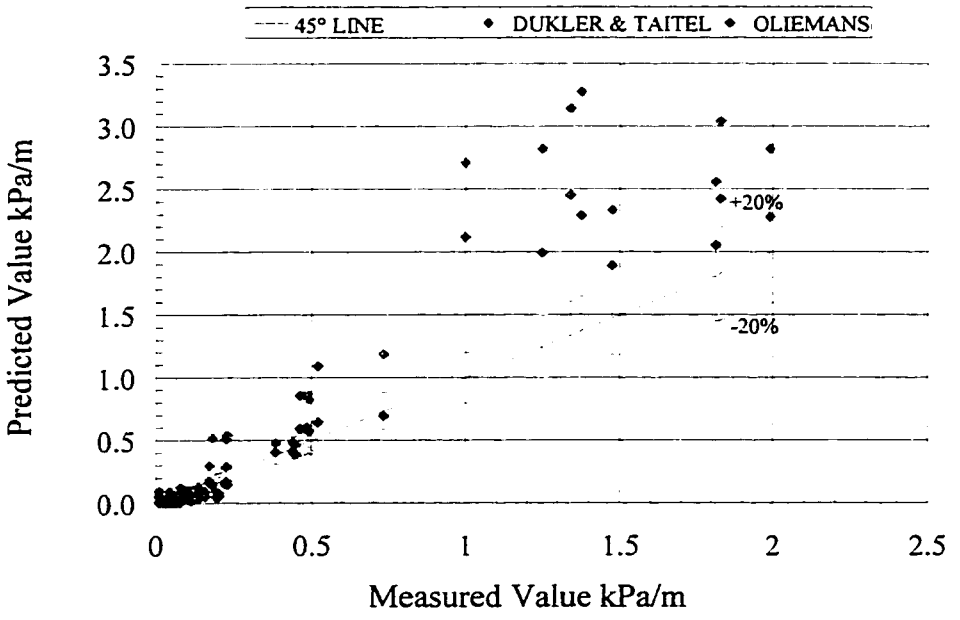

Figure 4.31 Pressure Gradient Stratified Flow
SMFD Dataset # 4

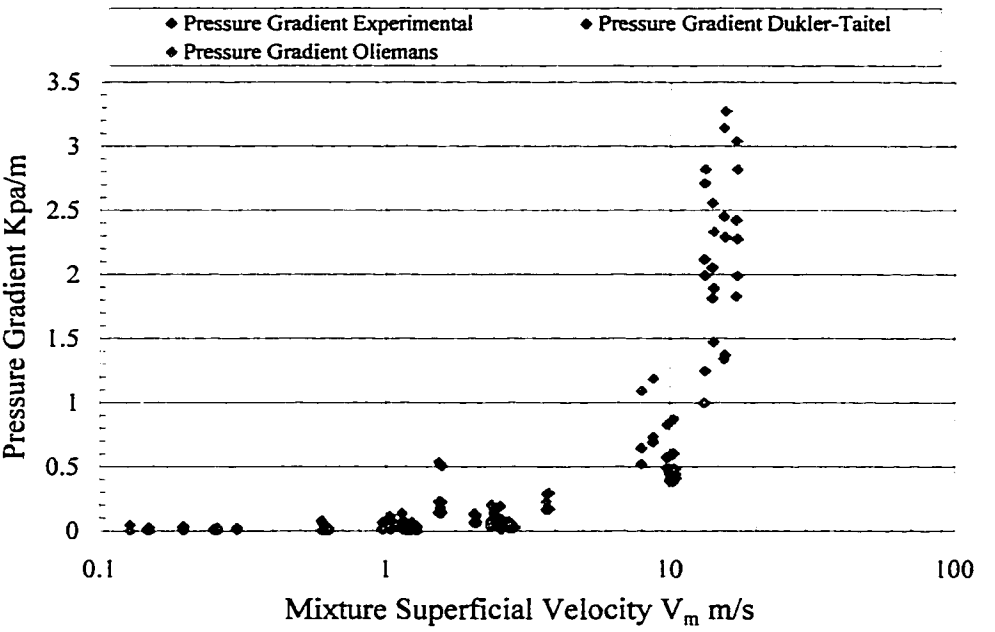

Figure 4.32 Pressure Gradient in Stratified Flow
SMFD Dataset # 4

Data Set # 5

As shown in Figure 4.33 the great majority of the data points are within the stratified regime boundaries. Therefore, this data set is considered valid for further analysis.

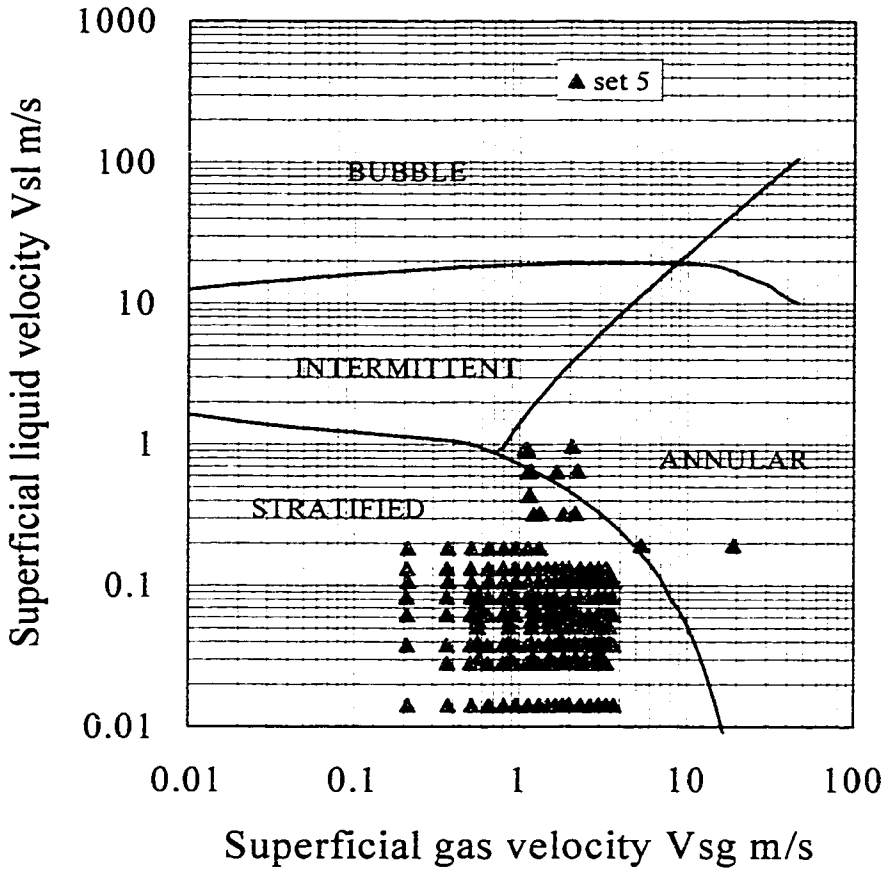

Figure 4.33 Flow Pattern Map
Flow Data Sets # 5 SU-8-10-22-24

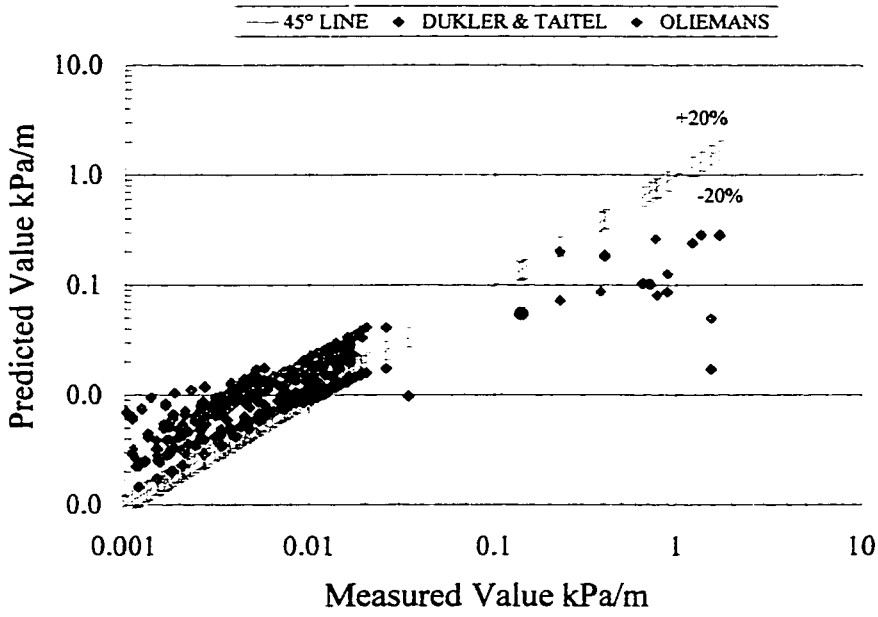

Figure 4.34 Pressure Gradient Stratified Flow
SMFD Dataset # 5

Figure 4.34 shows that the agreement between the predicted and measured values of pressure gradient is poor, most of the points are outside the ± 20 percent error band. Table 4.2 shows the average percentage error for the pressure gradient being 367% for the Taitel and Dukler model and 195% for the Oliemans model. This is due to the large amount of data points with near zero values (< 0.01), which give an unnecessarily large percent error. These near zero points cannot be removed since they form the majority of the data.

4.2 Horizontal Annular Flow

4.2.1. Liquid Holdup

Data Set # 6

For sub sets SU-199 and SU-200 the flow regime maps are shown in Figures 4.2 and 4.3. Most of the data is within the annular regime boundaries, except for a few data points located in the vicinity of the stratified-annular transition.

Figure 4.35 shows a comparison for the measured liquid holdup with the calculated holdup from Xiao and Oliemans methods. The Xiao method underpredicts the liquid holdup, with an average percentage error of –63% and a standard percentage deviation of 57% as shown in Table 4.3. The Oliemans model agreement with the measured data is excellent with all the valid points within the ± 20 percent error band and an average percentage error of 12% and a standard percentage deviation of 23%. The Xiao model did not predict the liquid holdup as accurately as the Oliemans model. It should be noted that the results for liquid holdup with near zero values (< 0.01) were not included, as they tend to produce artificially large errors. The good performance shown by the Oliemans model confirms the validity of the liquid holdup data. It is surprising that such a simple model, which does not account for liquid entrainment fraction, could produce such good results. Xiao et al (1990) did not provide the regression coefficients (β_i) for the liquid entrainment fraction correlation they used. In this study the regression coefficients (β_i) developed by Oliemans for vertical annular flow was used.

Table 4.3 Statistical Comparison of Liquid Holdup Results for Annular Flow

Data Set	SU	No of Points	Model	ε_1	ε_2	σ
6	ALL	150	Xiao et al.	-63.0	63.1	57.6
6	ALL	150	Oliemans	11.9	17.5	21.3

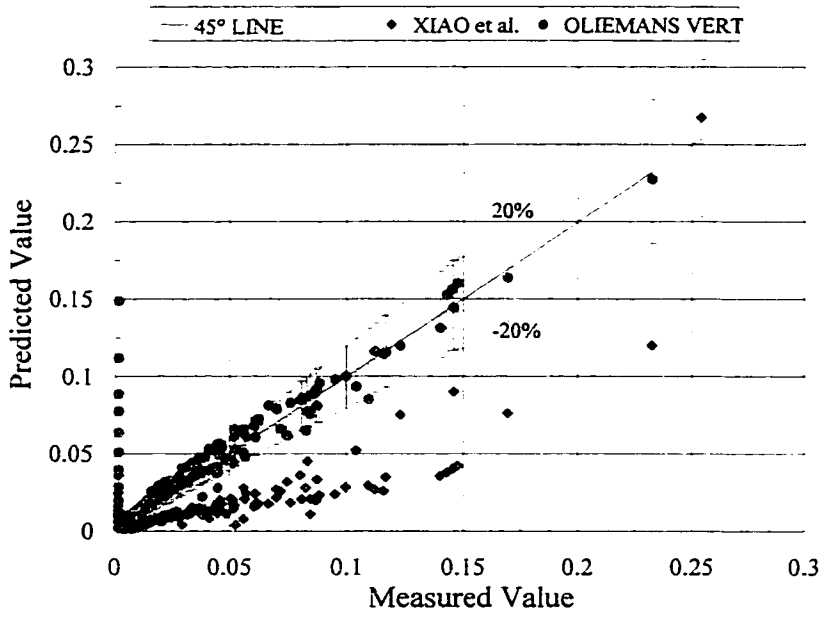

Figure 4.35 Holdup Annular Flow
SMFD Dataset # 6

The Xiao's liquid holdup expression was solved for the liquid film thickness to diameter ratio (δ/D) using the experimental liquid holdup as a parameter. These results along with the theoretical liquid film ratio were plotted against the calculated liquid holdup as shown in Figure 4.36. The experimental based liquid film ratio exhibits a nearly perfect linear relationship to liquid holdup, while the calculated liquid film ratio shows a steeper and sparser trend. This indicates the inability of the Xiao model to accurately predict the liquid holdup. Again, this could be attributed to the poor performance of the correlation used by Xiao for the liquid entrainment fraction.

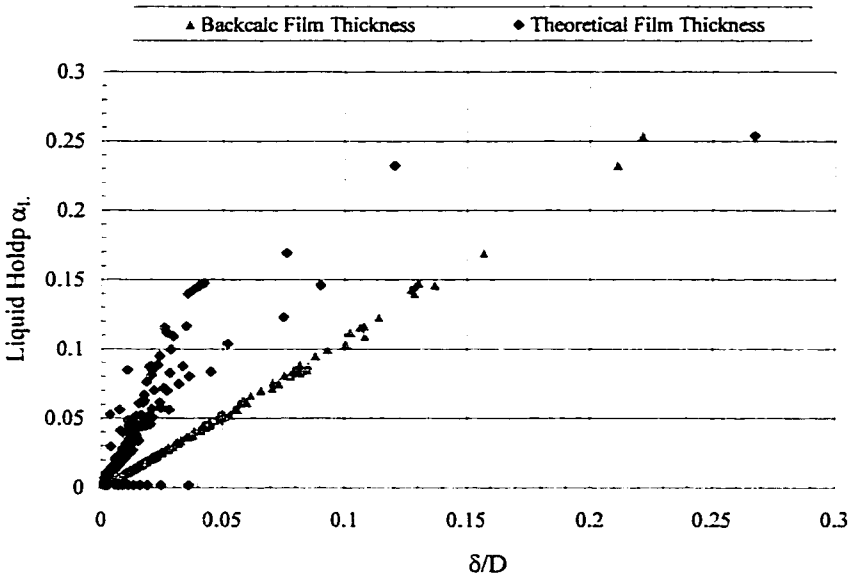

Figure 4.36 Film Thickness v/s Holdup Annular Flow
SMFD Dataset # 6

4.2.2. Pressure Gradient

Data Set # 6

Figure 4.37 shows the results for the pressure gradient comparisons between measured and calculated values. The Xiao model shows a poor agreement with the experimental data, with an average percentage error of 155% and a standard percentage deviation of 551% as shown in Table 4.4. Also, for values below 1 kPa/m the Xiao pressure gradient is almost constant. Also, the Xiao model overpredicts the pressure gradient in the region below 1 kPa/m, and underpredicts the pressure gradient in the region above 1 kPa/m. In order to clarify the validity of the data, the pressure gradient was also calculated using the experimental regressed liquid film ratio in the Xiao model. The results display a underestimated pressure gradient trend, as shown in Figure 4.37. The Oliemans pressure gradient was also plotted in Figure 4.35. It seems to show good agreement with the experimental pressure gradient up to 1 kPa/m, at which points it reaches

a maximum value and it continues with a decreasing trend. This lack of agreement between the models and the data could be attributed to poor quality of the coefficient for the liquid entrainment correlation.

Table 4.4 Statistical Comparison of Pressure Gradient Results for Annular Flow

Data Set	SU	No of Points	Model	ε_1	ε_2	σ
6	ALL	181	Xiao, FE-1	155.8	170.9	551.2
7	ALL	85	Xiao, FE-1	82.6	85.9	101.3
7	ALL	85	Xiao, FE-2	492.9	492.9	480.2
8	ALL	8	Xiao, FE-1	-45.2	45.2	6.1
8	ALL	8	Xiao, FE-2	101.4	145.0	209.2
9	ALL	176	Xiao, FE-1	228.0	299.3	282.9
9	ALL	176	Xiao, FE-2	480.1	480.8	1663.0

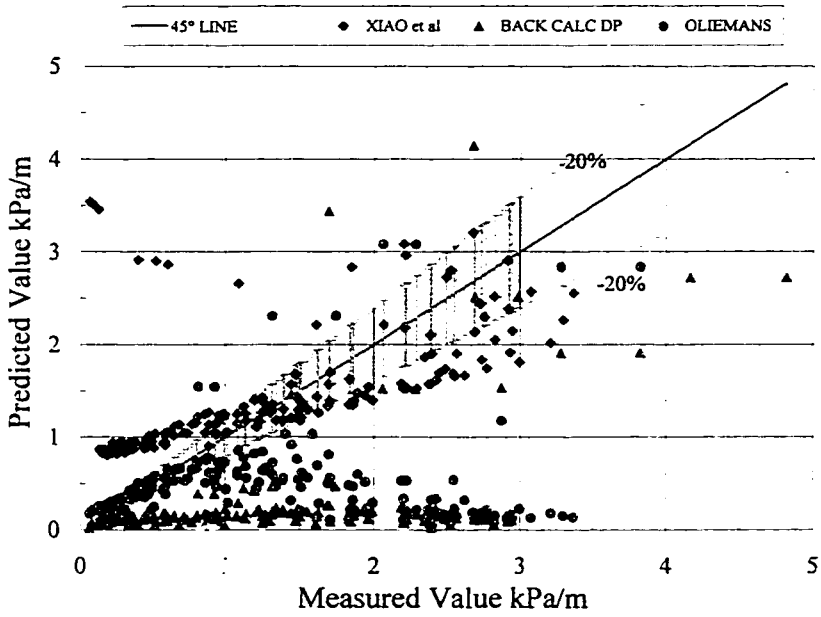

Figure 4.37 Pressure Gradient Annular Flow
SMFD Dataset # 6

Data Set # 7

As shown in Figure 4.27 all the data points are located at the annular-stratified regime transition boundary. Because this data set is located in the vicinity of this transition, within the error band, it should be considered valid for further analysis.

The pressure gradient for this data set exhibits similar performance to data set 6, as shown in Figure 4.38. Again, the Xiao and Oliemans pressure gradient show the wrong trend, with an average percentage errors of 83% and a standard percentage deviation of 101% as shown in Table 4.4. Moreover, the pressure gradient for the Xiao model was also computed using the liquid entrainment correlation of Wallis (1969) shown in Equation (2.159). The results obtained using the Oliemans liquid entrainment faction correlation were labelled FE-1, while the results obtained using Wallis liquid entrainment faction correlation were labelled FE-2. The results are extremely poor, with average percentage errors of 492% and a standard percentage deviation of 480% as shown in Table 4.4. This indicates the sensitivity of the Xiao pressure gradient model to the liquid entrainment fraction.

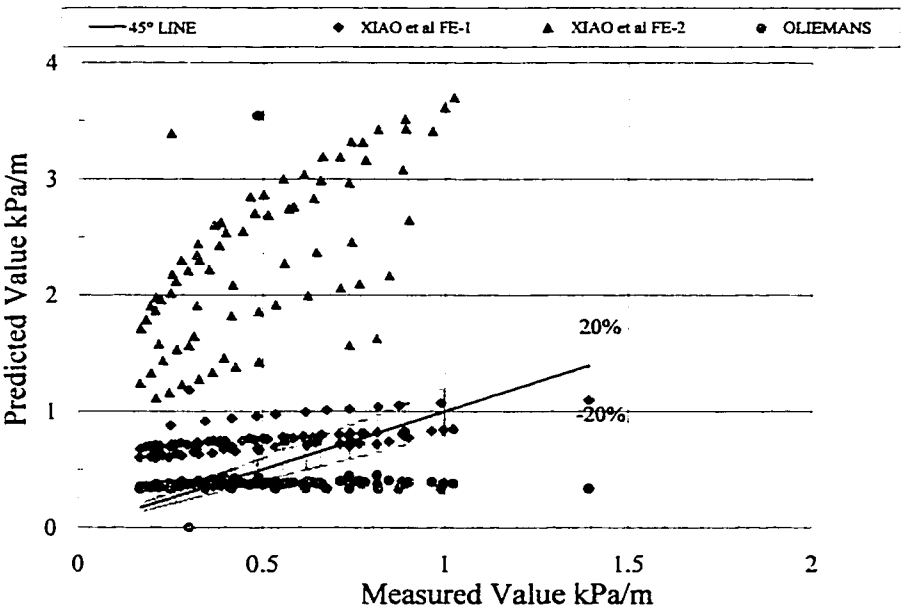

Figure 4.38 Pressure Gradient Annular Flow
SMFD Dataset # 7

Data Set # 8

Even though this data set has very few points, it has been included because it is field data. The fluid system is liquid–gas hydrocarbon at high pressures. This data set exhibits a similar performance to data sets 6 and 7 as shown in Figure 4.38. The Xiao model underpredicts the pressure drop with an average percentage error of -45% and a standard percentage deviation of 6% for the Oliemans liquid entrainment factor as shown in Table 4.4. The number of experimental data points is too small to perform any analysis or reach any conclusions.

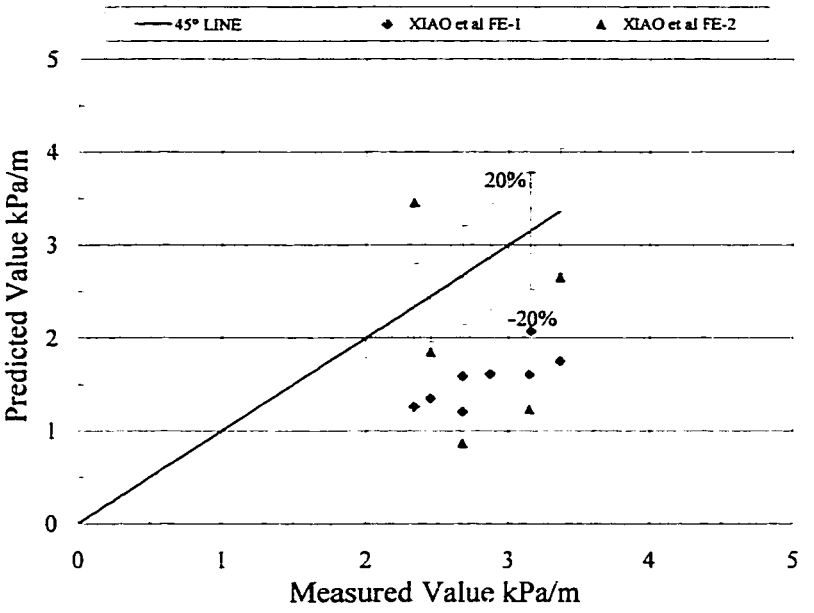

Figure 4.39 Pressure Gradient Annular Flow
SMFD Dataset # 8

Data Set # 9

Figures 4.2 and 4.3 show that most of the data is within the annular regime boundaries, except for a very few data points.

The same trends observed for the previous data sets are exhibited here. Both the Xiao and Oliemans models grossly underpredict the pressure gradient, while the Xiao model using the Wallis liquid entrainment correlation grossly overpredicts it. The Xiao model performed very poorly with average percentage errors of 228% and a standard percentage deviation of 282% as shown in Table 4.4. Figure 4.40 shows the comparison between the measured and the predicted pressure gradients.

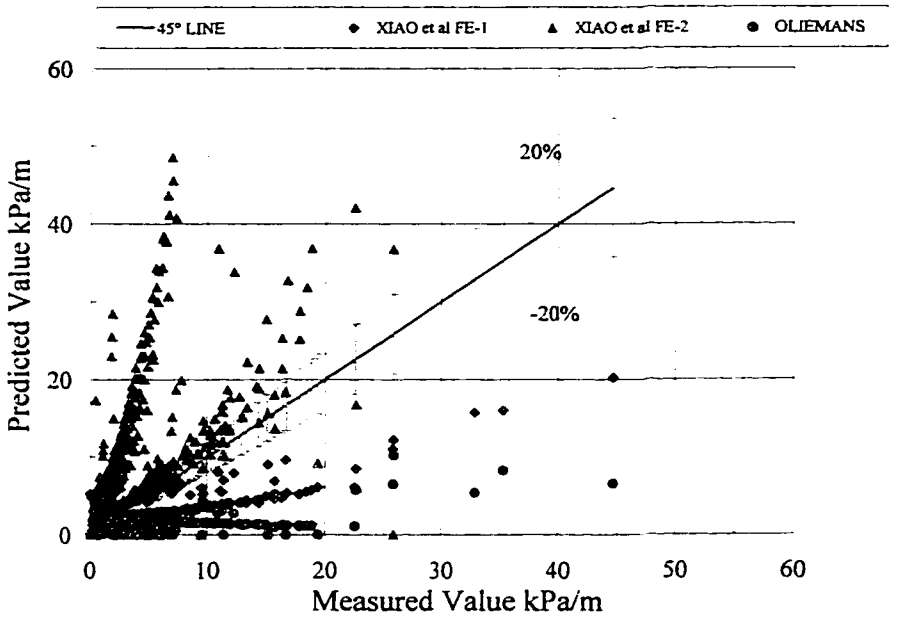

Figure 4.40 Pressure Gradient Annular Flow
SMFD Dataset # 9

4.3 Horizontal Slug Flow

4.3.1. Liquid Holdup

Data Set # 10

Figures 4.1, 4.2 and 4.3 show the flow regime map for this entire data set. Most of the data points are distributed between stratified and annular flow. As observed in these maps the liquid velocities are too low to fall within the intermittent flow regime transition. Nonetheless, most of the data is in the vicinity of the intermittent flow regime transition; hence, the analysis for this data was performed assuming that the data were valid.

Figure 4.41 shows the comparison between the measured liquid holdup and the liquid holdup predicted by the simplified Xiao model. The agreement between measured and predicted liquid

holdup is excellent, with an average percentage error of -3.3% and the standard percentage deviation is 25% as shown in Table 4.5. Most of the predicted liquid holdup is within the 20% error band. The large number of experimental data points validates this model for air-water systems with small pipe diameters. Unfortunately, it was not possible to test this model with other fluid systems because there was not liquid holdup data available in the database.

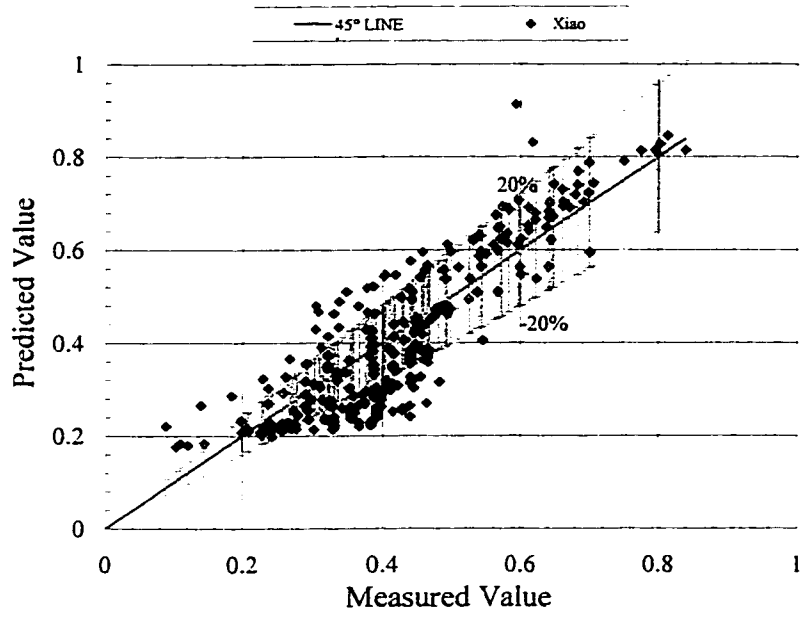

Figure 4.41 Holdup Slug Flow
SMFD Dataset # 10

Table 4.5 Statistical Comparison of Liquid Holdup Results for Slug Flow

Data Set	SU	No of Points	Model	ε_1	ε_2	σ
10	ALL	268	Xiao et al.	-3.3	19.2	25.0

4.3.2. Pressure Gradient

Data Set # 10

Figure 4.42 shows the comparison of measured pressure gradient and predicted results obtained with Xiao model. The agreement between measured and predicted pressure gradient is good in spite of the scatter of the data, with an average percentage error of 33% and the standard percentage deviation of 126% as shown in Table 4.6. Even though, the average percent error is positive due to greater positive deviations, the trend of this model is to underpredict the pressure gradient.

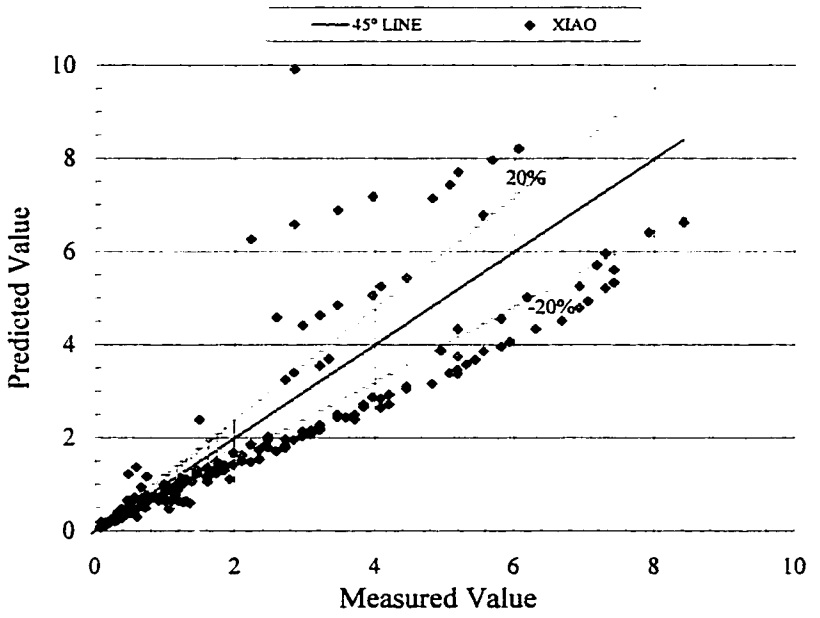

Figure 4.42 Pressure Gradient Slug Flow
SMFD Dataset # 10

Table 4.6 Statistical Comparison of Pressure Gradient Results for Slug Flow

Data Set	SU	No of Points	Model	ε_1	ε_2	σ
10	ALL	268	Xiao	33.1	59.1	126.0
11	ALL	108	Xiao	111.0	115.2	174.8

Data Set # 11

The fluid system for this data set is liquid and gas hydrocarbons obtained at field conditions as noted in Table 3.3. The agreement is poor, with an average percentage error of 111% and a standard percentage deviation of 175% as shown in Table 4.6. Most of the data is outside of the intermittent regime transition boundary, as shown in Figure 4.43, which could be the cause for this poor agreement.

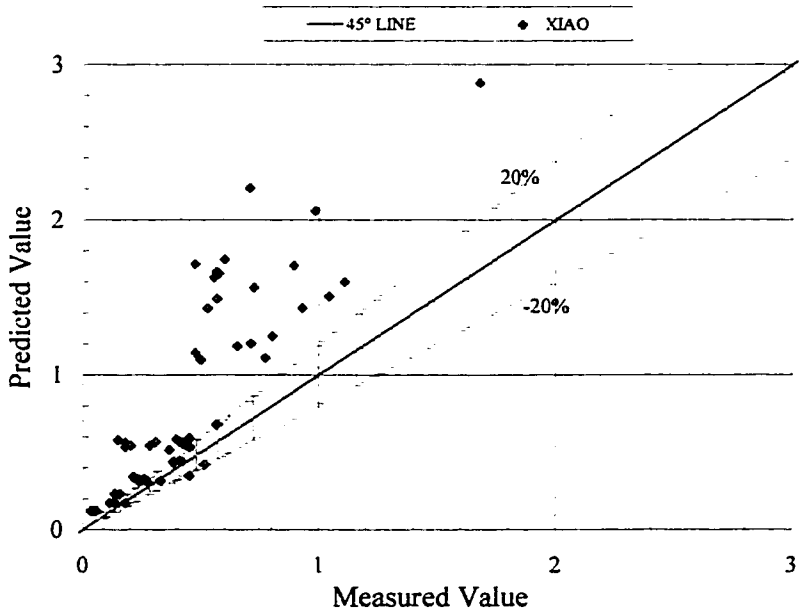

Figure 4.43 Pressure Gradient Slug Flow
SMFD Dataset # 11

4.4 Horizontal Bubble and Dispersed Bubble Flow

4.4.1. Liquid Holdup

Data Set # 12

Figures 4.2 shows the flow regime map for this entire data set. Most of the data points are distributed between stratified and annular flow. As observed in this map the liquid velocities are lower than would be required to fall within the bubble flow regime transition. Nonetheless, most of the data is in the vicinity of the bubble flow regime transition; therefore the analysis for this data was performed assuming that the data were valid.

Figure 4.44 shows the comparison of measured liquid holdup and predicted results obtained with Xiao model. The agreement between measured and predicted liquid holdup is good. Table 4.7 shows that the homogeneous model performed slightly better than the drift flux model. The homogeneous model exhibited an average percentage error of −18% and a standard percentage deviation of 29%, whereas the drift flux model results exhibited an average percentage error of 21.3% and the standard percentage deviation of 17.5%. Moreover, the measured and predictive liquid holdup were plotted against the Martinelly parameter as shown in Figure 4.45. The data is very scattered for X values below 20, after which the liquid holdup increases, rapidly with the Martinelly parameter. The difference between the liquid volume fraction and the predicted liquid holdup is large along the X values up to X=40, and converges asymptotically for X values greater than 40. The region for $X > 40$ is where the homogeneous flow assumption is valid. The value for the distribution parameter C_o constant, which normally fluctuates from 1.2 to 1.25, was found to be too large. When the value for this parameter was changed to 1.0 and the overall performance improved to an average percentage error of 12%, as shown in Table 4.7.

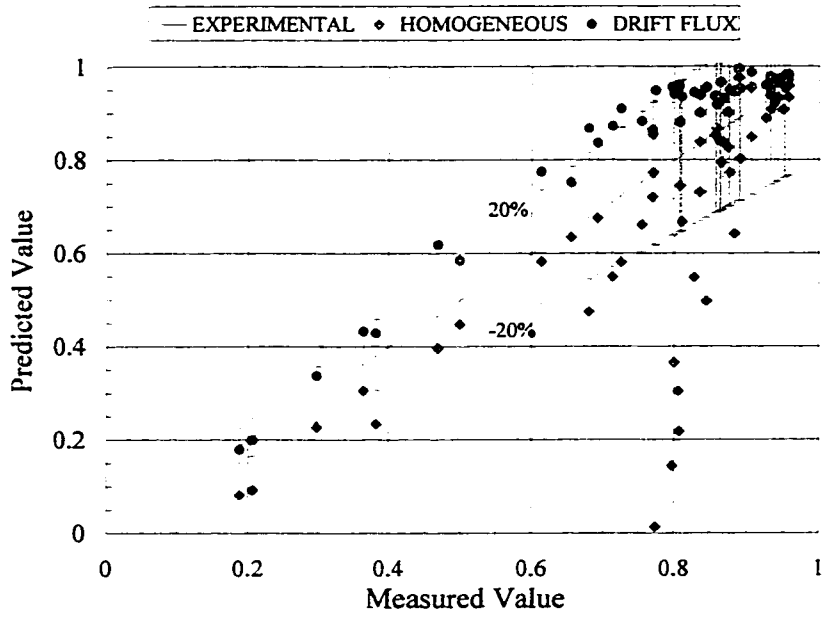

Figure 4.44 Holdup Bubble Flow
SMFD Dataset # 12

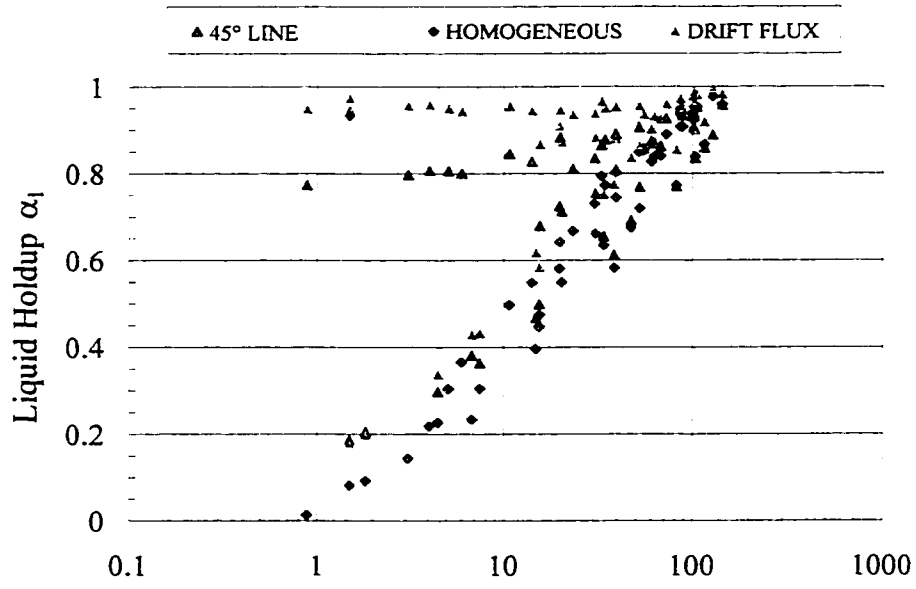

Figure 4.45 Liquid Holdup in Bubble Flow
SMFD Dataset # 12

Table 4.7 Statistical Comparison of Liquid Holdup Results for Bubble Flow

Data Set	SU	No of Points	Model	ε_1	ε_2	σ
12	ALL	62	Homogeneous	-17.8	18.5	29.2
12	ALL	62	Drift Flux Co =1.25	21.3	21.3	17.5
12	ALL	62	Drift Flux Co =1	11.9	12.4	10.3

4.4.2. Pressure Gradient

Data Set # 12

Figure 4.46 shows that the agreement between the predicted and measured values for the pressure gradient is very poor. As shown in Table 4.8 the average percent error for the pressure gradient is 35% for the Homogeneous model and 110% for the Drift Flux model.

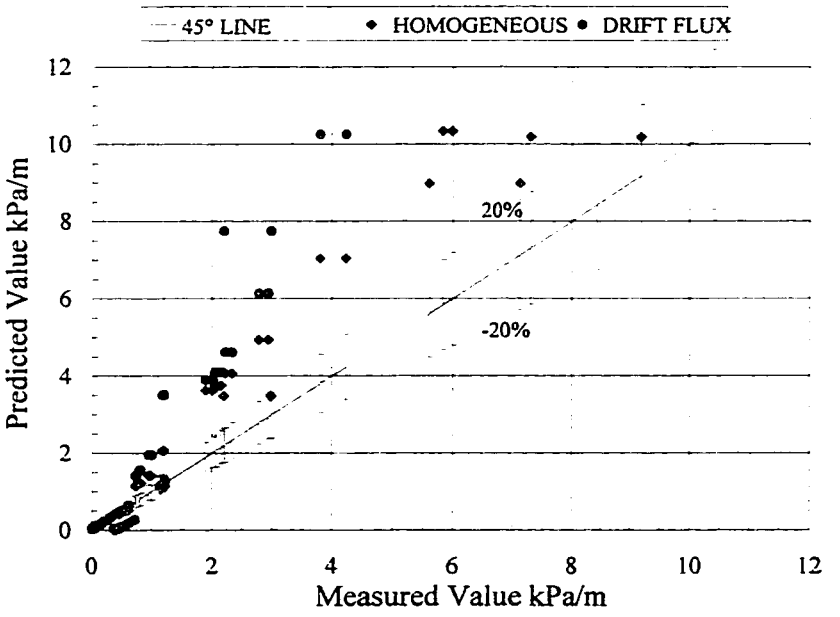

Figure 4.46 Pressure Gradient Bubble Flow
SMFD Dataset # 12

The homogeneous model performed better than the drift flux model, which is quite surprising considering that the data is not quite the bubble flow regime conditions were homogeneous flow applies. The drift velocity in the drift flux model tends to excessively increase the pressure gradient to account for bubble swirls, which is appropriate when in the fully developed bubble flow regime.

Table 4.8 Statistical Comparison of Pressure Gradient Results for Bubble Flow

Data Set	SU	No of Points	Model	ε_1	ε_2	σ
12	ALL	62	Homogeneous	35.3	85.7	151.1
12	ALL	62	Drift Flux	109.8	157.1	229.4
13	ALL	145	Homogeneous	94.9	123.2	392.4
13	ALL	145	Drift Flux	587.7	597.5	1258.7

Data Set # 13

Figure 4.47 shows the flow regime boundaries for this data set. Most of the data points are well below the bubble flow regime transition. Therefore, this data set is considered faulty and was not used for further analysis.

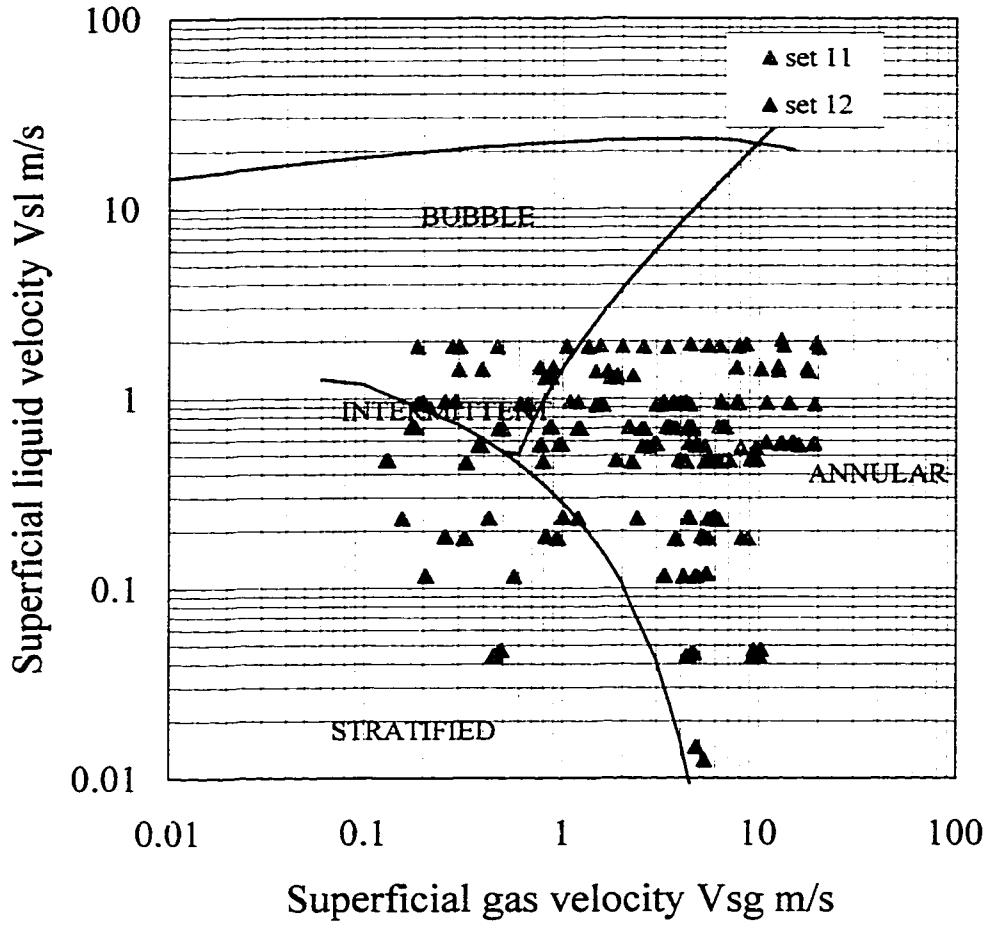

Figure 4.47 Flow Pattern Map
Data Sets # 11 SU-109-110

4.5 Vertical Annular Flow

4.5.1. Liquid Holdup

Data Set # 14

As shown in Figure 4.48 most of the data is within the annular flow regime boundaries. Thus, this data set is valid for further analysis.

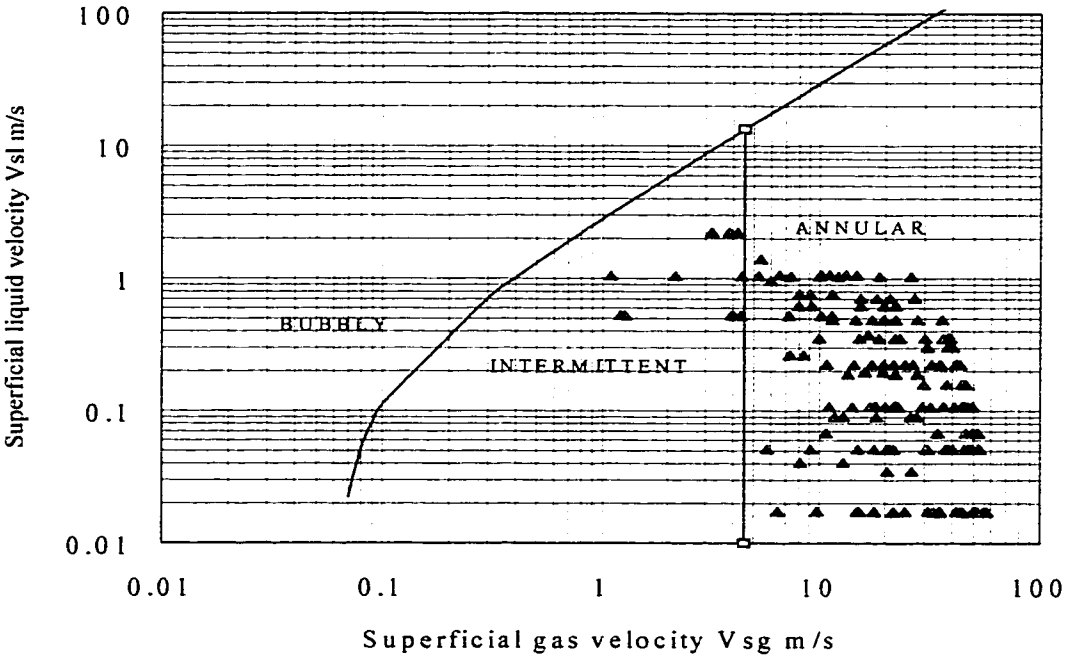

Figure 4.48 Flow Pattern Map
Flow Data Sets # 14 SU-203

Figure 4.49 shows a comparison between the measured liquid holdup and the calculated holdup using the Rajan et al. (1996) and Oliemans (1986) methods. The Oliemans model agreement is good with an average percentage error of 31% and a standard deviation of 93% as shown in Table 4.9. Even though there is some scatter of the predicted values, there is also a defined trend that follows the 45° line. The Rajan et al. model underpredicts the liquid holdup, with an average percentage error of -18.2% a standard deviation of 168%. This artificially low average percentage error in the Rajan et al. model is probably due to the mutual cancellation of the positive and negative deviations that are scattered over the measured range. Note, that the Oliemans correlation for liquid entrainment factor, Equation (2.116), was used for predicting the liquid holdup for the Rajan model, since the Wallis correlation, Equation (2.159), which Rajan recommended yielded too many negative values. The results obtained from the Rajan model were unsatisfactory. It was expected that this model, which accounts for liquid entrainment, would perform better than the Oliemans model. On the other hand the good agreement obtained with the Oliemans model was surprisingly remarkable and coincides with the results obtained for horizontal annular flow.

Table 4.9 Statistical Comparison of Liquid Holdup Results for Annular Flow

Data Set	SU	No of Points	Model	ε_1	ε_2	σ
14	ALL	196	Oliemans	-18.2	90.3	167.8
14	ALL	196	Rajan	31.1	37.4	93.4

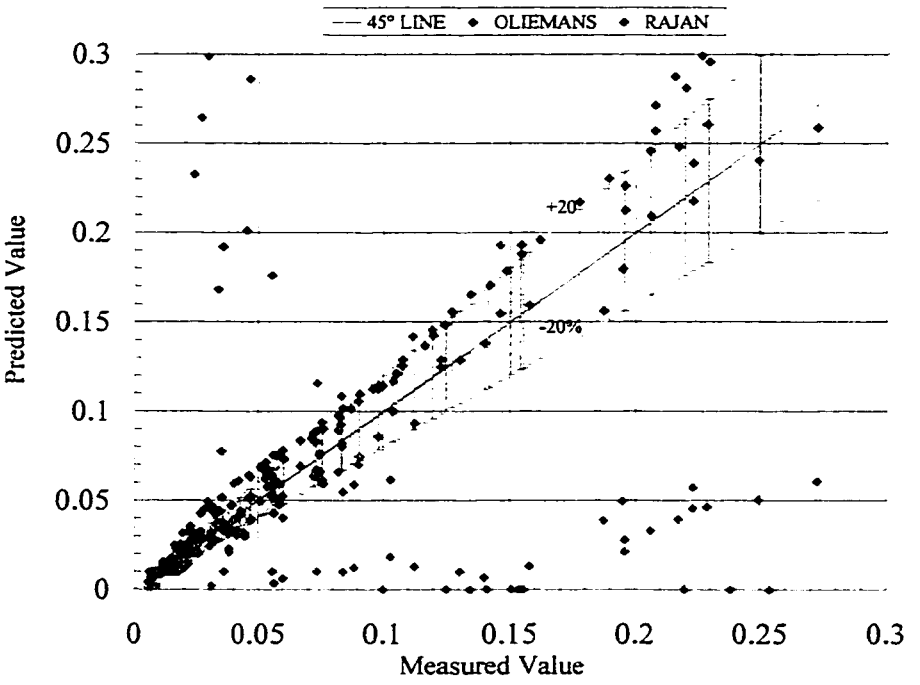

Figure 4.49 Holdup Annular Flow
SMFD Dataset # 14

4.5.2. Pressure Gradient

Data Set # 14

Figure 4.50 shows the results for the pressure gradient comparisons between measured and calculated values. The Oliemans model shows a very poor agreement with the experimental data, with an average percentage error of 625% and a standard percentage deviation of 1695% as shown in Table 4.10. The Rajan model shows a poor agreement also with an average percentage error of -96% and a standard percentage deviation of 1284%. The large scatter of the predicted values makes it impossible to postulate any trends. This lack of agreement between the models and the data could be attributed to faulty data for pressure gradient.

Table 4.10 Statistical Comparison of Pressure Gradient Results for Annular Flow

Data Set	SU	No of Points	Model	ε_1	ε_2	σ
14	ALL	196	Oliemans	625.8	654.8	1694.8
14	ALL	196	Rajan	-96.2	437.8	1284.4

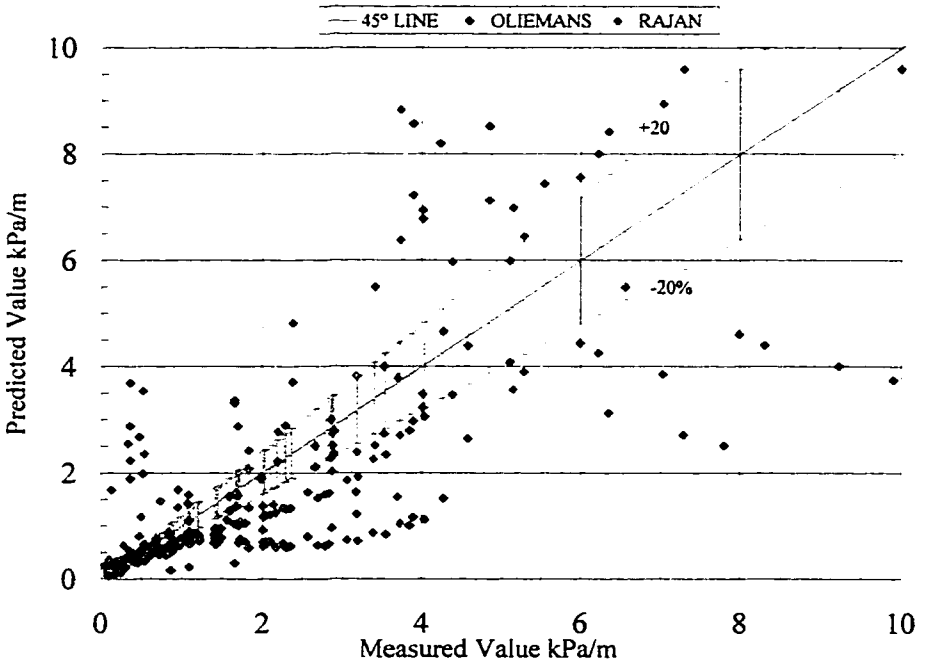

Figure 4.50 Pressure Gradient Annular Flow
SMFD Dataset # 14

4.6 Vertical Slug Flow

4.6.1. Liquid Holdup

Data Set # 15

As shown in Figure 4.51 all of the data are within the intermittent (slug) flow regime boundaries. The intermittent pattern is usually subdivided into elongated bubble, slug and froth-churn flow. A transition from slug to froth-churn flow is assumed to occur when the liquid holdup in the slug cylinder becomes less than 0.48. When the gas holdup within this liquid slug reaches the maximum bubble volumetric packing, the continuity of the liquid slug is destroyed by bubble agglomeration resulting in transition to churn flow.

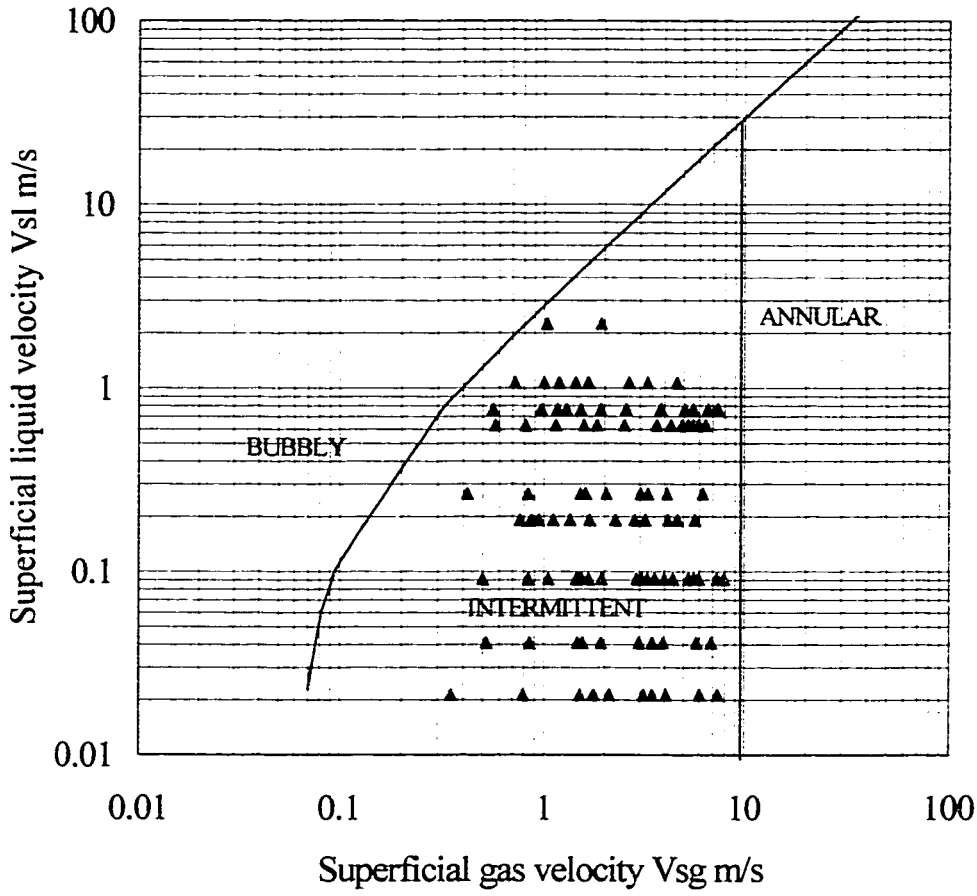

Figure 4.51 Flow Pattern Map
Flow Data Sets # 15 SU-66

Figure 4.52 shows a comparison for the measured liquid holdup with the predicted liquid holdup from Ansari model. The agreement of the Ansari et al (1994) model with the measured data is excellent with all the valid points within the ± 20 percent error band. The average percentage error was 1.4% and the standard percentage deviation was 32% as shown in Table 4.11. The good performance shown by the Ansari model confirms the validity of the liquid holdup data. It is surprising that a simple model, which uses empirical relationships for the Taylor bubble velocity, the slug length and the void fractions, could produce such good results.

Table 4.11 Statistical Comparison of Liquid Holdup Results for Slug Flow

Data Set	SU	No of Points	Model	ε_1	ε_2	σ
15	66	97	Ansari-94	1.4	18.0	32.0

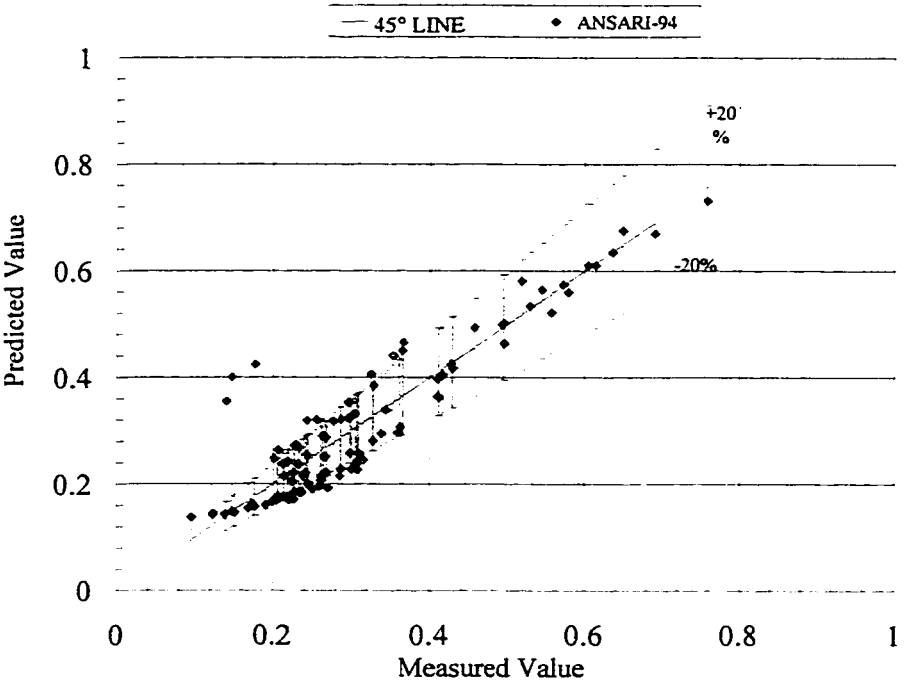

Figure 4.52 Holdup Slug Flow
SMFD Dataset # 15

4.6.2. Pressure Gradient

Data Set # 15

Figure 4.53 shows the comparison of measured pressure gradient and that predicted by the Ansari model. The agreement between measured and predicted pressure gradient is good in spite of the scatter, with an average percentage error of -31% and the standard percentage deviation of 39% as shown in Table 4.12. This model tends to underpredict the pressure gradient. This underprediction of the pressure gradient could be explained by the acceleration pressure gradient that was neglected by the Ansari model assuming fully developed stable slug flow. This acceleration pressure gradient becomes a significant factor for non stable slug flow or froth-churn

flow. Nonetheless, the agreement is fairly good and is within the accuracy required for engineering calculations. Unfortunately, without testing systems other than the laboratory air-water mixtures available, more general conclusion can not be substantiated.

Table 4.12 Statistical Comparison of Pressure Gradient Results for Slug Flow

Data Set	SU	No of Points	Model	ε_1	ε_2	σ
15	66	97	Ansari-94	-30.6	34.1	39.4

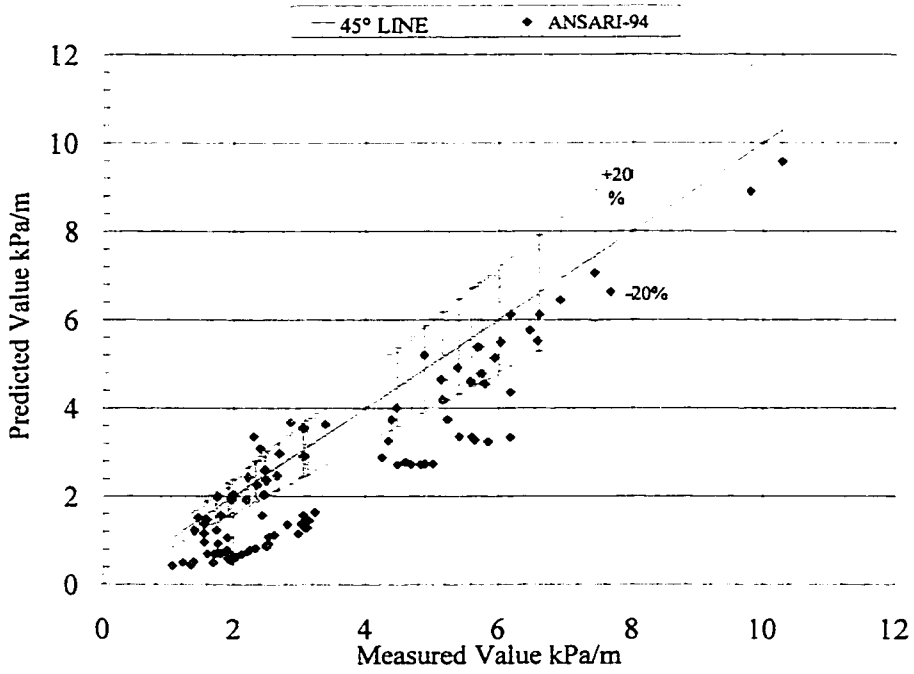

Figure 4.53 Pressure Gradient Slug Flow
SMFD Dataset # 15

4.7 Vertical Bubbly Flow

4.7.1. Liquid Holdup

Data Set # 16

Figures 4.54 shows the flow regime map for this data set of the data is within the bubbly flow regime boundaries, with the exception of a few data points located at the vicinity of the bubbly flow regime transition. Therefore, the analysis for this data was performed assuming that the data is valid.

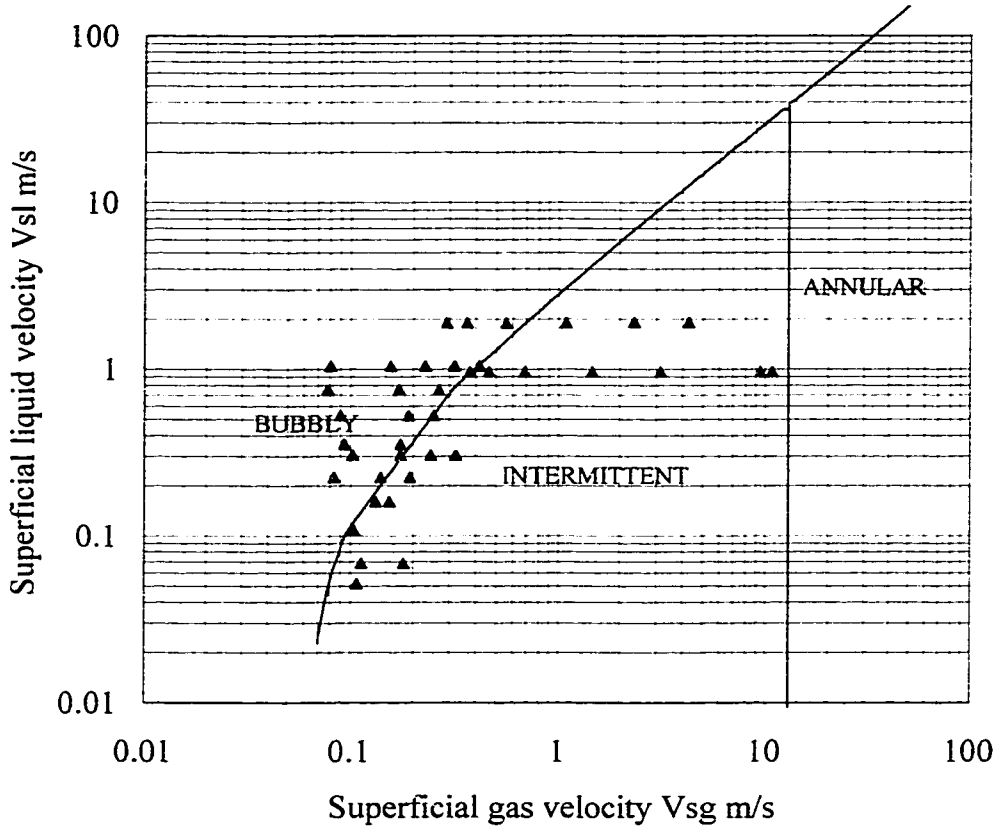

Figure 4.54 Flow Pattern Map
Flow Data Sets # 16 SU-204

Figure 4.56 shows the comparison of measured liquid holdup and predicted results obtained with the Ansari's (1994) and the Homogenous model. The agreement between measured and predicted liquid holdup is fairly good. Table 4.13 shows that Ansari's drift-flux model performed slightly better than the homogeneous model with an average percentage error of –8% and a standard percentage deviation of 18%, whereas the homogeneous model had an average percentage error of 14% and the standard percentage deviation of 88%. This validates the quality of the data, since bubbly flow is probably the simplest flow regime model, and therefore the easiest one to model accurately. The trends showed by these models are that the Ansari model slightly overpredicts the liquid holdup, whereas the homogeneous model underpredicts it. Two values were used for the coefficient n in Equation (2.145) for liquid holdup, 0.1 and 0.5, respectively. Both values gave almost identical results.

Table 4.13 Statistical Comparison of Liquid Holdup Results for Bubbly Flow

Data Set	SU	No of Points	Model	ε_1	ε_2	σ
16	ALL	39	Ansari-94	-8.1	13.4	18.4
16	ALL	39	Homogeneous	-14.2	73.3	88.2

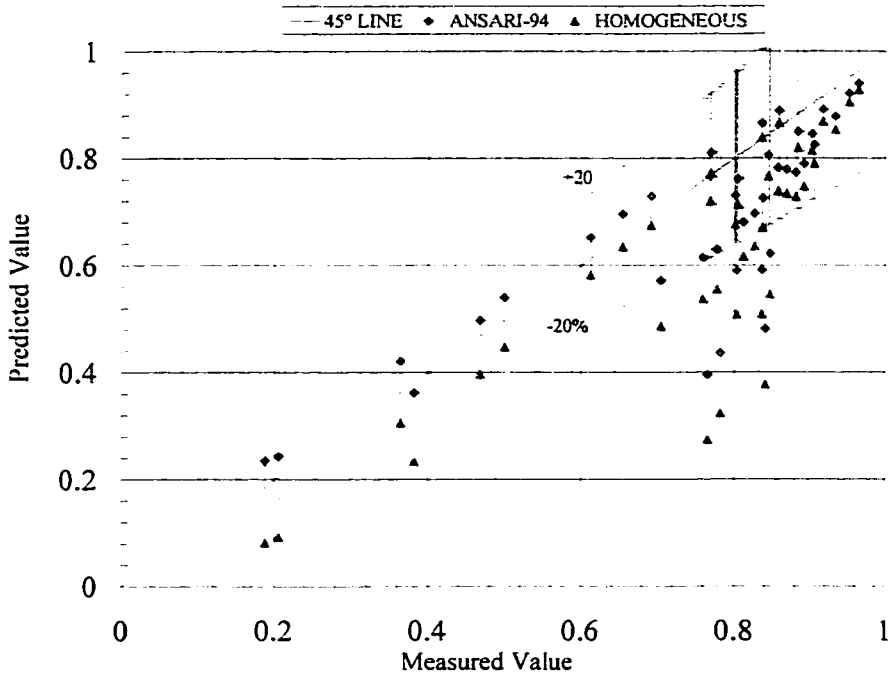

Figure 4.55 Holdup Bubbly Flow
SMFD Dataset # 16

4.7.2. Pressure Gradient

Data Set # 16

Figure 4.57 shows that the agreement between the predicted and measured values for the pressure gradient is very poor. As shown in Table 4.14 the average percent error for the pressure gradient is 79% for the Ansari (1994) model and -99% for the homogeneous model. For the pressure gradient range between 0 and 1.0, the homogeneous model predicted very low pressure gradient values. The corresponding superficial gas velocity is lower than the liquid, which invalidates the bubbly flow regime assumption. It should be noted that all the data points, which match this condition, are outside the bubbly flow regime boundary.

Table 4.14 Statistical Comparison of Pressure Gradient Results for Bubble Flow

Data Set	SU	No of Points	Model	ε_1	ε_2	σ
16	ALL	39	Sylvester-94	78.7	110.9	226.0
16	ALL	39	Homogeneous	-99.4	99.4	51.3

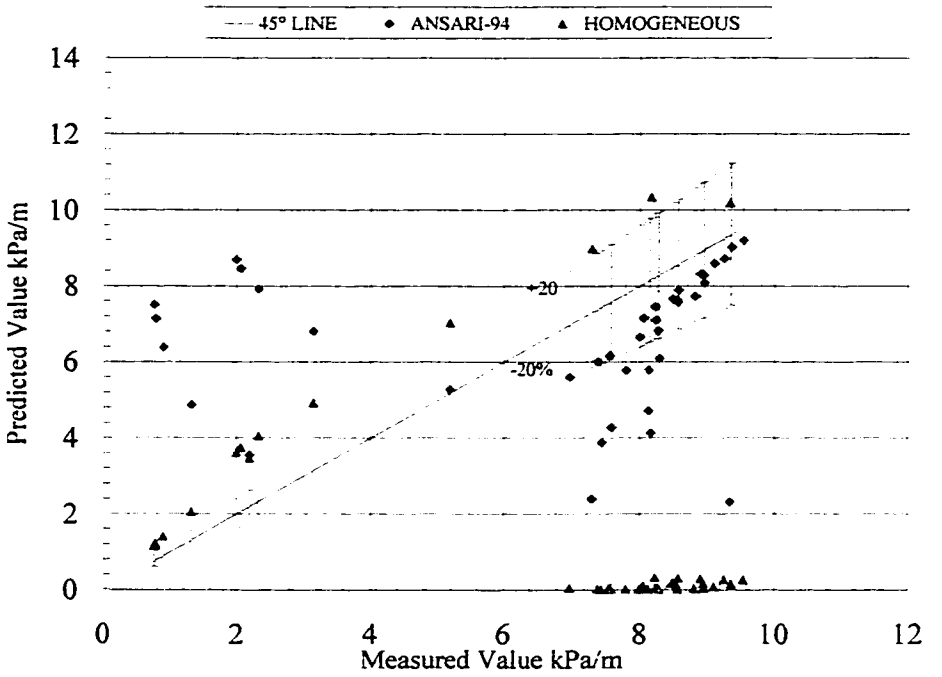

Figure 4.56 Pressure Gradient Bubbly Flow
SMFD Dataset # 16

4.8 Summary

This chapter presented the results for the testing of the mechanistic models under evaluation for horizontal and vertical flow. The flow regimes included stratified, annular, slug, bubble, and bubbly flow. The data collected from the Stanford database was screened using flow regime

transition maps. The majority of the data was found to be inside the boundaries of the flow regime recorded in the database, with the exception of bubble and bubbly flow regime. It is shown that, in general the models reduced well to simple air-water, small diameter systems. Out of the two variables under evaluation, liquid holdup, and pressure gradient, the former was predicted with better accuracy by all the models. However, the performance of the pressure gradient models, for vertical and horizontal flow, was inferior. The pressure gradient model for annular flow was found to be unacceptably inaccurate.

Chapter 5
CONCLUSIONS AND RECOMMENDATIONS

5.1 Conclusions

The purpose of this research project was to evaluate the performance of mechanistic models for the prediction of liquid holdup and pressure gradient. Several data sets from the Stanford database covering the main flow regimes for horizontal and vertical flow were tested. The liquid holdup and pressure gradient data from these data sets were compared with prediction from well accepted models. Based on the results obtained from these comparisons the following conclusions can be made.

The liquid holdup for stratified flow was compared against the Taitel and Dukler (1976) and the Oliemans (1986) models. The Oliemans model yielded slightly better results than the Taitel and Dukler model, for horizontal flow and inclined flows. It was also found that the liquid holdup is a strong function of the f_i/f_{sg} ratio. The data tested consisted mainly of air-water mixtures flowing in small pipes at low pressures. Thus, the models are adequate for the prediction of liquid holdup for these types of systems. However, the models for horizontal flow should be independently tested. Testing should be done for hydrocarbon fluid systems flowing in large diameter pipelines at high pressures, with known physical properties, and sufficient liquid holdup and frictional pressure gradient data points, to emphasize the models.

The liquid holdup was found to be sensitive to inclination angle. The Oliemans model predicted the liquid holdup fairly well in upward inclined flow, whereas the Taitel and Dukler model did not.

Out of all the data sets tested, including a hydrocarbon fluid mixture operating at high pressure, the pressure gradient predicted by the Oliemans method yielded better results than the Taitel and Dukler model, probably due to its flow dependent interfacial friction

factor correlation. The low constant value for the interfacial holdup used by the Taitel and Dukler model resulted in trends that underpredicted when compared to the measured data.

Annular flow is the flow regime where the level of understanding is the least satisfactory. The mechanisms are not clear and the extent of basic modelling is still very limited. The measured liquid holdup for annular flow in a horizontal pipe was compared against the Xiao et al (1990) and Oliemans (1986) models. The predictions obtained with the Oliemans model were excellent, whereas the Xiao model yielded poor results for all the data sets tested. This lack of agreement from the Xiao model was attributed to the liquid entrainment correlation, which was developed for vertical flow. The regression coefficients for this liquid entrainment correlation should be correlated with horizontal entrainment data to improve the model. None of these models could accurately predict the pressure gradient. The liquid entrainment correlations of Wallis (1969) and Oliemans (1986) were used for testing in the Xiao et al (1990) model, it was found that the Wallis correlation grossly overpredicts the pressure gradient.

The results obtained for the liquid holdup predictions using the Xiao et al (1990) simplified model for slug flow regime were very good. Unfortunately, only air-water data was found in the Standford database for testing. The pressure gradient predictions were not as good, the air-water mixture tested showed underpreding trend for the pressure gradient, while the hydrocarbon-hydrocarbon field data tested showed an overpredicting trend.

The bubble flow regime data tested was not completely within the bubble flow regime transition boundaries. The Xiao (1990) version of the drift flux model and a simple homogeneous model yielded good liquid holdup predictions. However, both of them poorly predicted the pressure gradient. Probably due to faulty data since this is the simplest flow regime to model when the assumption for homogeneous flow holds.

For vertical annular flow the liquid holdup results were similar to those obtained for

horizontal flow. The Olieman model outperformed the more mechanistic Rajan et al. (1996) model, however, the pressure gradients predictions with both models were very poor.

For vertical slug flow the experimental liquid holdup was compared to the Ansari et al. (1994) model. The agreement found was excellent, which was surprising for a model which depends on empirical correlations for its closure relationships. The pressure gradient results were fairly good in spite of some slightly underprediction of the measured data. The performance of this model is quite remarkable, considering that the acceleration gradient was neglected and that most of the data points were in the churn flow regime, rather than the slug flow regime being studied. This verifies the good extrapolating capabilities of the model.

The Ansari et al. (1996) model for vertical bubbly flow showed similar trends to the horizontal counterpart. The liquid holdup yielded good agreement between measured and predicted data, while the pressure gradients predictions were very poor.

In summary, there seems to be a consistent trend, which indicates that the pressure gradient is a weak function of liquid holdup. Most of the liquid hold up prediction are probably accurate for design purposes, which is the ultimate goal of modeling. The pressure gradient models, on the other hand did not performed as well as expected, only the models for stratified flow and slug flow (horizontal and vertical) are accurate enough to be used for design purposes. The quality of the data is questionable for some flow regimes, since a large portion of the data was found to be outside of the flow regime for which it was classified in the database.

5.2 Recommendations and Future Work

The effect of the predicted fluid properties on liquid holdup and pressure gradient was not considered in this work. Future work should include a parametric study of the effect of fluid viscosity, density and surface tension, as well as the empirical parameters on liquid holdup and pressure gradient predictions models. Thus, determining the relative weight of these parameters in the models, and consequently focusing the research on improvements to areas where progress could be maximised.

The current Stanford Multiphase Flow database is mainly composed of water-air systems at low pressures in small diameter pipes. The data should be enlarged to include compositional data in large diameter pipes at high pressures. This would permit extension of the models to real field situations.

Further theoretical analysis of two-phase flow should aimed at eliminating the empiricism involve in the current models used to predict liquid hold and pressure gradients.

Bibliography

Agrawal, S.S., "Horizontal Two Phase Stratified Flow in Pipes," M.Sc. Thesis, University of Calgary, Calgary (1971).

Agrawal, S.S., G.A. Gregory and G.W.Govier, "An Analysis of Horizontal Stratified Two-Phase Flow in Pipes," Can. J. Chem. Eng., 51, 280-286 (1973).

Ansari, A.M., and Sylvester, N.D., "A Mechanistic Model for Two-Phase Bubble Flow in Vertical Pipes", AIChE J., Vol. 34, No. 8, (1988).

Ansari, A.M., Sylvester, N.D., Shoham, O., and Brill, J.P., "A Comprehensive Mechanistic Model for Upward Two-Phase Flow in Wellbores," SPE Prod. & Facilities 151-165 (1990).

Ansari, A.M., Sylvester, N.D., Sarica, C., Shoham, O., and Brill, J.P., "A Comprehensive Mechanistic Model for Upward Two-Phase Flow in Wellbores," SPE Prod. & Facilities 143-152 (1994).

Aziz, K., Govier, G.W., and Fogarasi, M., "Pressure Drop in Wells Producing Oil and Gas, "J. Can. Pet. Tech., 38-47, (1972).

Baker, O., "Simultaneous Flow of Oil and Gas," Oil Gas J., 53, 185-190 (1954).

Baker, O., "Effect of Hills on Two-Phase Pressure Drop," Oil Gas J., 55, 150-152, November 11 (1957).

Baker, O., "Experience with Two-Phase Pipelines," Canadian Oil and Gas Industries, 14, 43-53 (1961).

Baker, A., Nielsen, K. and Gabb, A.: "Pressure Loss, Liquid Holdup Calculations Developed, " Oil & Gas J., 55-59 (March 14, 1988).

Barnea, D., O. Shoham and Y. Taitel, "Flow Pattern Transitions for Gas-Liquid Flow In Horizontal and Inclined Pipes: Comparison of Experimental Data With Theory, "Int. J. Multiphase Flow, 6, 217-225 (1980a).

Barnea, D., O. Shoham and Y. Taitel, "Flow Pattern Transitions for Vertical Down-Ward Two Phase Flow, "Chem.Eng. Sci., 37, 741-746 (1982a).

Barnea, D., O. Shoham and Y. Taitel, "Flow Pattern Transition for Downward Inclined Two Phase Flow: Horizontal to Vertical, "Chem. Eng. Sci., 37, 735-740 (1982b).

Barnea, D., O. Shoham and Y. Taitel, "Gas Liquid Flow in Inclined Tubes; Flow Pattern Transitions for Upward Flow," Chem. Eng. Sci., 40, 131-136 (1985).

Barnea, D. and N. Brauner, "Holdup of Liquid Slug in Two Phase Intermittent Flow," Int.J. Multiphase Flow, 11, 43-49 (1985).

Barnea, D., "Transition from Annular Flow and from Dispersed Bubble Flow–Unified Models for the Whole Range of Pipe Inclinations,"Int.J. Multiphase Flow , 12, 733-744 (1986).

Barnea, D., "A Unified Model for Predicting Flow-Pattern Transitions for the Whole Range of Pipe Inclinations," Int. Journal Multiphase Flow, No. 13, 1-12 (1987).

Barnea, D., Y. Taitel, "Structural and Interfacial Stability of Possible Solutions For Stratified Flow," Int. Journal of Multiphase Flow, Vol. 18, No. 16, (1992).

Baroczy, C.J., "A Systematic Correlation for Two-Phase Pressure Drop," Chem. Eng. Prog. Symp. Ser., 62, 232-249 (1965).

Beggs, H.D. and J.P. Brill, "A Study of Two Phase Flow in Inclined Pipes, " J.Pet. Technol, 25, 607-617 (1973).

Brill, J.P., Beggs, H. "Two-Phase Flow in Pipes", 6th Edition, January 1991.

Bendiksen, K. H., "An Experimental Investigation of the Motion of Long Bubbles in Inclined Tubes," Int. Journal Multiphase Flow 10, No. 4, 467-483 (1984).

Brown, R.A.S., G.A. Sullivan and G.W. Govier, "The Upward Vertical Flow of Air-Water Mixtures – III Effect of Gas Phase Density on Flow Patterns, Holdup and Pressure Drop," Can. J. Chem. Eng., 38, 62-66 (1960).

Browne, E.J.P., "Practical Aspects of Predicting Errors in Two-Phase Pressure Loss Correlations," SPE Paper 5000, presented at the 49th Annual SPE Fall Meeting, Houston, Texas (1974).

Chawla, J.M., "Friction Pressure Drop in Flow of Liquid-Gas Mixtures in Horizontal Pipes," Forsch. Ingenieurwes., 34, 53 (1968).

Chisholm, D., "A Theoretical Basis for the Lockhart-Martinelli Correlation for Two-Phase Flow," Int. J. Heat Mass Transfer, 10, 1767 – 1778 (1967).

Churchill, S.W. (1977) Chem. Eng., 91-92, Nov. 1991

Cohen, L.S. and T.J. Hanratty, "Effect of Waves at a Gas-Liquid Interface on a Turbulent Air Flow," J. Fluid Mechanics, 3, 467 – 479 (1968).

Colebrook, C.F. and White, C.M. J. Inst. Civil Engineers , London, 11(133), (1939).

Corteville, J., Lagiere M. & Roux A. 1983 Designing and Operating Two-Phase Oil and Gas Pipelines Preprint of the 11th World Petroleum Congress, London, SP 10 (1983).

Danesh, A., "Discussion of Evaluation of Inclined-Pipe Two-Phase Liquid Holdup and Pressure Loss Correlations Using Experimental Data," J. Pet. Technol., 32, 169-170 (1980).

Davidson, J.F. and O.G. Schuler, "Bubble Formation at an Orifice in an Inviscid Liquid," Trans. Inst. Chem. Engrs., 38, 335 – 342 (1960).

Davies, R.M., and Taylor, G.I., "The Mechanics of Large Bubbles Rising Through Extended Liquids and Through Liquids in Tubes," Proc. Roy. Soc. A200, 375 (1950).

Dukler, A.E., M. Wicks III and R.G. Cleveland, "Frictional Pressure Drop in Two-Phase Flow: B. An Approach Through Similarity Analysis," AIChE J., 10, (1964).

Dukler, A. E. and M.G. Hubbard, "A Model for Gas-Liquid Slug Flow in Horizontal and Near Horizontal Tubes," Ind. Eng. Chem. Fundam., 14, 337-347 (1975).

Dukler, A.E. and Y. Taitel, "Flow Patterns in Horizontal and Near Horizontal Pipes", Design Manual FM-3, DIMP/AIChE, New York, (1982).

Dukler, A.E. and Y. Taitel, "Flow Patterns for Steady Upward Gas-Liquid Flow in Vertical Tubes", Design Manual VUFP-1, DIMP/AIChE, New York, (1984).

Dukler, A.E., D.M. Maron and N. Brauner, "A Physical Model for Predicting the Minimum Stable Slug Length," Chem. Eng. Sci., 40, 1379 – 1385 (1985).

Duns Jr., H. and N.C.J. Ros, "Vertical Flow of Gas and Liquid Mixtures from Boreholes, "Proceedings of the 6th World Petroleum Congress, Section 2, Paper 22, Frankfurt (1963).

Eaton, B.A., D.E. Andrews, C.R. Knowles, I.H. Silberberg and K.E. Brown, "The Prediction of Flow Patterns, Liquid Holdup and Pressure Losses Occurring During Continuous Two-Phase Flow in Horizontal Pipelines, " J. Pet. Technol., 19, 815-828 (1967).

Ellis, S.R.M. and B. Gay, "The Parallel Flow of Two Fluid Streams: Interfacial Shear and Fluid-Fluid Interaction," Trans. Inst. Chem. Engrs., 37, 206 (1959).

Espanol, J.H., C.S. Holmes and K.E. Brown, "A Comparison of Existing Multiphase Flow Methods for the Calculation of Pressure Drop in Vertical Wells,: SPE Paper 2553 presented at the 1969 SPE Annual Meeting, Denver (1969).

Fernandes, R.C., R. Semiat and A.E. Dukler, "Hydrodynamic Model for Gas-Liquid Slug Flow in Vertical Tubes," AIChE J., 29, 981-989 (1983).

Flanigan, O., "Effect of Uphill Flow on Pressure Drop in Design of Two-Phase Gathering Systems," Oil Gas J., 56, 132-141, March 10 (1958).

Govier, G.W., B.A. Radford and J.S.C. Dunn, "The Upward Vertical Flow of Air-Water Mixtures: I Effect of Air and Water Rates on Flow Patterns, Holdup and Pressure Drop," Can. J. Chem. Eng., 35, 58 (1957).

Govier, G.W. and M.M. Omer, "The Horizontal Flow of Air-Water Mixtures," Can. J. Chem. Eng. 40, 93-104 (1962).

Govier, G.W. and K. Aziz, The Flow of Complex Mixtures in Pipes, Van Nostrand Reinhold Company, New York (1972).

Gregory, G.A., "Comments on the Prediction of Liquid Holdup for Gas-Liquid Flow in Inclined Pipe," Can. J. Chem. Eng., 13, 463-467 (1974)

Gregory, G.A., "Comparison of Methods for the Prediction of Liquid Holdup for Upward Gas-Liquid Flow in Inclined Pipes," Can. J. Chem. Eng., 14, 384-388 (1975).

Gregory, G.A., Nicolson, M.K. and Aziz, K., "Correlation of the Liquid Volume Fraction in the Slug for Horizontal Gas-Liquid Slug Flow", Int. J. Multiphase Flow 4, 33-39, (1978).

Gregory, G.A. , M. Fogarasi and K. Aziz,, "Analysis of Vertical Two-Phase Flow Calculations: Crude Oil-Gas Flow in Well Tubing," J.Can. Pet. Technol., 19, 86-91 (1980).

Gregory, G.A. , M. Fogarasi, Mattar, L. and K. Aziz,, "Multiphase Flow in Pipes and Its Applications to Production and Transportation of Oil and Gas", Course Notes, Dept. of Chemical Engineering, University of Calgary, April 1980.

Gregory, G.A. , and M. Fogarasi , "A Critical Evaluation of Multiphase Gas-Liquid Pipelines Calculation Methods" proceedings of 2nd International Conference On Multi-Phase Flow, London, 93-108, June 1985.

Griffith, P. and G.B. Wallis, "Two-Phase Slug Flow," J. Heat Transfer, 83, 307-320 (1961).

Hagedorn, A.R. and K.E. Brown, "Experimental Study of Pressure Gradients Occurring During Continuous Two-Phase Flow in Small Diameter Vertical Conduits," J. Pet. Technol., 17, 475-484 (1965).

Harmathy, T.Z., "Velocity of Large Drops and Bubbles in Media of Infinite Or Restricted Extent," AIChE J., 6, 28 (1960).

Hasan, A.R. and C.S. Kabir, "Predicting Multiphase Flow Behavior in a Deviated Well," SPE paper 15449 presented at the 61st Annual Technical Meeting, New Orleans (1986).

Hetsroni, G., Handbood of Multiphase Systems, McGraw-Hill Company, (1982)

Hewitt, G.F. and N.S. Hall-Taylor, Annular Two Phase Flow, Pergomon Press, Oxford (1970).

Hinze, J.O., " Fundamentals of the Hydrodynamic Mechanism of Splitting In Dispersion Processes. AIChE J. 1, 289-295, (1955).

Hoogendoorn, C.J., "Gas-Liquid Flow in Horizontal Pipes," Chem. Eng. Sci., 9, 205-217 (1959).

Hoogendoorn, C.J. and A.A. Buitelaar, "The Effect of Gas Density and Gradual Vaporization on Gas-Liquid Flow in Horizontal Lines," Chem. Eng. Sci., 16, 208-221 (1961).

Hughmark, G.A. and B.S. Pressburg, "Holdup and Pressure Drop with Gas-Liquid Flow in a Vertical Pipe," AIChE J., 7, 677-682 (1961).

Hughmark, G.A., "Holdup in Gas-Liquid Flow," Chem. Eng. Prog., 58, 62-73 (1962).

James, P.W., Wilkes, N.S., Conkie, W. and Burns, A., Developments in the Modelling of Horizontal Annular Two-Phase Flow", Int. J. Multiphase Flow 13, No. 2, 173-198, (1987).

Kabir, C.S. and A.R. Hasan, "A Study of Multiphase Flow Behaviour in Vertical Oil Wells: Part II-Field Applications," SPE Paper 15139 presented at The 56th California Regional Meeting, Oakland, California (1986).

Kosterin, S.I., "An Investigation of the Influence of the Diameter and Inclination of a Tube in the Hydrostatic Resistance and Flow Structure Of Gas-Liquid Mixture," Izv. Akad. Nauk SSSR, Otd., Tekh. Nauk., No. 12, 1824-1830 (1949).

Laurinat, J. E., Hanratty, T.J. and Jepson, W.P. "Film Thickness Distribution For Gas-Liquid Annular Flow in a Horizontal Pipe", Int. J. Multiphase Flow 6, No.1 and 2, 179-195, (1985).

Lawson, J.D. and J.P. Brill, "A Schematic Evaluation of Methods Used to Predict Pressure Losses for Multiphase Flow in Vertical Oilwell Tubing," J. Pet. Technol., 26, 903-913 (1974).

Levich, V.G., Physiochemical Hydrodynamics, Prentice Hall, Englewood Cliff, New Jersey (1962).

Lockhart, R.W. and R.C. Martinelli, "Proposed Correlation of Data for Isothermal Two-Phase, Two-Component Flow in Pipes," Chem. Eng. Prog., 45, 39-48 (1949).

Manabe, R. Tochikawa, Tetsuro, Tsukuda, M., and Arihara, N., "Experimental and Modeling Studies of Two-Phase Flow in Pipelines", SPE Production & Facilities v 12n 4, Nov. 1997.

Mandhane, J.M., G.A. Gregory and K. Aziz, "A Flow Pattern Map for Gas-Liquid Flow in Horizontal Pipes, "Int. J. Multiphase Flow, 1, 537-553 (1974).

Mandhane, J.M., G.A. Gregory and K. Aziz, "Critical Evaluation of Holdup Prediction Methods for Gas-Liquid Flow in Horizontal Pipes," J.Pet. Technol., 27, 1017-1026 (1975).

Mandhane, J.M.,G.A. Gregory and K. Aziz, "Critical Evaluation of Pressure Drop Prediction Methods for Gas-Liquid Flow in Horizontal Pipes," J. Pet. Technol., 29, 1348-1358 (1977).

Maron, D.M., N.Y. Yacoub and N. Brauner, "New Thoughts on the Mechanism of Gas-Liquid Slug Flow," Letters in Heat and Mass Transfer, 9, 333-342 (1982).

Masud, B., "Most Accurate Two-Phase Pressure-Drop Correlation Identified " Oil & Gas J., 90-95 (September 16, 1991).

Minami, K., O., Shoham, "Pigging Dynamics in Two-Phase Flow Pipelines: Experiment and Modeling," SPE Production & Facilities (1995).

Mukherjee, H., "An Experimental Study of Inclined Two-Phase Flow," Ph.D.

Dissertation, University of Tulsa, Oklahoma (1979).

Nguyen, T, White-Stevens, D., "Design of Multiphase Pipeline Systems" Australia's Bicentennial International Conference for the Process Industries, Sydney, August (1988).

Nicholson, M.K., K. Aziz and G.A. Gregory, "Intermittent Two-Phase Flow in Horizontal Pipes: Predictive Models," Can. J. Chem. Eng., 56, 653-663 (1978).

Oliemans, R.V.A., B.F. Pots, and N. Trompe, "Modelling of Annular Dispersed Two-Phase Flow in Vertical Pipes", Int. Jl. Of Multiphase Flow, Vol.12 No. 5, 711-732, (1986).

Oliemans, R.V.A., "Modelling of Gas-Condensate Flow in Horizontal and Inclined Pipes", Proc., ASME Symp., etce, P 73 Dallas, Texas (1987).

Orkiszewski, J., "Predicting Two-Phase Pressure Drop in Vertical Pipe," J.Pet. Technol., 19, 829-838 (1967).

Palmer, C.M., "Evaluation of Inclined Pipe Two-Phase Liquid Holdup Correlations Using Experimental Data," M.S. Thesis, University of Tulsa, Oklahoma (1975).

Payne, G.A., C.M. Palmer, J.P. Brill and H.D. Beggs, "Evaluation of Inclined –Pipe Two-Phase Liquid Holdup and Pressure-Loss Correlations Using Experimental Data," J. Petrol. Tech., 31, 1198-1208 (1979).

Petalas, N. and Aziz, K. "Standford Multiphase Flow Database ", User's Manual Version 0.1, Dept. of Petroleum Engineering Standford University, (1994).

Poettmann, F.H. and P.G. Carpenter, "The Multiphase Flow of Gas, Oil and Water Through Vertical Flow Strings with Application to the Design of Gas Lift Installations," Drilling and Production Practice, API, 257-317 (1952).

Rajan, N., Schmidt, Z., Doty, D., "Experimental Study and the Development of Mechanistic Model for Two-Phase Flow Through Vertical Tubing" SPE 35676, 255 – 267, (1996).

Scott, S.L., "Modelling Slug Growth in Pipelines", Ph.D. Dissertation, The University of Tulsa (1987).

Shoham, O. and Y. Taitel, "Stratified Turbulent-Turbulent Gas-Liquid Flow in Horizontal and Inclined Pipes," AIChE., 30, 377-385 (1984).

Sylvester, N.E., "A Mechanistic Model for Two-Phase Vertical Slug Flow In Pipes", J. Energy Resour. Technol., Vol. 109, 206, (1987).

Taitel, Y. and A.E. Dukler, "A Model for Prediction of Flow Regime in Horizontal and Near Horizontal Gas-Liquid Flow," AIChE J., 22, 47-55 (1976).

Taitel, Y., D. Barnea and A.E. Dukler, "Modeling Flow Pattern Transitions for Steady Upward Gas-Liquid Flow in Vertical Tubes," AIChE J.,26, 345-354 (1980).

Taitel, Y. and A.E. Dukler, "A Model for Slug Frequency During Gas-Liquid Flow in Horizontal and Near Horizontal Pipes," Int. J. Multiphase Flow,3, 585-596 (1977).

Taitel, Y., Barnea, D. and Dukler, A.E. "Modeling Flow Pattern Transition for Steady Upward Gas-Liquid Flow in Vertical Tubes", AIChE j. 26, 345-354, (1980).

Taitel, Y. and Barnea, D. " A Consistent Approzch for Calculating Pressure Drop in Inclined Slug Flow", Chemical Engineering Science, Vol. 45, No. 5, (1990).

Wallis, G.B., One Dimensional Two Phase Flow, McGraw Hill Book Company, New York (1969).

Xiao, J.J., O. Shoham, and J.P. Brill, "A Comprehensive Mechanistic Model for Two-Phase Flow in Pipelines," SPE 20631 presented at the 65th Annual Technical Conference of The Society of Petroleum Engineers, New Orleans (1990).

Zuber, N., and Hench, J., "Steady State and Transient Void Fraction of Bubbling Systems and their Operating Limits, Part 1: Steady State Operations", General Electric Reports, 62GL100 (1962).

Appendix A

Raw Data

An electronic copy of the database used in this work is available in the attached Compact Disk.

Appendix B

Sample Calculations

Determine the liquid holdup and pressure gradient for test loop sub set SU-96, node 2, run 50, flowing under stratified flow regime conditions.

Input data:

Property		Liquid	Gas
Density	kg/m3	997.57	1.29
Viscosity	cp	0.99	0.018
Surface Tension	dyne/cm	72.59	-
Pressure	Kpag	244.69	244.69
Temperature	°C	20.55	20.55
Pipe Parameters		**Value**	
Diameter	m	0.026	
Angle of Inclination	°	0	
Relative Roughness	-	0	
Database Main Parameters		**Measured Value**	
Liquid Holdup	-	0.8873	
Pressure Gradient	Kpa/m	0.05968	

Calculation Procedure steps:

Property	Equation	1st Iteration	2nd Iteration	Converged
Liquid Superficial Velociy m/s	Eq. 2.2	0.305	0.305	0.305
Gas Superficial Velociy m/s	Eq. 2.2	0.045	0.045	0.045
Reynolds Number Liquid -	Eq. 2.22	7987.180	7987.180	7987.180
Reynolds Number Gas -	Eq. 2.23	84.616	84.616	84.616
Friction factor Liquid -	Eq. 2.26	0.033	0.033	0.033
Friction factor Gas -	Eq. 2.26	0.756	0.756	0.756
Pressure Gradient Liquid Kpa	Eq. 2.30	5.86E-02	5.86E-02	5.86E-02
Pressure Gradient Gas Kpa	Eq. 2.30	3.75E-05	3.75E-05	3.75E-05
Martinelly X parameter	Eq. 2.30	39.54	39.54	39.54
Martinelly Y parameter	Eq. 2.31	0	0	0
h/d	-	0.1	0.9	0.885023
Sg	Eq. 2.35	2.498	0.644	0.692
Sl	Eq. 2.34	0.644	2.498	2.450
Si	Eq. 2.36	0.600	0.600	0.638
Ag	Eq. 2.33	0.745	0.041	0.050
Al	Eq. 2.32	0.041	0.745	0.735
Vl	Eq. 2.37	19.215	1.055	1.068
Vg	Eq. 2.38	1.055	19.215	15.661
Dl	Eq. 2.24	0.254	1.192	1.201
Dg	Eq. 2.25	0.961	0.131	0.151
Objective Function	Eq. 2.29	6.62E+06	-4.00E+03	-2.95E-05
γ Rad	Eq. 2.70			4.8994
α_l -	Eq. 2.69			0.9361
PressureGradient Kpa/m	Eq. 2.76			0.04951